Electronic Supporting Information

# Tuning reactivity through implementation of the HSAB concept in oxygen- and sulphur-bridged Al/P and Ga/P FLPs

Julian Buth, Yury V. Vishnevskiy, Jan-Hendrik Lamm, Beate Neumann, Hans-Georg Stammler,

and Norbert W. Mitzel*

Lehrstuhl für Anorganische Chemie und Strukturchemie
Fakultät für Chemie, Universität Bielefeld
Universitätsstraße 25, 33615 Bielefeld (Germany)
E-Mail: mitzel@uni-bielefeld.de

## Table of contents

## Experimental details

### General methods

All reactions and manipulations with air and moisture sensitive compounds were carried out under conventional Schlenk techniques or in a glove box using argon as inert gas. Volatile compounds were handled in a vacuum line. The solvents *n*-hexane, toluene, toluene-$d_8$ and benzene-$d_6$ were dried over a Na/K alloy, dichloromethane over $CaH_2$, and were also distilled and degassed prior to use. $Bis_2AlH$,[1] $Bis_2GaBr$,[2] $Bis_2GaOP^tBu_2$,[2] and $^tBu_2P(S)H$[3] were prepared according to literature procedures. $CO_2$ (99.5%, Linde), $SO_2$ (99.98%, Air Liquid), and $N_2O$ (extracted from a cream capsule) were used without further purification. $CS_2$ (99.9%, J.T. Baker) was dried over $P_4O_{10}$, distilled and degassed prior to use. Propylene sulphide (98%, TCI) was distilled and degassed prior to use. NMR spectra were recorded using a Bruker Avance III 500, Avance III 500 HD, Ascend 500 neo2K or Ascend 500 neo3K spectrometer at ambient temperature unless otherwise stated. Chemical shifts were referenced to the residual proton or carbon signal of the solvent (benzene-$d_6$: $^1$H: 7.16 ppm, $^{13}$C: 128.1 ppm; toluene-$d_8$: $^1$H: 2.09 ppm) or externally ($^{29}$Si: $SiMe_4$, $^{31}$P: 85% $H_3PO_4$ in $H_2O$). Elemental analyses were carried out using a HEKATECH EURO Elemental Analyzer.

#### Synthetic procedures

**$^tBu_2P(S)H$**: In an ampoule fitted with a greaseless tap, $^tBu_2PCl$ (1.14 g, 6.31 mmol) was dissolved in toluene (5 mL), degassed and pressurised with $H_2S$ (1022 mbar, 16.5 mmol). After stirring for 8 d at 100°C all volatiles were removed under reduced pressure. The residue was dissolved in dichloromethane (15 mL) and dried in *vacuo* again. *Via* sublimation (60 °C, 0.02 mbar) $^tBu_2P(S)H$ was isolated as a fluffy colourless solid (709 mg, 4.00 mmol, 63%). $^1$H NMR (500 MHz, $C_6D_6$): $\delta$ [ppm] = 1.04 (d, $^3J_{P,H}$ = 16.2 Hz, 18H, C**H**$_3$), 5.51 (d, $^1J_{P,H}$ = 414.7 Hz, 1H, P**H**). $^{13}$C{$^1$H} NMR (126 MHz, $C_6D_6$): $\delta$ [ppm] = 27.3 (s, C(**C**H$_3$)$_3$), 35.6 (d, $^1J_{P,C}$ = 42.7 Hz, **C**(CH$_3$)$_3$). $^{31}$P{$^1$H} NMR (202 MHz, $C_6D_6$): $\delta$ [ppm] = 74.2 (s).

**$Bis_2AlSP^tBu_2$** (**AlSP**): $^tBu_2P(S)H$ (189 mg, 1.06 mmol) was dissolved in *n*-hexane (10 mL) and added to a solution of $Bis_2AlH$ (368 mg, 1.06 mmol) in *n*-hexane (10 mL), observing gas formation. After stirring for 1 h, all volatiles were removed under reduced pressure and the residue dried in *vacuo*. **AlSP** was obtained as a colourless crystalline solid (555 mg, 1.06 mmol, quant.). $^1$H NMR (500 MHz, $C_6D_6$): $\delta$ [ppm] = 0.27 (s, 2H, AlC**H**), 0.34 (s, 36H, Si(C**H**$_3$)$_3$), 1.24 (d, $^3J_{P,H}$ = 11.6 Hz, 18H, C(C**H**$_3$)$_3$). $^{13}$C{$^1$H} NMR (126 MHz, $C_6D_6$): $\delta$ [ppm] = 4.6 (s, Si(**C**H$_3$)$_3$), 10.5 (s, Al**C**H), 29.8 (d, $^2J_{P,C}$ = 15.4 Hz, C(**C**H$_3$)$_3$), 34.9 (d, $^1J_{P,C}$ = 34.3 Hz, **C**(CH$_3$)$_3$). $^{29}$Si{$^1$H} NMR (99 MHz, $C_6D_6$): $\delta$ [ppm] = −3.3 (s). $^{31}$P{$^1$H} NMR (202 MHz, $C_6D_6$): $\delta$ [ppm] = 69.2 (s). Elemental analysis calcd (%) for $C_{22}H_{56}AlPSSi_4$ ($M_r$ = 523.05): C 50.52, H 10.79, S 6.13; found C 49.88, H 10.76, S 6.09.

**$Bis_2GaSP(^tBu)_2$** (**GaSP**): $(^tBu)_2P(S)H$ (467 mg, 2.62 mmol) and $Bis_2GaBr$ (1.240 g, 2.65 mmol) were dissolved in *n*-hexane (15 mL). Potassium hexamethyldisilazanide (539 mg, 2.70 mmol) was added as a solid in portions over 30 min. The milky suspension was stirred for 1 h, then filtered and all volatiles were removed under reduced pressure. The residue was dried under reduced pressure. **GaSP** was obtained as a colourless crystalline solid (1.417 g, 2.50 mmol, 96%). $^1$H NMR (500 MHz, $C_6D_6$): $\delta$ [ppm] = 0.32 (s, 36H, Si(C**H**$_3$)$_3$), 1.06 (s, 2H, GaC**H**), 1.27 (d, $^3J_{P,H}$ = 11.5 Hz, 18H, C(C**H**$_3$)$_3$). $^{13}$C{$^1$H} NMR (126 MHz, $C_6D_6$): $\delta$ [ppm] = 4.2 (s, Si(**C**H$_3$)$_3$), 18.3 (s, Ga**C**H), 30.0 (d, $^2J_{P,C}$ = 15.7 Hz, C(**C**H$_3$)$_3$), 34.9 (d, $^1J_{P,C}$ = 33.8 Hz, **C**(CH$_3$)$_3$). $^{29}$Si{$^1$H} NMR (99 MHz, $C_6D_6$): $\delta$ [ppm] = −2.8 (s). $^{31}$P{$^1$H} NMR (202 MHz, $C_6D_6$): $\delta$ [ppm] = 68.5 (s). Elemental analysis calcd (%) for $C_{22}H_{56}GaPSSi_4$ ($M_r$ = 565.79): C 46.86, H 10.12, S 5.88; found C 46.70, H 9.98, S 5.67.

**Bis$_2$AlSP$^t$Bu$_2$**·HBr (**AlSP**·HBr): $^t$Bu$_2$P(S)H (16 mg, 90 µmol) was dissolved in toluene (2 mL) and added to Bis$_2$AlBr (38 mg, 90 µmol). After stirring for 1 h, all volatiles were removed under reduced pressure and **AlSP**·HBr was isolated as a colourless solid (54 mg, 90 µmol, quant.). Crystals of **AlSP**·HBr suitable for X-ray diffraction were obtained by slow evaporation of a solution in $C_6D_6$. $^1$H NMR (500 MHz, $C_6D_6$): $\delta$ [ppm] = −0.41 (s, 2H, AlC**H**), 0.45 (s, 36H, Si(C**H**$_3$)$_3$), 0.91 (d, $^3J_{P,H}$ = 17.2 Hz, 18H, C**H**$_3$), 6.02 (d, $^1J_{P,H}$ = 444.8 Hz, 1H, P**H**). $^{13}$C{$^1$H} NMR (126 MHz, $C_6D_6$): $\delta$ [ppm] = 5.0 (s, Si(**C**H$_3$)$_3$), 8.9 (s, Al**C**H), 27.6 (d, $^2J_{P,C}$ = 2.3 Hz, C(**C**H$_3$)$_3$), 35.9 (d, $^1J_{P,C}$ = 39.3 Hz, **C**(CH$_3$)$_3$). $^{29}$Si{$^1$H} NMR (99 MHz, $C_6D_6$): $\delta$ [ppm] = −1.8 (s). $^{31}$P{$^1$H} NMR (121 MHz, $C_6D_6$): $\delta$ [ppm] = 69.7 (s). Elemental analysis calcd (%) for $C_{22}H_{57}BrAlSPSi_4$ ($M_r$ = 587.90): C 43.75, H 9.51, S 5.31; found C 43.34, H 9.52, S 5.65.

**Procedure for the CO$_2$ adducts Bis$_2$EXP$^t$Bu$_2$**·CO$_2$ (**EXP**·CO$_2$)

**EXP** was dissolved in *n*-hexane (4 mL), degassed (3 × freeze-pump-thaw) and pressurised with an atmosphere of carbon dioxide (1 atm.). After stirring for 24 h, all volatiles were removed under reduced pressure and the residue dried in *vacuo*. Crystals of **GaOP**·CO$_2$ and **AlSP**·CO$_2$ suitable for X-ray diffraction were obtained by slow evaporation of a solution in $C_6D_6$.

**Bis$_2$GaOP$^t$Bu$_2$**·CO$_2$ (**GaOP**·CO$_2$) was obtained as a colourless solid (42 mg, 71 µmol, quant.). $^1$H NMR (500 MHz, $C_6D_6$): $\delta$ [ppm] = −0.35 (s, 2H, GaC**H**), 0.37 (s, 18H, Si(C**H**$_3$)$_3$), 0.39 (s, 18H, Si(C**H**$_3$)$_3$), 1.06 (d, $^3J_{P,H}$ = 15.1 Hz, 18H, C(C**H**$_3$)$_3$). $^{13}$C{$^1$H} NMR (126 MHz, $C_6D_6$): $\delta$ [ppm] = 4.6 (s, Si(**C**H$_3$)$_3$), 4.8 (s, Ga**C**H), 26.7 (s, C(**C**H$_3$)$_3$), 34.7 (d, $^1J_{P,C}$ = 45.4 Hz, **C**(CH$_3$)$_3$), 167.2 (d, $^1J_{P,C}$ = 98.5 Hz, P**C**O$_2$). $^{29}$Si{$^1$H} NMR (99 MHz, $C_6D_6$): $\delta$ [ppm] = −1.2 (s). $^{31}$P{$^1$H} NMR (202 MHz, $C_6D_6$): $\delta$ [ppm] = 57.1 (s). Elemental analysis calcd (%) for $C_{23}H_{56}GaO_3PSi_4$ ($M_r$ = 593.73): C 46.53, H 9.51; found C 46.30, H 9.78.

**Bis$_2$AlSP$^t$Bu$_2$**·CO$_2$ (**AlSP**·CO$_2$) was obtained as a colourless solid (39 mg, 69 µmol, quant.). $^1$H NMR (500 MHz, $C_6D_6$): $\delta$ [ppm] = −0.79 (s, 2H, AlC**H**), 0.41 (s, 18H, Si(C**H**$_3$)$_3$), 0.42 (s, 18H, Si(C**H**$_3$)$_3$), 1.05 (d, $^3J_{P,H}$ = 16.8 Hz, 18H, C(C**H**$_3$)$_3$). $^{13}$C{$^1$H} NMR (126 MHz, $C_6D_6$): $\delta$ [ppm] = 5.1 (s, Si(**C**H$_3$)$_3$), 5.3 (s, Si(**C**H$_3$)$_3$), 5.7 (s, Al**C**H), 27.3 (s, C(**C**H$_3$)$_3$), 38.3 (d, $^1J_{P,C}$ = 26.4 Hz, **C**(CH$_3$)$_3$), 163.3 (d, $^1J_{P,C}$ = 79.0 Hz, P**C**O$_2$). $^{29}$Si{$^1$H} NMR (99 MHz, $C_6D_6$): $\delta$ [ppm] = −1.7 (s), −1.3 (s). $^{31}$P{$^1$H} NMR (202 MHz, $C_6D_6$): $\delta$ [ppm] = 73.3 (s). Elemental analysis calcd (%) for $C_{23}H_{56}AlO_2PSSi_4$ ($M_r$ = 567.05): C 48.72, H 9.95, S 5.65; found C 48.93, H 10.23, S 5.48.

**Bis$_2$GaSP$^t$Bu$_2$**·CO$_2$ (**GaSP**·CO$_2$): **GaSP** forms a temperature-dependent equilibrium with **GaSP**·CO$_2$ under an atmosphere of CO$_2$. VT NMR studies were conducted in the range between 253 – 373 K. $^1$H NMR (500 MHz, $C_6D_6$): $\delta$ [ppm] = −0.27 (s, 2H, GaC**H**), 0.40 (s, 36H, Si(C**H**$_3$)$_3$), 1.13 (d, $^3J_{P,H}$ = 16.4 Hz, 18H, C(C**H**$_3$)$_3$). $^{13}$C{$^1$H} NMR (126 MHz, $C_6D_6$): $\delta$ [ppm] = 4.9 (s, Si(**C**H$_3$)$_3$), 11.8 (s, Ga**C**H), 27.6 (s, C(**C**H$_3$)$_3$), 38.1 (d, $^1J_{P,C}$ = 27.0 Hz, **C**(CH$_3$)$_3$), 164.2 (d, $^1J_{P,C}$ = 75.1 Hz, P**C**O$_2$). $^{29}$Si{$^1$H} NMR (99 MHz, $C_6D_6$): $\delta$ [ppm] = −0.6 (s). $^{31}$P{$^1$H} NMR (202 MHz, $C_6D_6$): $\delta$ [ppm] = 67.9 (s).

**Procedure for the CS$_2$ adducts Bis$_2$EXP$^t$Bu$_2$**·CS$_2$ (**EXP**·CS$_2$):

**EXP** was dissolved in *n*-hexane (3 mL) carbon disulfide (excess) was added, and the solutions show colourations within 5 min for **GaOP**·CS$_2$ (blue) and **AlSP**·CS$_2$ (green). For **GaSP**·CS$_2$ the reaction was slower and within 24 h a deep yellow colouration resulted. After stirring for 48 h, all volatiles were removed under reduced pressure and the residue dried in *vacuo*. Recrystallization from *n*-hexane gave violet crystals in all cases.

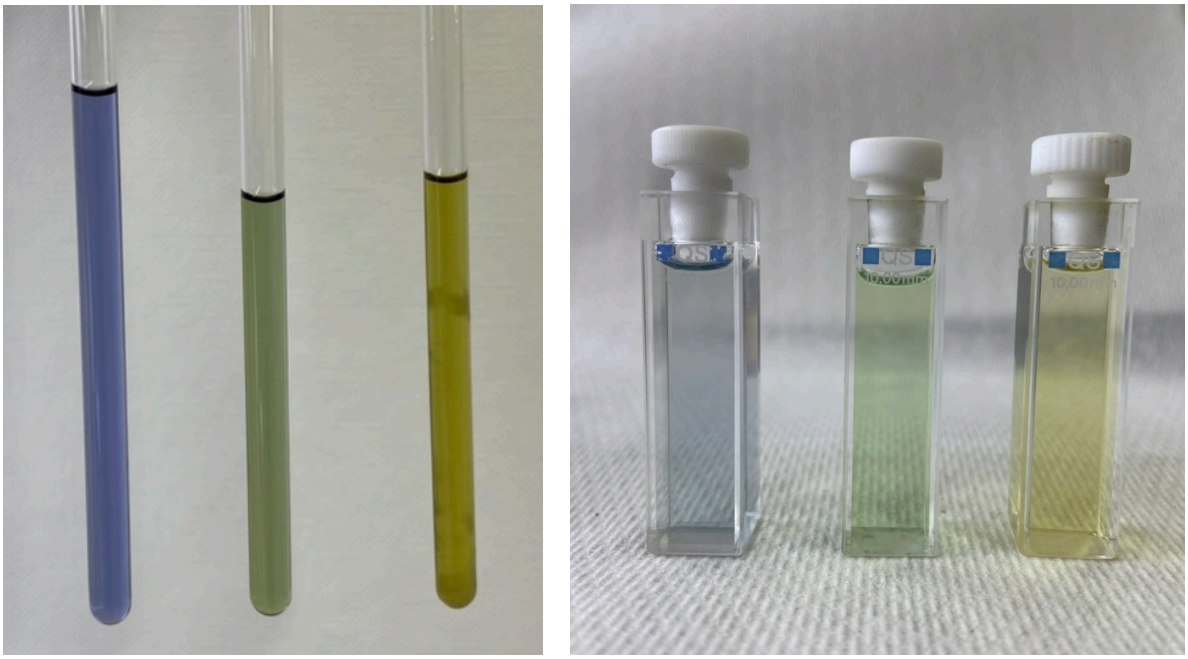

**Figure S1. GaOP**·$CS_2$ (blue), **AlSP**·$CS_2$ (green) and **GaSP**·$CS_2$ (yellow) in Young NMR tubes ($C_6D_6$) and in cuvettes (*n*-hexane).

**Bis$_2$GaOP$^t$Bu$_2$**·$CS_2$ (**GaOP**·$CS_2$) crystallises as wide, violet needles (11 mg, 18 µmol, 31%) from a concentrated *n*-hexane solution at −18 °C. $^1$H NMR (500 MHz, $C_6D_6$): $\delta$ [ppm] = −0.17 (s, 2H, GaCH), 0.36 (s, 36H, Si($CH_3$)$_3$), 1.14 (d, $^3J_{P,H}$ = 14.9 Hz, 18H, C($CH_3$)$_3$). $^{13}$C{$^1$H} NMR (126 MHz, $C_6D_6$): $\delta$ [ppm] = 4.7 (s, Si($CH_3$)$_3$), 4.8 (s, Si($CH_3$)$_3$), 11.4 (s, GaCH), 27.3 (s, C($CH_3$)$_3$), 36.6 (d, $^1J_{P,C}$ = 51.0 Hz, C($CH_3$)$_3$), 237.8 (d, $^1J_{P,C}$ = 42.4 Hz, $PCS_2$). $^{29}$Si{$^1$H} NMR (99 MHz, $C_6D_6$): $\delta$ [ppm] = −1.5 (s), −0.9 (s). $^{31}$P{$^1$H} NMR (202 MHz, $C_6D_6$): $\delta$ [ppm] = 63.5 (s). Elemental analysis calcd (%) for $C_{23}H_{56}GaOPS_2Si_4$ ($M_r$ = 625.86): C 44.14, H 9.02, S 10.25; found C 44.35, H 8.93, S 10.17.

**Bis$_2$AlSP$^t$Bu$_2$**·$CS_2$ (**AlSP**·$CS_2$) crystallises as small violet blocks (22 mg, 37 µmol, 47%) from a concentrated *n*-hexane solution at −18 °C. $^1$H NMR (500 MHz, $C_6D_6$): $\delta$ [ppm] = −0.59 (s, 2H, AlCH), 0.40 (s, 18H, Si($CH_3$)$_3$), 0.42 (s, 18H, Si($CH_3$)$_3$), 1.14 (d, $^3J_{P,H}$ = 16.5 Hz, 18H, C($CH_3$)$_3$). $^{13}$C{$^1$H} NMR (126 MHz, $C_6D_6$): $\delta$ [ppm] = 5.5 (s, Si($CH_3$)$_3$), 7.0 (s, AlCH), 28.4 (s, C($CH_3$)$_3$), 41.7 (d, $^1J_{P,C}$ = 29.5 Hz, C($CH_3$)$_3$), 232.7 (d, $^1J_{P,C}$ = 18.3 Hz, $PCS_2$). $^{29}$Si{$^1$H} NMR (99 MHz, $C_6D_6$): $\delta$ [ppm] = −1.5 (s), −1.4 (s). $^{31}$P{$^1$H} NMR (202 MHz, $C_6D_6$): $\delta$ [ppm] = 91.9 (s). Elemental analysis calcd (%) for $C_{23}H_{56}AlPS_3Si_4$ ($M_r$ = 599.18): C 46.11, H 9.42, S 16.05; found C 46.44, H 9.80, S 15.69.

**Bis$_2$GaSP$^t$Bu$_2$**·$CS_2$ (**GaSP**·$CS_2$): crystallises as small violet blocks (56 mg, 87 µmol, 46%) from a concentrated *n*-hexane solution at −18 °C. 'classical' adduct (**GaSCP**-connectivity): $^1$H NMR (500 MHz, $C_6D_6$): $\delta$ [ppm] = −0.12 (s, 2H, GaCH), 0.38 (s, 18H, Si($CH_3$)$_3$), 0.39 (s, 18H, Si($CH_3$)$_3$), 1.19 (d, $^3J_{P,H}$ = 16.3 Hz, 18H, C($CH_3$)$_3$). $^{13}$C{$^1$H} NMR (126 MHz, $C_6D_6$): $\delta$ [ppm] = 5.0 (s, Si($CH_3$)$_3$), 5.1 (s, Si($CH_3$)$_3$), 12.6 (s, GaCH), 28.6 (s, C($CH_3$)$_3$), 41.7 (d, $^1J_{P,C}$ = 30.1 Hz, C($CH_3$)$_3$), 233.0 (d, $^1J_{P,C}$ = 16.2 Hz, $PCS_2$). $^{29}$Si{$^1$H} NMR (99 MHz, $C_6D_6$): $\delta$ [ppm] = −0.6 (s), −0.5 (s). $^{31}$P{$^1$H} NMR (202 MHz, $C_6D_6$): $\delta$ [ppm] = 91.7 (s). 'inverted' adduct (**GaCSP**-connectivity): $^1$H NMR (500 MHz, $C_6D_6$): $\delta$ [ppm] = −0.13 (s, 2H, GaC**H**), 0.24 (s, 36H, Si(C**H**$_3$)$_3$), 1.44 (d, $^3J_{P,H}$ = 16.0 Hz, 18H, C(C**H**$_3$)$_3$). $^{13}$C{$^1$H} NMR (126 MHz, $C_6D_6$): $\delta$ [ppm] = 4.2 (s, Si(**C**H$_3$)$_3$), 13.2 (s, Ga**C**H), 28.6 (s, C(**C**H$_3$)$_3$), 40.7 (d, $^1J_{P,C}$ = 36.4 Hz, **C**(CH$_3$)$_3$), 255.8 (s, Ga**C**S$_2$). $^{29}$Si{$^1$H} NMR (99 MHz, $C_6D_6$): $\delta$ [ppm] = −0.3 (s). $^{31}$P{$^1$H} NMR (202 MHz, $C_6D_6$): $\delta$ [ppm] = 97.1 (s). Elemental analysis calcd (%) for $C_{23}H_{56}GaPS_3Si_4$ ($M_r$ = 641.92): C 43.04, H 8.79, S 14.98; found C 43.28, H 9.05, S 14.87.

**Procedure for Bis$_2$EXP$^t$Bu$_2$·SO$_2$ (EXP·SO$_2$):**

**EXP** was dissolved in *n*-hexane (3 mL), degassed (3 × freeze-pump-thaw) and $SO_2$ (excess) was condensed onto the frozen solution. After stirring for 24 h, all volatiles were removed under reduced pressure and the residue dried in *vacuo*. **EXP**·$SO_2$ were obtained as colourless solids. Crystals of **EXP**·$SO_2$ suitable for X-ray diffraction were obtained by slow evaporation of a solution in $C_6D_6$.

**Bis$_2$GaOP$^t$Bu$_2$**·$SO_2$ (**GaOP**·$SO_2$) was obtained as a colourless solid (23 mg, 38 µmol, quant.). $^1$H NMR (500 MHz, $C_6D_6$): $\delta$ [ppm] = −0.31 (br. s, 1H, GaC**H**), −0.03 (br. s, 1H, GaC**H**), 0.37–0.49 (m, 36H, Si(C**H**$_3$)$_3$), 0.87 (d, $^3J_{P,H}$ = 14.5 Hz, 9H, C(C**H**$_3$)$_3$), 1.21 (d, $^3J_{P,H}$ = 15.1 Hz, 9H, C(C**H**$_3$)$_3$). $^{13}$C{$^1$H} NMR (126 MHz, $C_6D_6$): $\delta$ [ppm] = 4.8 (s, Si(**C**H$_3$)$_3$), 5.0 (s, Si(**C**H$_3$)$_3$), 12.2 (br. s, Ga**C**H), 26.7 (s, C(**C**H$_3$)$_3$), 27.1 (s, C(**C**H$_3$)$_3$), 37.0 (d, $^1J_{P,C}$ = 21.1 Hz, **C**(CH$_3$)$_3$), 39.3 (d, $^1J_{P,C}$ = 21.2 Hz, **C**(CH$_3$)$_3$). $^{29}$Si{$^1$H} NMR (99 MHz, $C_6D_6$): $\delta$ [ppm] = −1.3 (s), −0.9 (s). $^{31}$P{$^1$H} NMR (202 MHz, $C_6D_6$): $\delta$ [ppm] = 88.1 (s). Elemental analysis calcd (%) for $C_{22}H_{56}GaO_3PSSi_4$ ($M_r$ = 613.78): C 43.05, H 9.20, S 5.22; found C 42.51, H 9.03, S 5.30.

**Bis$_2$AlSP$^t$Bu$_2$**·$SO_2$ (**AlSP**·$SO_2$) was obtained as a colourless solid (21 mg, 37 µmol, quant.). $^1$H NMR (500 MHz, $C_6D_6$): $\delta$ [ppm] = −0.69 (br. s, 1H, AlC**H**), −0.57 (br. s, 1H, AlC**H**), 0.31–0.59 (m, 36H, Si(C**H**$_3$)$_3$), 0.89 (d, $^3J_{P,H}$ = 16.3 Hz, 9H, C(C**H**$_3$)$_3$), 1.18 (d, $^3J_{P,H}$ = 16.4 Hz, 9H, C(C**H**$_3$)$_3$). $^{13}$C{$^1$H} NMR (126 MHz, $C_6D_6$): $\delta$ [ppm] = 5.0 (s, Si(**C**H$_3$)$_3$), 5.2 (s, Si(**C**H$_3$)$_3$), 6.1 (s, Al**C**H), 8.5 (s, Al**C**H), 27.5 (s, C(**C**H$_3$)$_3$), 27.9 (s, C(**C**H$_3$)$_3$), 39.2 (d, $^1J_{P,C}$ = 21.3 Hz, **C**(CH$_3$)$_3$), 42.4 (d, $^1J_{P,C}$ = 18.9 Hz, **C**(CH$_3$)$_3$). $^{29}$Si{$^1$H} NMR (99 MHz, $C_6D_6$): $\delta$ [ppm] = −1.5 (s). $^{31}$P{$^1$H} NMR (202 MHz, $C_6D_6$): $\delta$ [ppm] = 117.0 (s). Elemental analysis calcd (%) for $C_{22}H_{56}AlO_2PS_2Si_4$ ($M_r$ = 587.10): C 45.01, H 9.61, S 10.92; found C 45.11, H 9.59, S 10.92.

**Bis$_2$GaSP$^t$Bu$_2$**·$SO_2$ (**GaSP**·$SO_2$) was obtained as a colourless solid (25 mg, 39 µmol, 95%). $^1$H NMR (500 MHz, $C_6D_6$): $\delta$ [ppm] = −0.08 (br. s, 2H, GaC**H**), 0.44 (s, 36H, Si(C**H**$_3$)$_3$), 1.07 (br. s, 18H, C(C**H**$_3$)$_3$). $^{13}$C{$^1$H} NMR (126 MHz, $C_6D_6$): $\delta$ [ppm] = 5.1 (s, Si(**C**H$_3$)$_3$), 28.3 (s, C(**C**H$_3$)$_3$), carbon atoms (Ga**C**H, **C**(CH$_3$)$_3$) not detected due to broadening. $^{29}$Si{$^1$H} NMR (99 MHz, $C_6D_6$): $\delta$ [ppm] = −1.1 (s). $^{31}$P{$^1$H} NMR (202 MHz, $C_6D_6$): $\delta$ [ppm] = 114.9 (s). Elemental analysis calcd (%) for $C_{23}H_{56}GaO_2PS_2Si_4$ ($M_r$ = 629.84): C 41.95, H 8.96, S 10.18; found C 42.38, H 9.07, S 9.99.

**Procedure for Bis$_2$EXP$^t$Bu$_2$·O (EXP·O):**

Bis$_2$EXP$^t$Bu$_2$ was dissolved in *n*-hexane (3 mL), degassed (3 × freeze-pump-thaw) and $N_2O$ (excess) was condensed onto the frozen solution. After stirring for 24 h, all volatiles were removed under reduced pressure and the residue dried in *vacuo*. **GaOP**·O (23 mg, 40 µmol, quant.) and **AlSP**·O (16 mg, 30 µmol, 92%) were obtained as colourless solids. **GaSP** shows no reaction with $N_2O$, even after heating to 70 °C. Crystals of **EXP**·O suitable for X-ray diffraction were obtained by slow evaporation of a solution in $C_6D_6$.

**Bis$_2$GaOP$^t$Bu$_2$**·O (**GaOP**·O) was obtained as a colourless solid (23 mg, 40 µmol, quant.). $^1$H NMR (500 MHz, $C_6D_6$): $\delta$ [ppm] = 0.18 (s, 2H, GaC**H**), 0.38 (s, 36H, Si(C**H**$_3$)$_3$), 1.18 (d, $^3J_{P,H}$ = 14.0 Hz, 18H, C(C**H**$_3$)$_3$). $^{13}$C{$^1$H} NMR (126 MHz, $C_6D_6$): $\delta$ [ppm] = 4.6 (s, Si(**C**H$_3$)$_3$), 13.3 (s, Ga**C**H), 27.5 (s, C(**C**H$_3$)$_3$), 35.7 (d, $^1J_{P,C}$ = 73.5 Hz, **C**(CH$_3$)$_3$). $^{29}$Si{$^1$H} NMR (99 MHz, $C_6D_6$): $\delta$ [ppm] = −1.3 (s). $^{31}$P{$^1$H} NMR (202 MHz, $C_6D_6$): $\delta$ [ppm] = 85.2 (s). Elemental analysis calcd (%) for $C_{22}H_{56}GaO_2PSi_4$ ($M_r$ = 565.72): C 46.71, H 9.98; found C 46.76, H 10.13.

**Bis$_2$AlSP$^t$Bu$_2$**·O (**AlSP**·O) was obtained as a colourless solid (16 mg, 30 µmol, 92%). $^1$H NMR (500 MHz, $C_6D_6$): $\delta$ [ppm] = −0.54 (br. s, 1H, AlC**H**), −0.47 (br. s, 1H, AlC**H**), 0.42 (s, 36H, Si(C**H**$_3$)$_3$), 1.09 (d, $^3J_{P,H}$ = 16.3 Hz, 18H, C(C**H**$_3$)$_3$). $^{13}$C{$^1$H} NMR (126 MHz, $C_6D_6$): $\delta$ [ppm] = 5.1 (s, Si(**C**H$_3$)$_3$), 5.5 (s, Si(**C**H$_3$)$_3$), 9.5 (s, Al**C**H), 27.0 (d, $^2J_{P,C}$ = 2.8 Hz, C(**C**H$_3$)$_3$), 35.7

(d, $^{1}J_{P,C}$ = 50.1 Hz, **C**$(CH_3)_3$). $^{29}Si\{^{1}H\}$ NMR (99 MHz, $C_6D_6$): $\delta$ [ppm] = −2.0 (s). $^{31}P\{^{1}H\}$ NMR (202 MHz, $C_6D_6$): $\delta$ [ppm] = 116.4 (s). Elemental analysis calcd (%) for $C_{22}H_{56}AlOPSSi_4$ ($M_r$ = 539.04): C 49.02, H 10.47, S 5.95; found C 49.20, H 10.64, S 5.83.

**Bis$_2$GaOP$^t$Bu$_2$**·S (**GaOP**·S): **GaOP** (96.1 mg, 0.17 mmol) was dissolved in toluene (3 mL), degassed (3 × freeze-pump-thaw) and propylene sulphide (20 mbar, excess) was condensed onto the frozen solution. After stirring for 24 h at 80 °C, all volatiles were removed under reduced pressure and the residue dried in *vacuo*. **GaOP**·S was obtained as a colourless solid (79 mg, 0.14 mmol, 78%). Crystals of **GaOP**·S suitable for X-ray diffraction were obtained by slow evaporation of a solution in $C_6D_6$.
$^{1}H$ NMR (500 MHz, $C_6D_6$): $\delta$ [ppm] = 0.22 (s, 2H, GaC**H**), 0.40 (s, 36H, Si(C**H**$_3)_3$), 1.17 (d, $^{3}J_{P,H}$ = 15.9 Hz, 18H, C(C**H**$_3)_3$). $^{13}C\{^{1}H\}$ NMR (126 MHz, $C_6D_6$): $\delta$ [ppm] = 4.6 (s, Si(**C**$H_3)_3$), Ga**C**H not detected, 27.4 (d, $^{2}J_{P,C}$ = 2.3 Hz, C(**C**$H_3)_3$), 39.6 (d, $^{1}J_{P,C}$ = 52.4 Hz, **C**$(CH_3)_3$). $^{29}Si\{^{1}H\}$ NMR (99 MHz, $C_6D_6$): $\delta$ [ppm] = −1.0 (s). $^{31}P\{^{1}H\}$ NMR (202 MHz, $C_6D_6$): $\delta$ [ppm] = 117.8 (br. s). Elemental analysis calcd (%) for $C_{22}H_{56}GaOPSSi_4$ ($M_r$ = 581.79): C 45.42, H 9.70, S 5.51; found C 45.60, H 9.42 S 5.51.

**Bis$_2$AlSP$^t$Bu$_2$**·$SC_3H_6$ (**AlSP**·$SC_3H_6$): **AlSP** (32.0 mg, 61 µmol) was dissolved in toluene (3 mL), degassed (3 × freeze-pump-thaw) and propylene sulphide (12 mbar, excess) was condensed onto the frozen solution. After stirring for 24 h at 80 °C, all volatiles were removed under reduced pressure and the residue dried in *vacuo*. **AlSP**·$SC_3H_6$ was obtained as a colourless solid (35 mg, 58 µmol, 95%). Crystals of **AlSP**·$SC_3H_6$ suitable for X-ray diffraction were obtained by slow evaporation of a solution in $C_6D_6$. $^{1}H$ NMR (500 MHz, $C_6D_6$): $\delta$ [ppm] = −0.54 (m, 2H, AlC**H**), 0.49 – 0.57 (m, 36H, Si(C**H**$_3)_3$), 0.80 (d, $^{3}J_{P,H}$ = 15.3 Hz, 9H, C(C**H**$_3)_3$), 0.91 (d, $^{3}J_{P,H}$ = 16.0 Hz, 9H, C(C**H**$_3)_3$), 1.46 (dd, 3H, C**H**$_3$), 1.62 (ddd, 1H, PC**H**$_2$), 1.82 (ddd, 1H, PC**H**$_2$), 3.12 (m, 1H, OC**H**). $^{13}C\{^{1}H\}$ NMR (126 MHz, $C_6D_6$): $\delta$ [ppm] = 5.3, 5.5, 5.6 (s, Si(**C**$H_3)_3$), 6.8 (s, Al**C**H), 26.7 (s, C(**C**$H_3)_3$), 27.1 (s, C(**C**$H_3)_3$), 28.9 (d, $^{3}J_{P,C}$ = 13.8 Hz, **C**$H_3$), 30.3 (d, $^{1}J_{P,C}$ = 40.0 Hz, **C**$H_2$), 31.4 (d, $^{2}J_{P,C}$ = 4.6 Hz, O**C**H), 37.6 (d, $^{1}J_{P,C}$ = 37.7 Hz, **C**$(CH_3)_3$), 38.7 (d, $^{1}J_{P,C}$ = 40.0 Hz, **C**$(CH_3)_3$). $^{29}Si\{^{1}H\}$ NMR (99 MHz, $C_6D_6$): $\delta$ [ppm] = −1.3 (s). $^{31}P\{^{1}H\}$ NMR (202 MHz, $C_6D_6$): $\delta$ [ppm] = 77.4 (s). Elemental analysis calcd (%) for $C_{25}H_{62}AlPS_2Si_4$ ($M_r$ = 597.19): C 50.28, H 10.47, S 10.74; found C 50.08, H 10.36, S 11.08.

NMR spectra

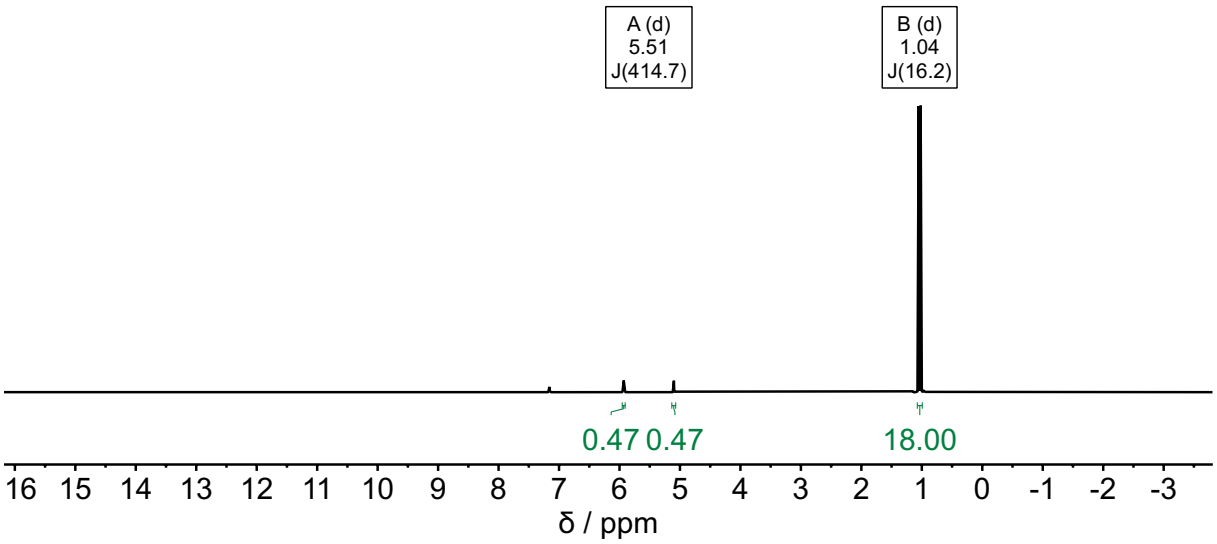


**Figure S2.** $^{1}H$ NMR spectrum of $^{t}Bu_2P(S)H$ in $C_6D_6$ (500 MHz, 298K).

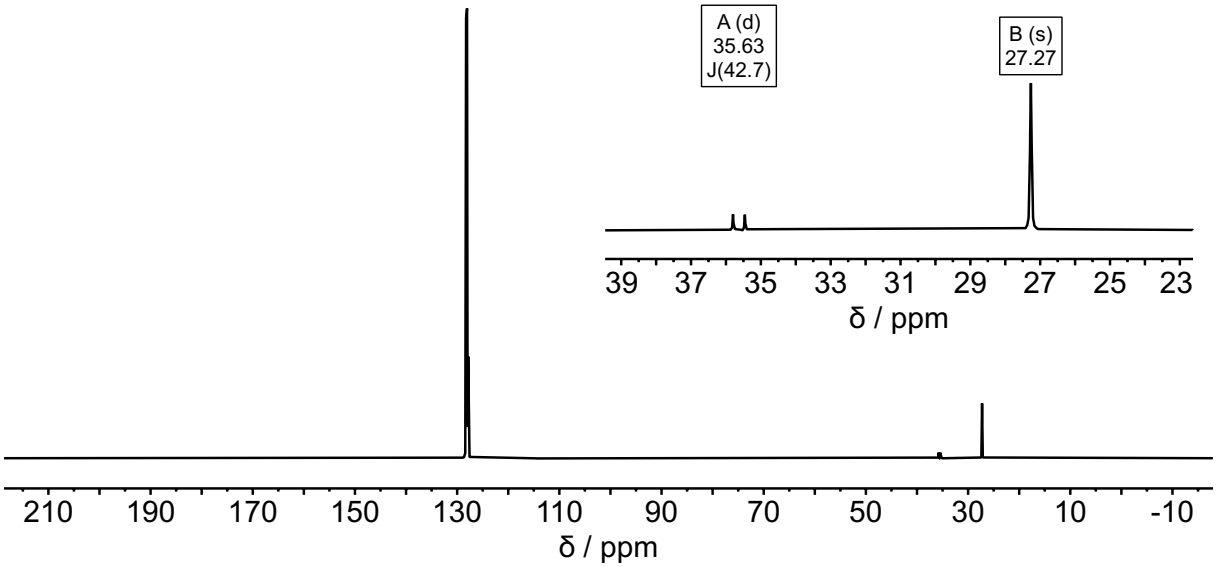


**Figure S3.** $^{13}C\{^{1}H\}$ NMR spectrum of $^{t}Bu_2P(S)H$ in $C_6D_6$ (126 MHz, 298K).

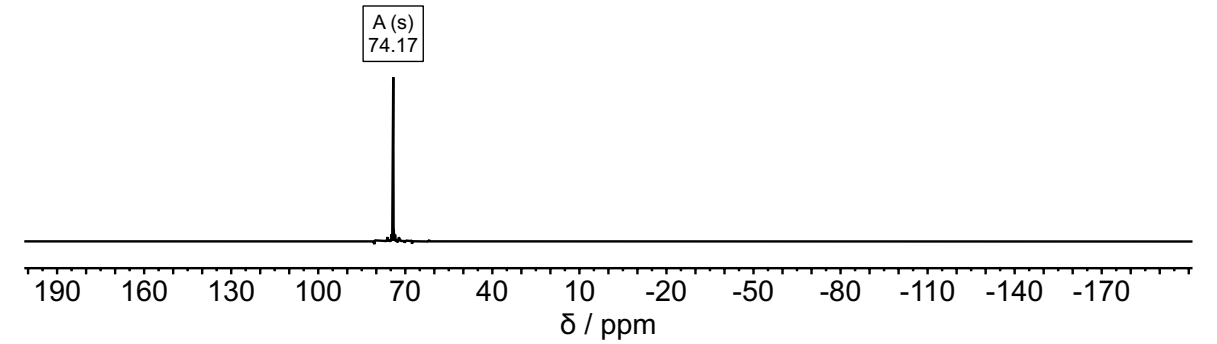


**Figure S4.** $^{31}P\{^{1}H\}$ NMR spectrum of $^{t}Bu_2P(S)H$ in $C_6D_6$ (202 MHz, 298K).

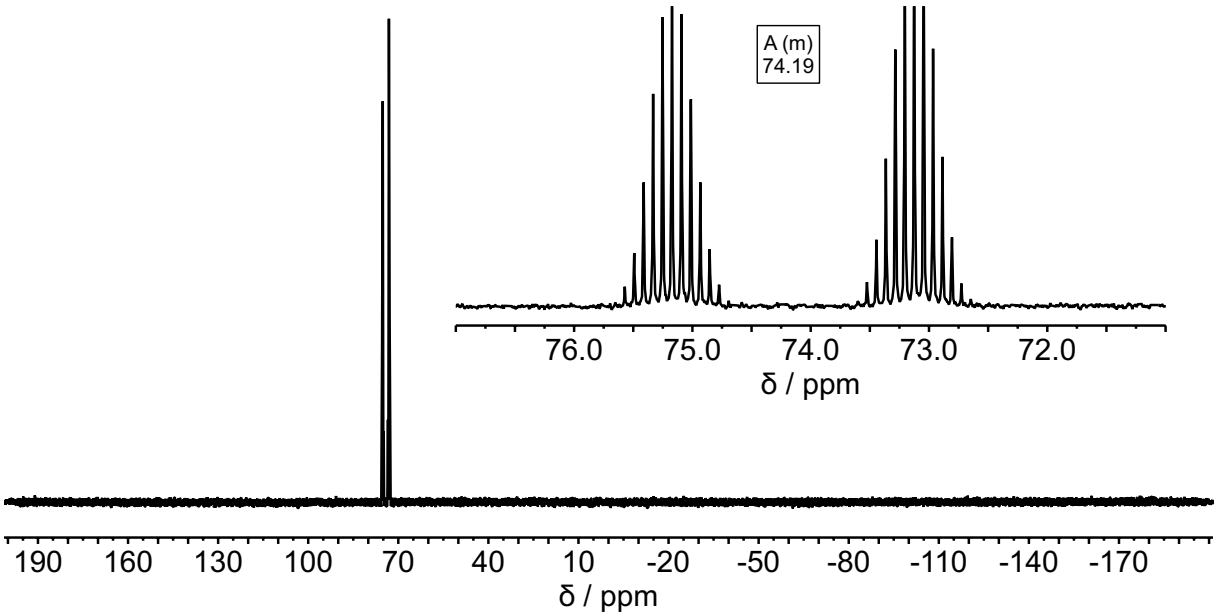


**Figure S5.** $^{31}$P NMR spectrum of $^{t}Bu_2P(S)H$ in $C_6D_6$ (202 MHz, 298K).

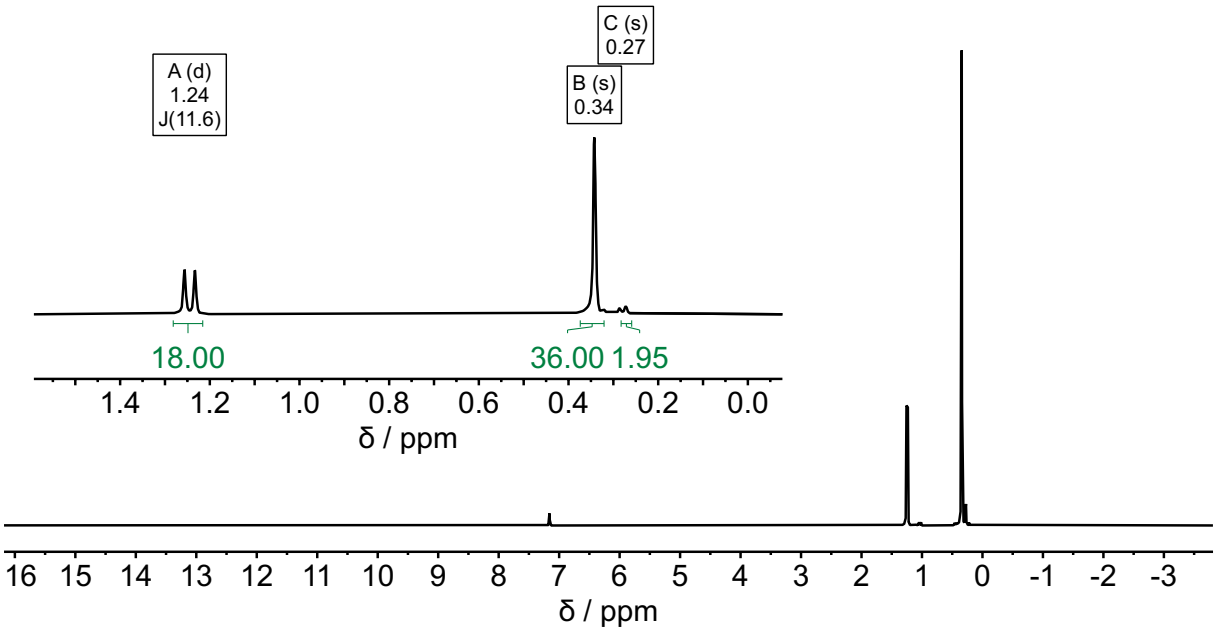


**Figure S6.** $^{1}$H NMR spectrum of $Bis_2AlSP^{t}Bu_2$ (**AlSP**) in $C_6D_6$ (500 MHz, 298K).

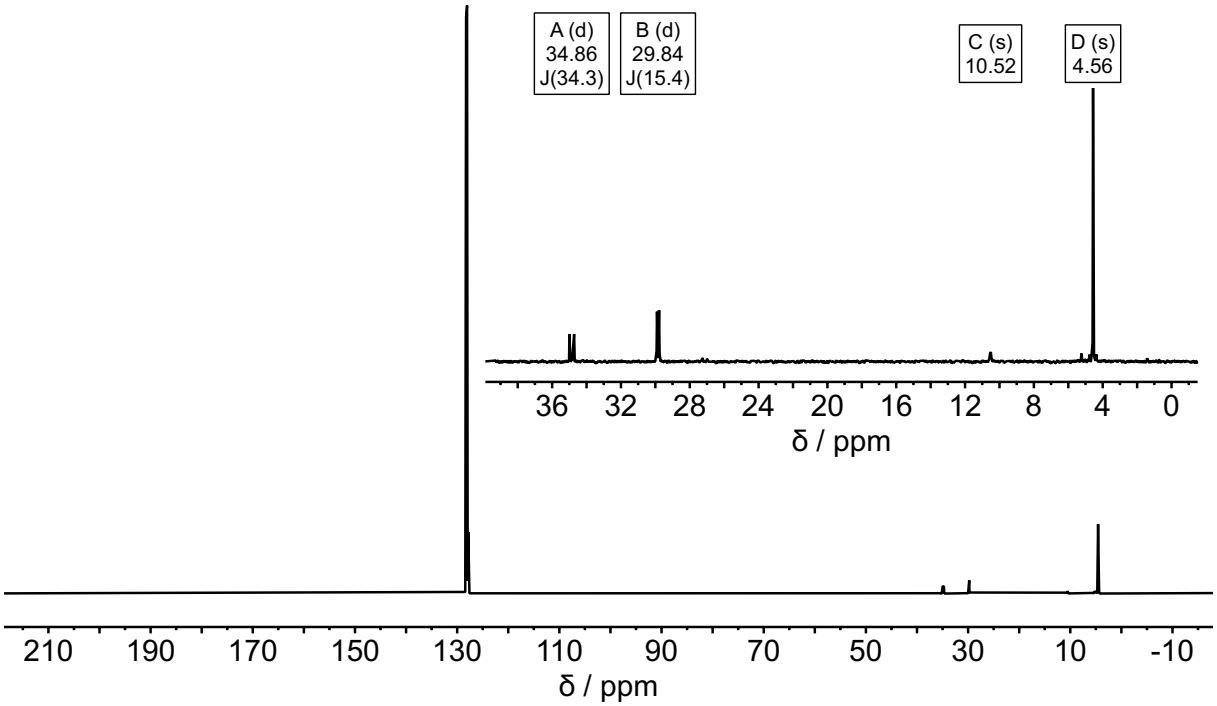


**Figure S7.** $^{13}C\{^{1}H\}$ NMR spectrum of $Bis_2AlSP^tBu_2$ (**AlSP**) in $C_6D_6$ (126 MHz, 298K).

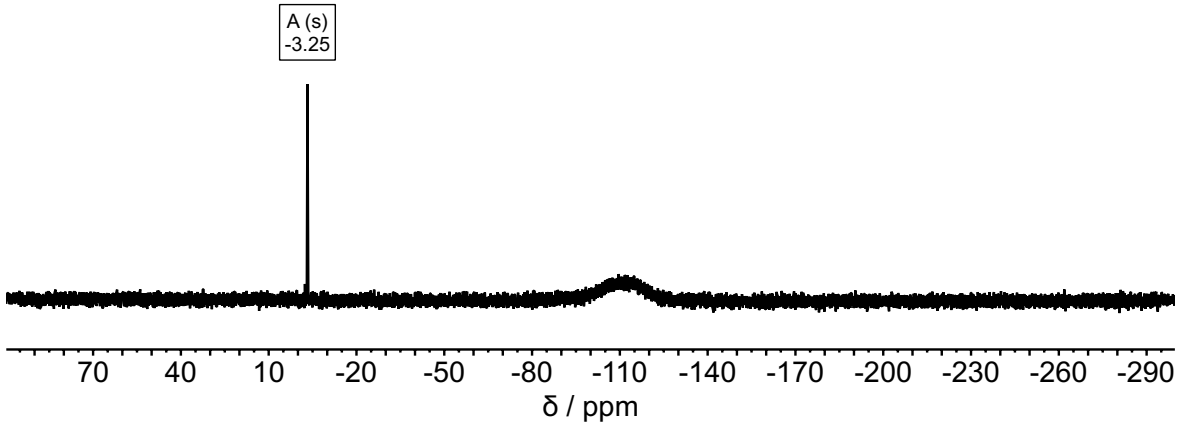


**Figure S8.** $^{29}Si\{^{1}H\}$ NMR spectrum of $Bis_2AlSP^tBu_2$ (**AlSP**) in $C_6D_6$ (99 MHz, 298K).

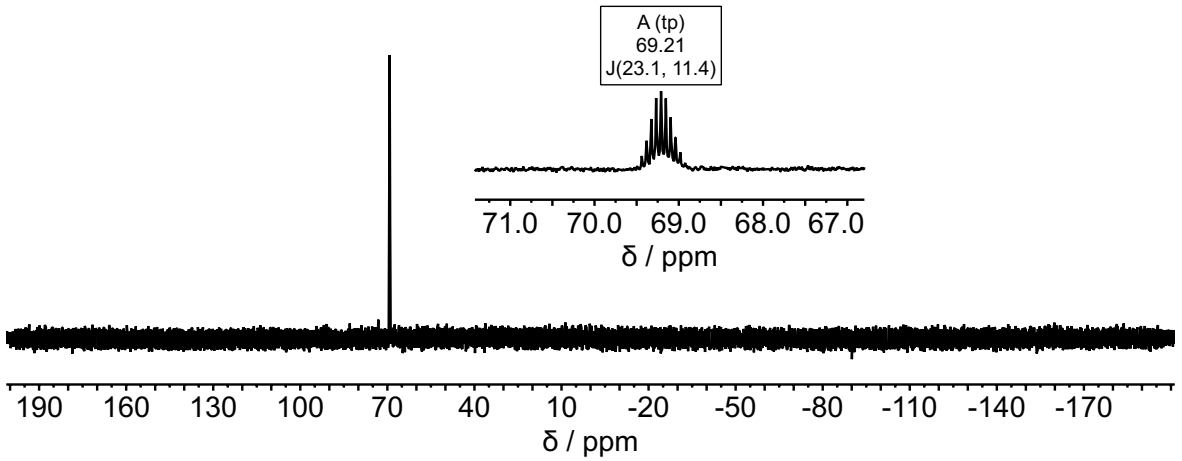


**Figure S9.** $^{31}P$ NMR spectrum of $Bis_2AlSP^tBu_2$ (**AlSP**) in $C_6D_6$ (202 MHz, 298K).

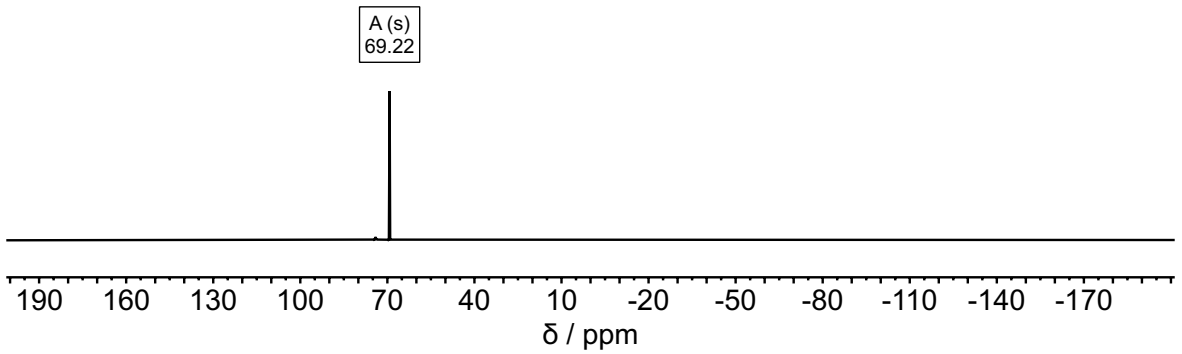


**Figure S10.** $^{31}P\{^{1}H\}$ NMR spectrum of $Bis_2AlSP^tBu_2$ (**AlSP**) in $C_6D_6$ (202 MHz, 298K).

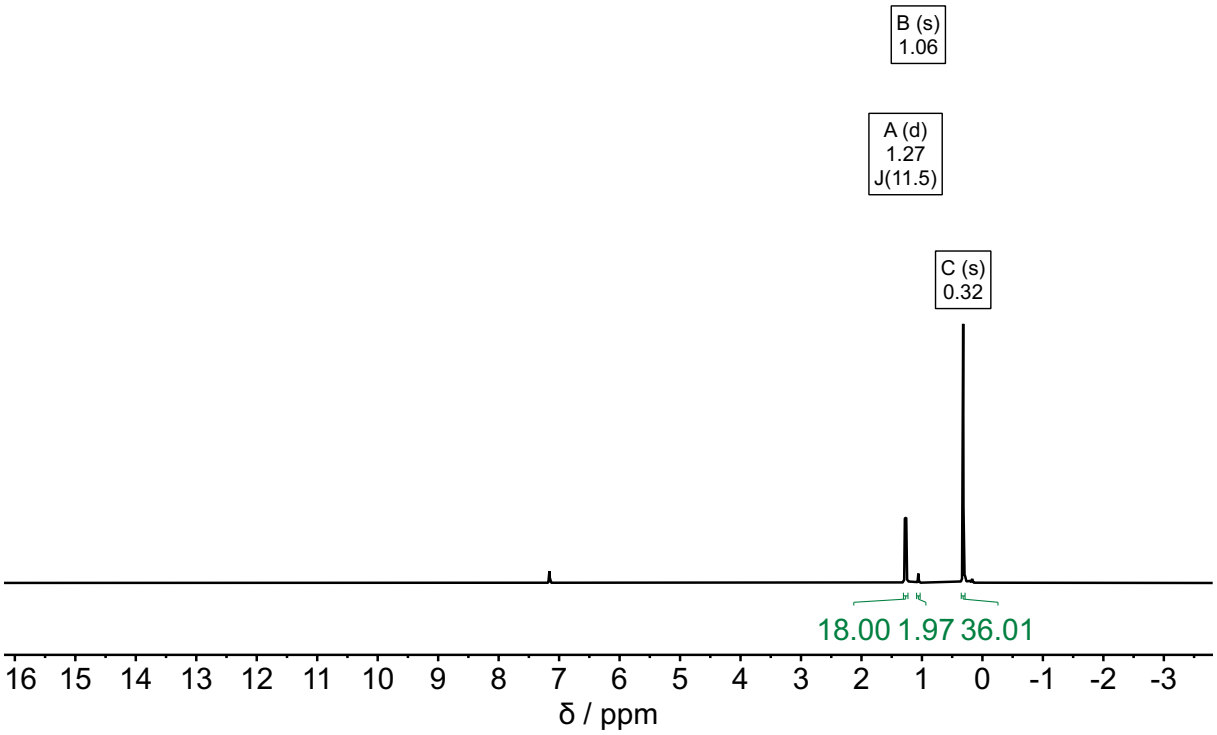


**Figure S11.** $^{1}H$ NMR spectrum of $Bis_2GaSP(^tBu)_2$ (**GaSP**) in $C_6D_6$ (500 MHz, 298K).

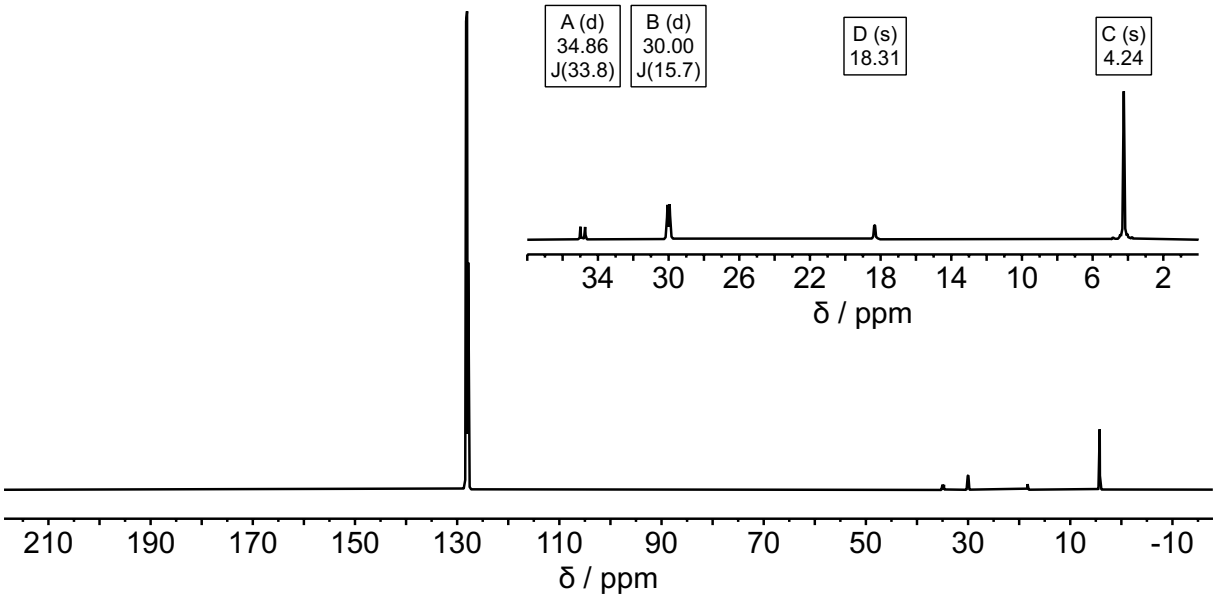


**Figure S12.** $^{13}C\{^{1}H\}$ NMR spectrum of $Bis_2GaSP(^tBu)_2$ (**GaSP**) in $C_6D_6$ (126 MHz, 298K).

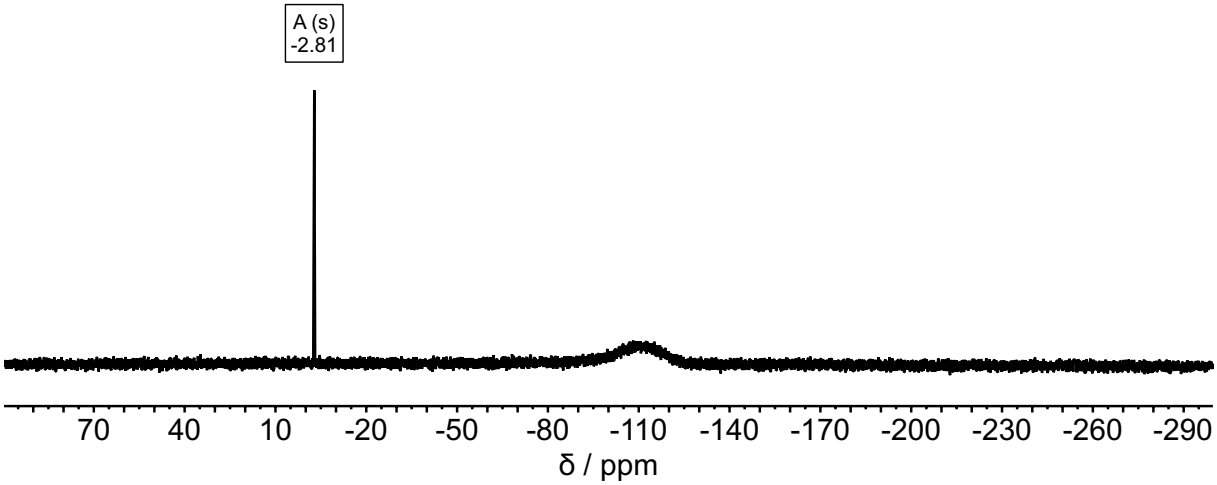


**Figure S13.** $^{29}Si\{^{1}H\}$ NMR spectrum of $Bis_2GaSP(^tBu)_2$ (**GaSP**) in $C_6D_6$ (99 MHz, 298K).

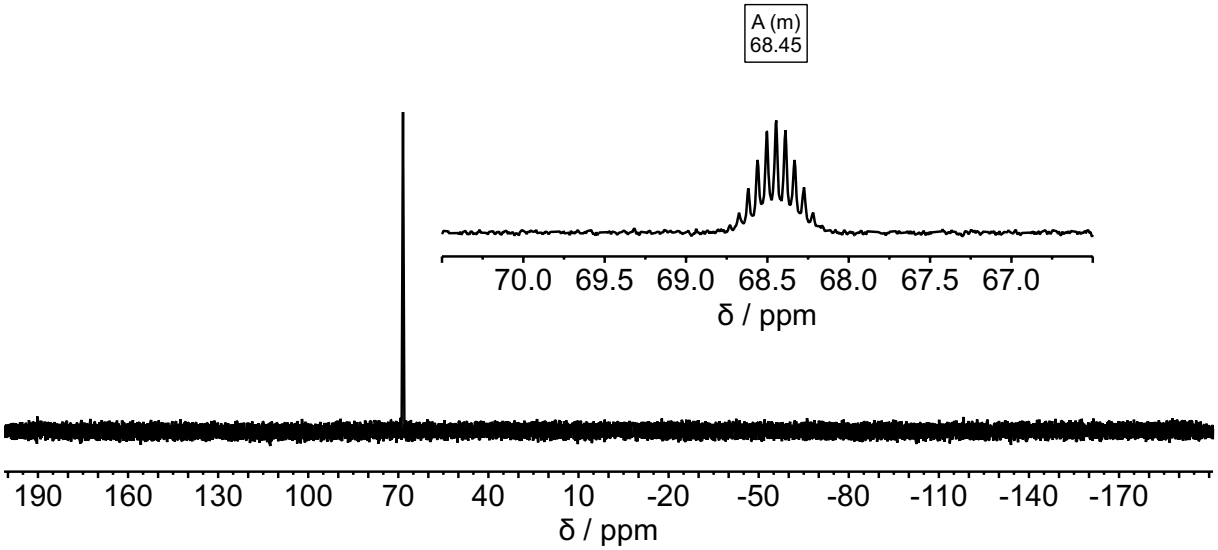


**Figure S14.** $^{31}P$ NMR spectrum of $Bis_2GaSP(^tBu)_2$ (**GaSP**) in $C_6D_6$ (202 MHz, 298K).

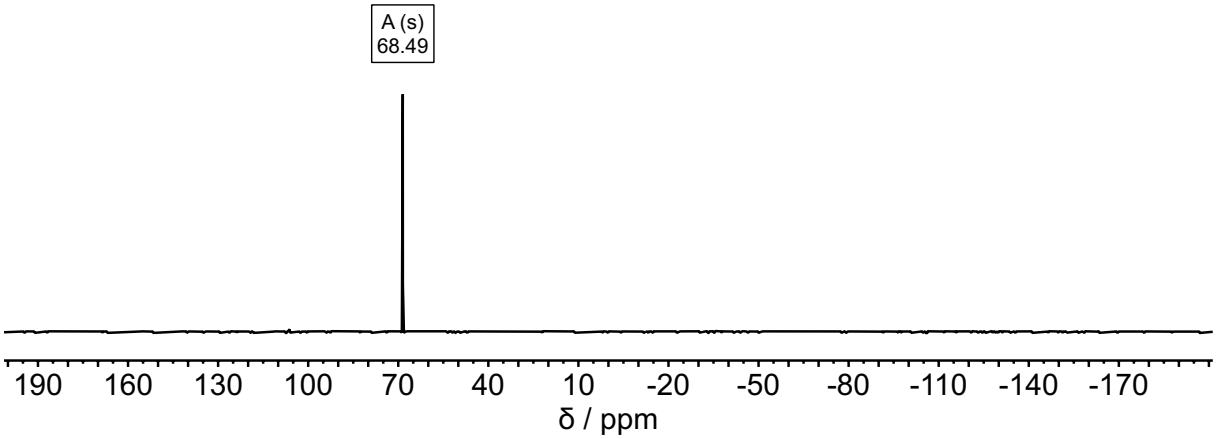


**Figure S15.** $^{31}P\{^{1}H\}$ NMR spectrum of $Bis_2GaSP(^tBu)_2$ (**GaSP**) in $C_6D_6$ (202 MHz, 298K).

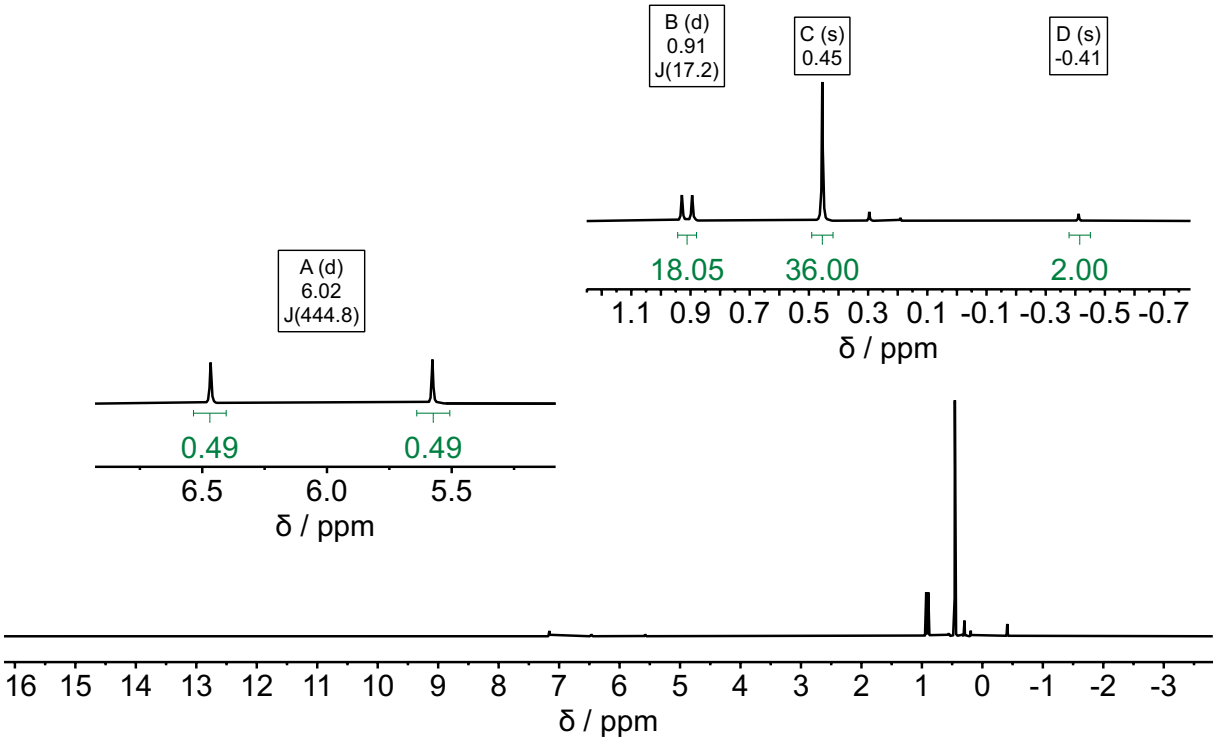


**Figure S16.** $^{1}H$ NMR spectrum of $Bis_2Al(Br)SP(H)^tBu_2$ (**AlSP**·HBr) in $C_6D_6$ (500 MHz, 298K).

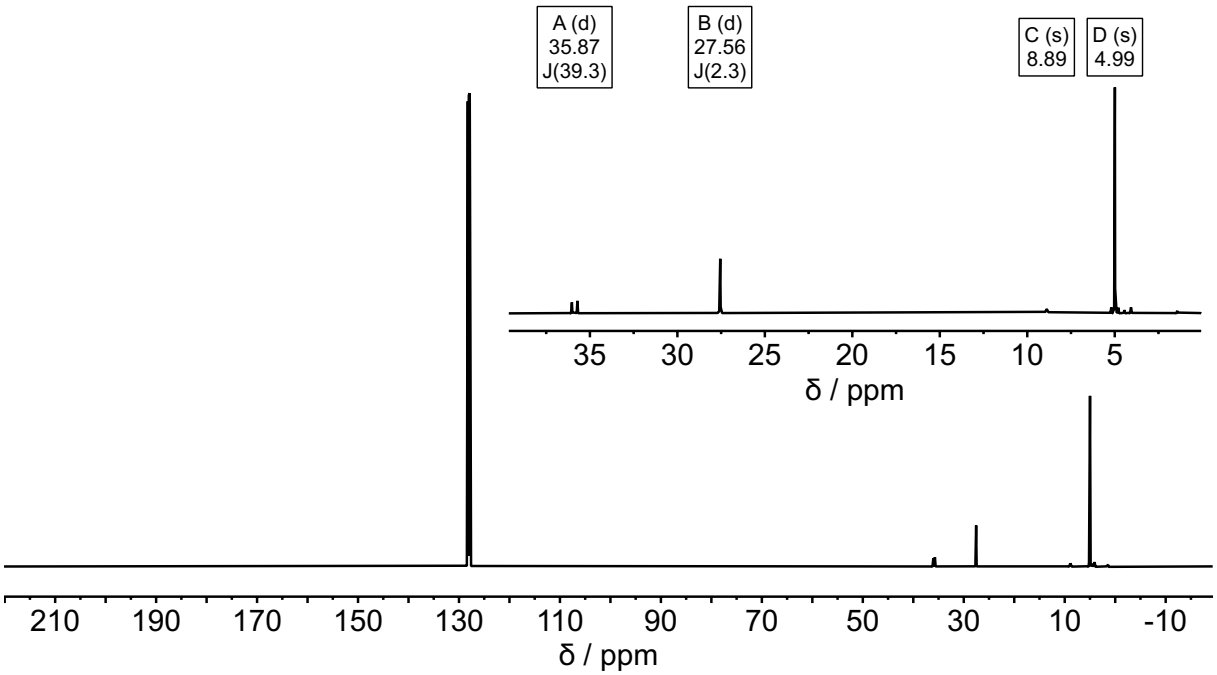


**Figure S17.** $^{13}C\{^{1}H\}$ NMR spectrum of $Bis_2Al(Br)SP(H)^tBu_2$ (**AlSP**·HBr) in $C_6D_6$ (126 MHz, 298K).

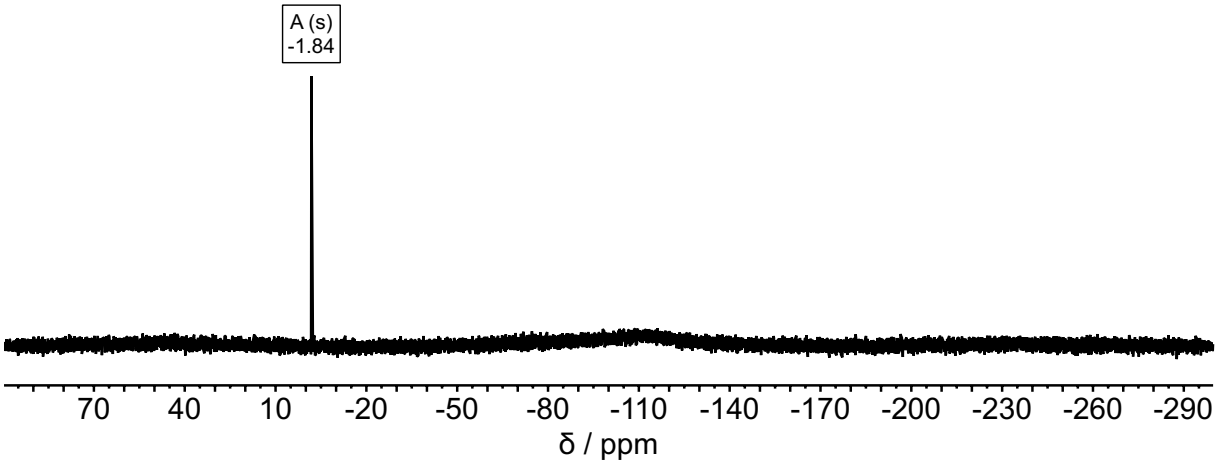


**Figure S18.** $^{29}Si\{^{1}H\}$ NMR spectrum of $Bis_2Al(Br)SP(H)^tBu_2$ (**AlSP**·HBr) in $C_6D_6$ (99 MHz, 298K).

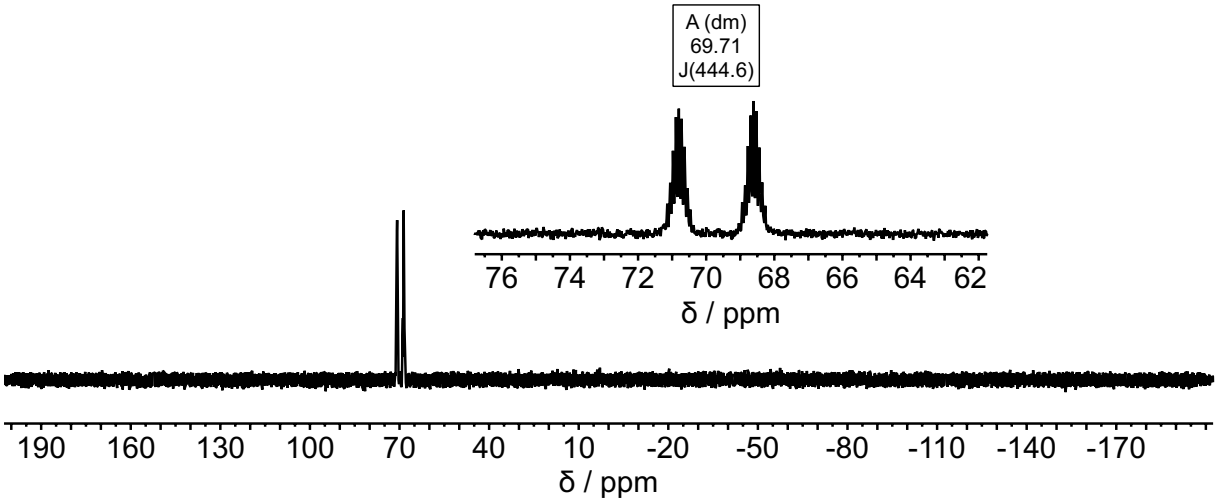


**Figure S19.** $^{31}P$ NMR spectrum of $Bis_2Al(Br)SP(H)^tBu_2$ (**AlSP**·HBr) in $C_6D_6$ (202 MHz, 298K).

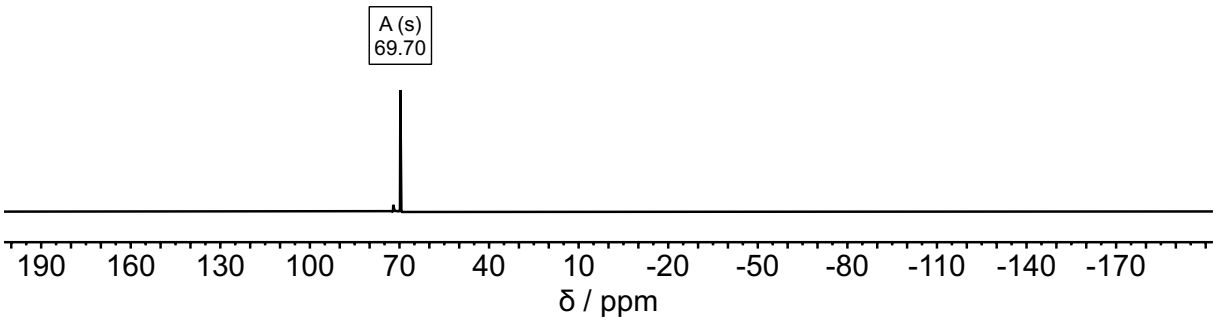


**Figure S20.** $^{31}P\{^{1}H\}$ NMR spectrum of $Bis_2Al(Br)SP(H)^tBu_2$ (**AlSP**·HBr) in $C_6D_6$ (202 MHz, 298K).

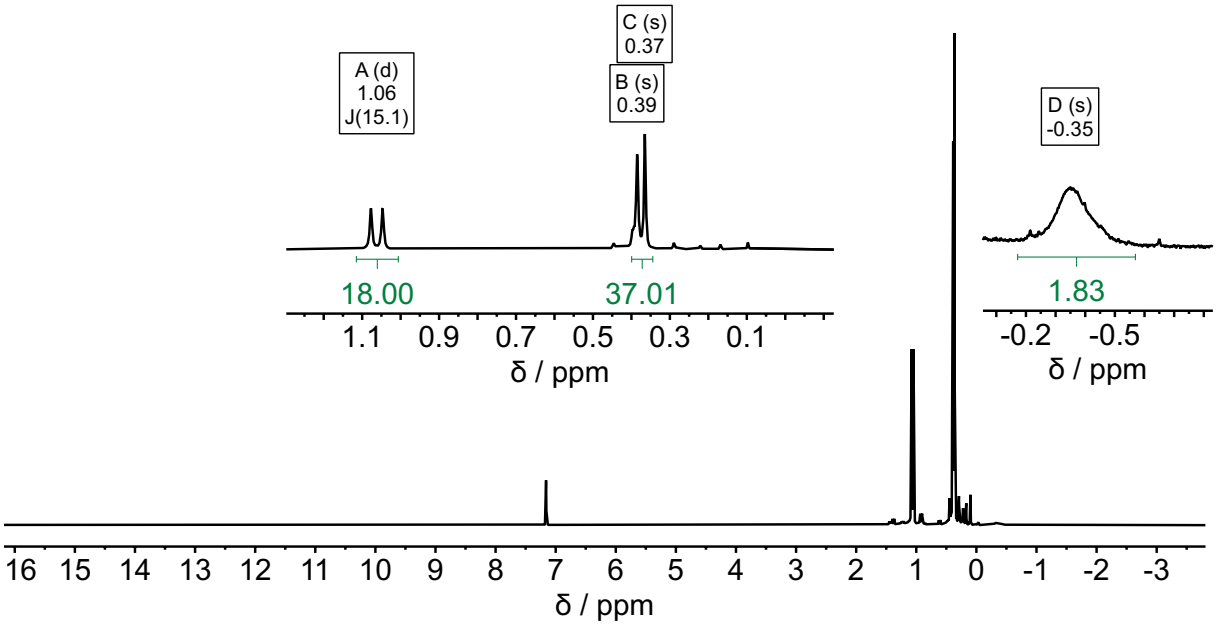


**Figure S21.** $^{1}H$ NMR spectrum of $Bis_2GaOP^tBu_2{\cdot}CO_2$ (**GaOP**·$CO_2$) in $C_6D_6$ (500 MHz, 298K).

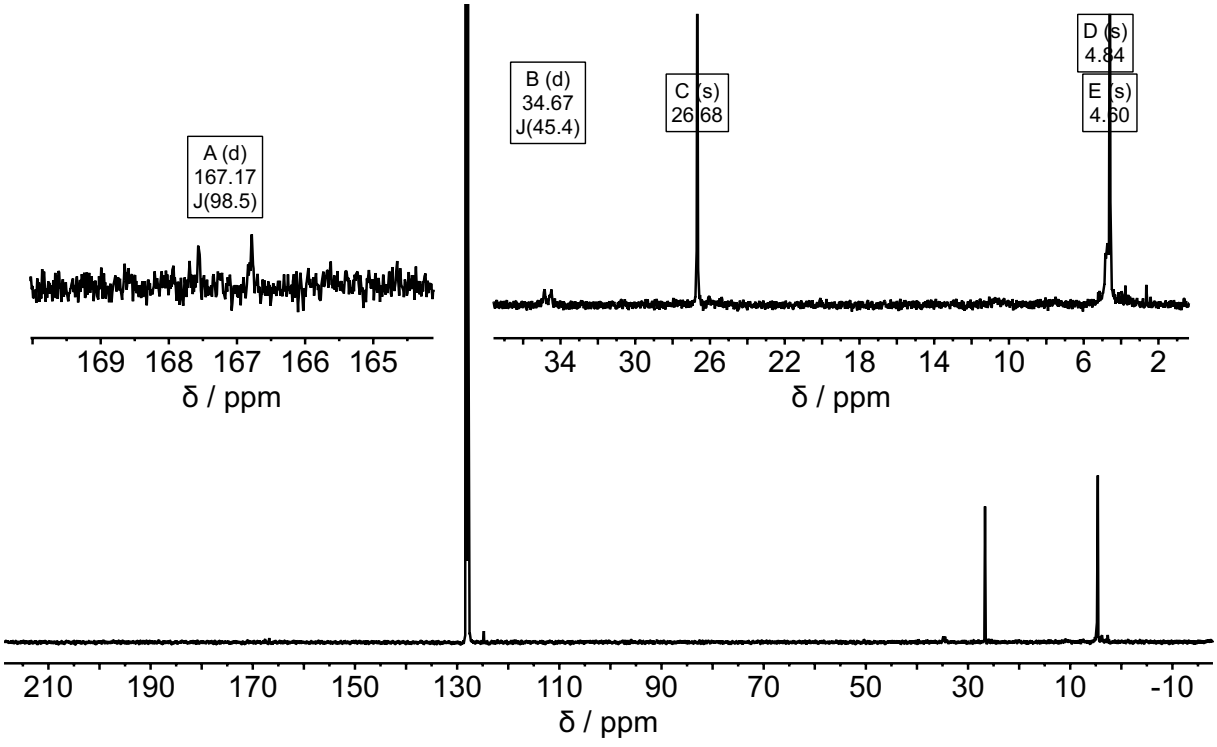


**Figure S22.** $^{13}C\{^{1}H\}$ NMR spectrum of $Bis_2GaOP^tBu_2{\cdot}CO_2$ (**GaOP**·$CO_2$) in $C_6D_6$ (126 MHz, 298K).

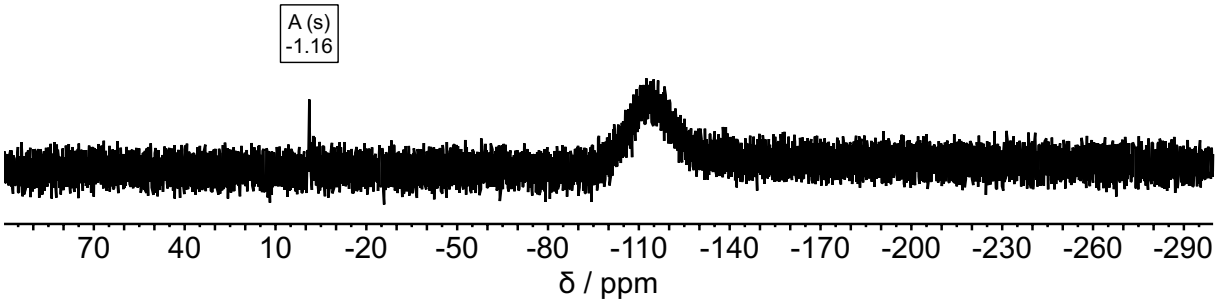


**Figure S23.** $^{29}Si\{^{1}H\}$ NMR spectrum of $Bis_2GaOP^tBu_2{\cdot}CO_2$ (**GaOP**·$CO_2$) in $C_6D_6$ (99 MHz, 298K).

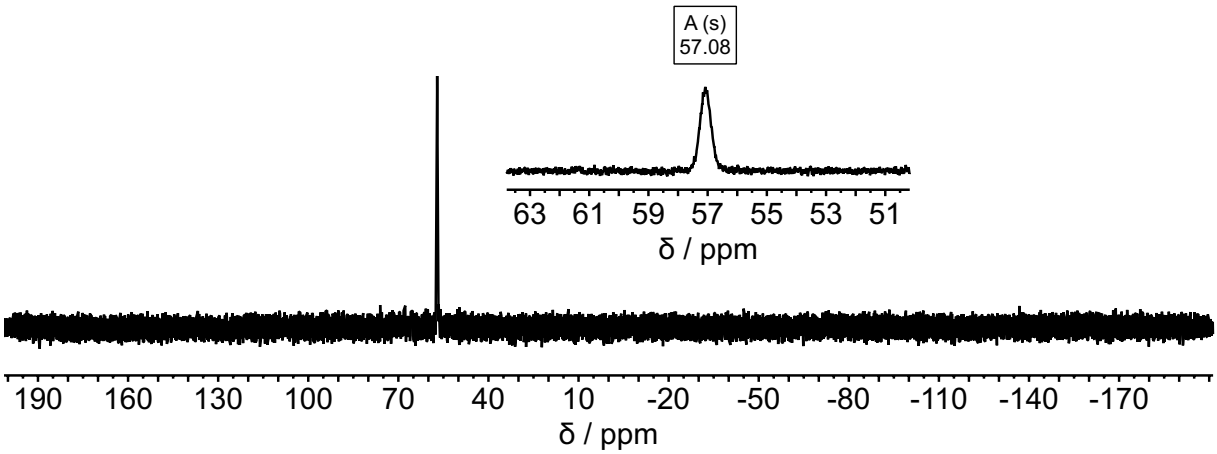


**Figure S24.** $^{31}P$ NMR spectrum of $Bis_2GaOP^tBu_2{\cdot}CO_2$ (**GaOP**·$CO_2$) in $C_6D_6$ (202 MHz, 298K).

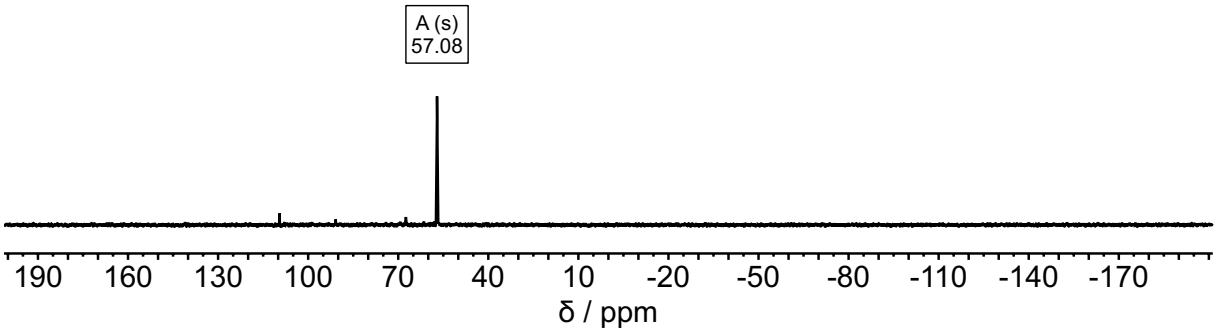


**Figure S25.** $^{31}P\{^{1}H\}$ NMR spectrum of $Bis_2GaOP^tBu_2{\cdot}CO_2$ (**GaOP**·$CO_2$) in $C_6D_6$ (202 MHz, 298K).

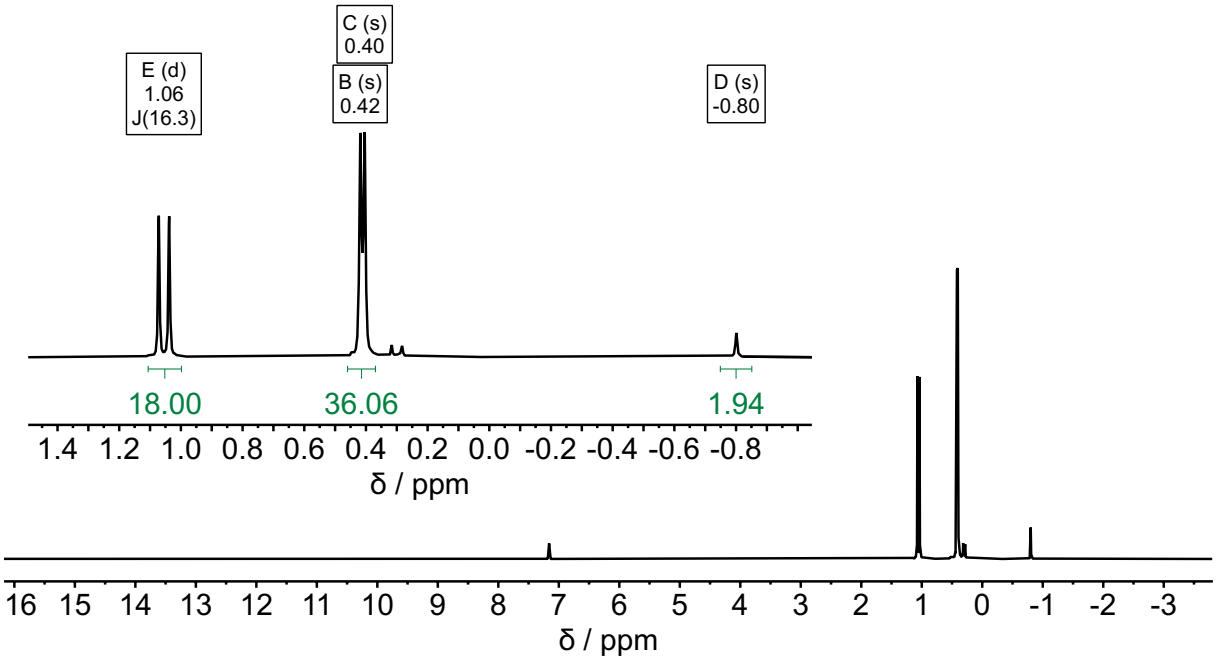


**Figure S26.** $^{1}H$ NMR spectrum of $Bis_2AlSP^tBu_2{\cdot}CO_2$ (**AlSP**·$CO_2$) in $C_6D_6$ (500 MHz, 298K).

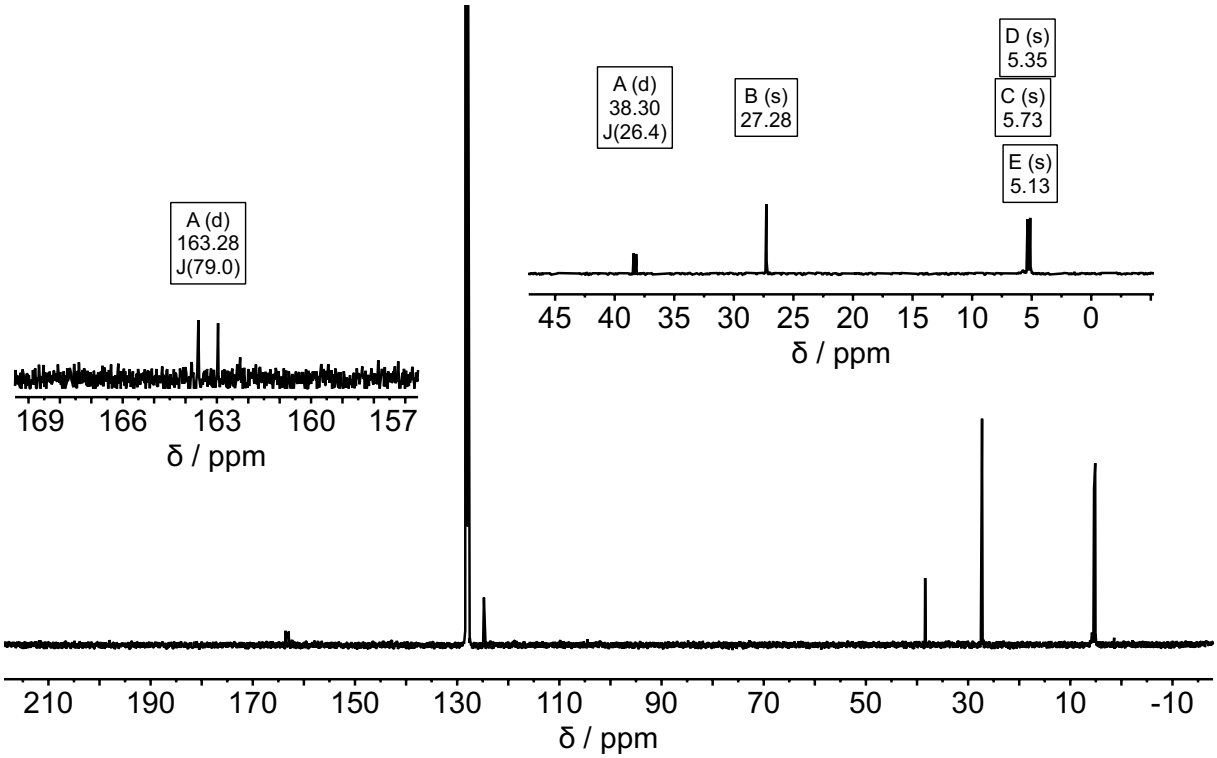


**Figure S27.** $^{13}C\{^{1}H\}$ NMR spectrum of $Bis_2AlSP^tBu_2{\cdot}CO_2$ (**AlSP**·$CO_2$) in $C_6D_6$ (126 MHz, 298K).

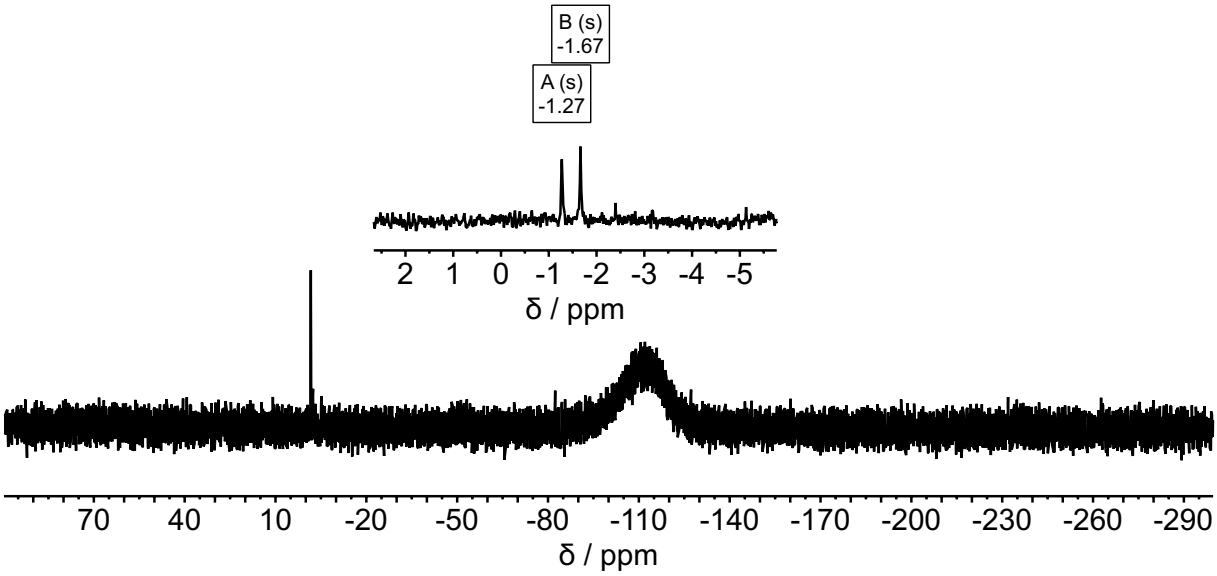


**Figure S28.** $^{29}Si\{^{1}H\}$ NMR spectrum of $Bis_2AlSP^tBu_2{\cdot}CO_2$ (**AlSP**·$CO_2$) in $C_6D_6$ (99 MHz, 298K).

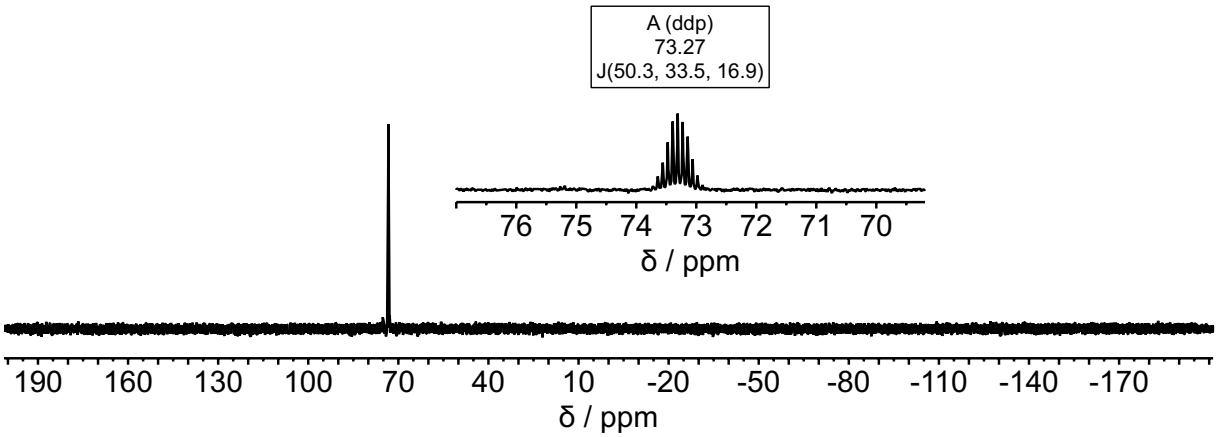


**Figure S29.** $^{31}P$ NMR spectrum of $Bis_2AlSP^tBu_2{\cdot}CO_2$ (**AlSP**·$CO_2$) in $C_6D_6$ (202 MHz, 298K).

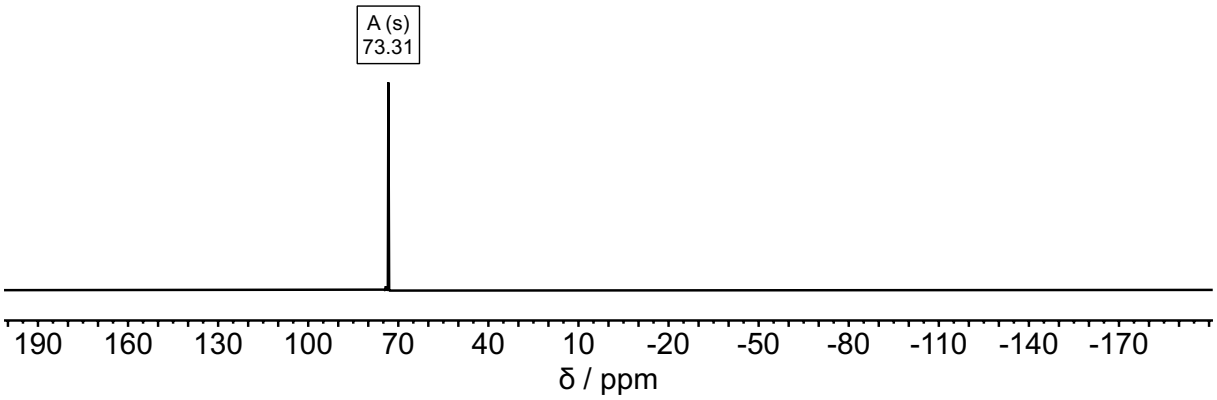


**Figure S30.** $^{31}P\{^{1}H\}$ NMR spectrum of $Bis_2AlSP^tBu_2{\cdot}CO_2$ (**AlSP**·$CO_2$) in $C_6D_6$ (202 MHz, 298K).

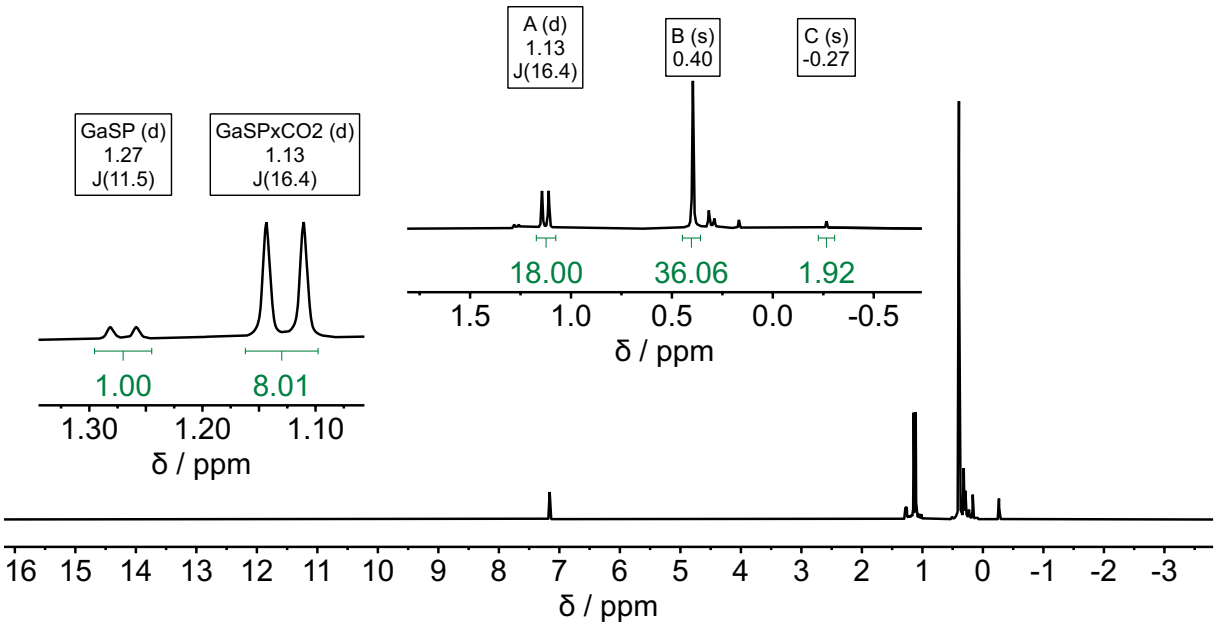


**Figure S31.** $^{1}H$ NMR spectrum of $Bis_2GaSP^tBu_2{\cdot}CO_2$ (**GaSP**·$CO_2$) in $C_6D_6$ (500 MHz, 298K).

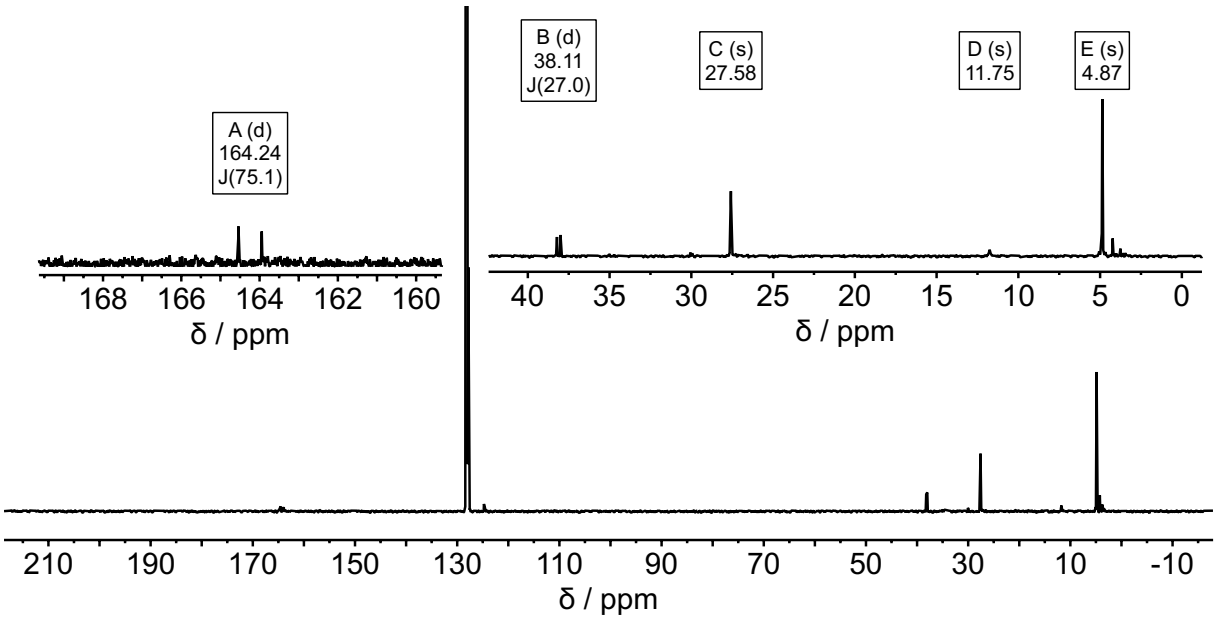


**Figure S32.** $^{13}C\{^{1}H\}$ NMR spectrum of $Bis_2GaSP^tBu_2{\cdot}CO_2$ (**GaSP**·$CO_2$) in $C_6D_6$ (126 MHz, 298K).

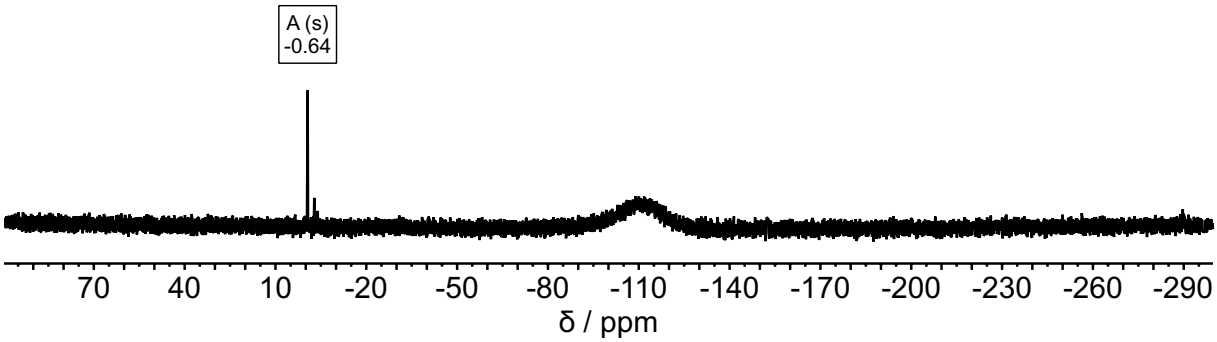


**Figure S33.** $^{29}Si\{^{1}H\}$ NMR spectrum of $Bis_2GaSP^tBu_2{\cdot}CO_2$ (**GaSP**·$CO_2$) in $C_6D_6$ (99 MHz, 298K).

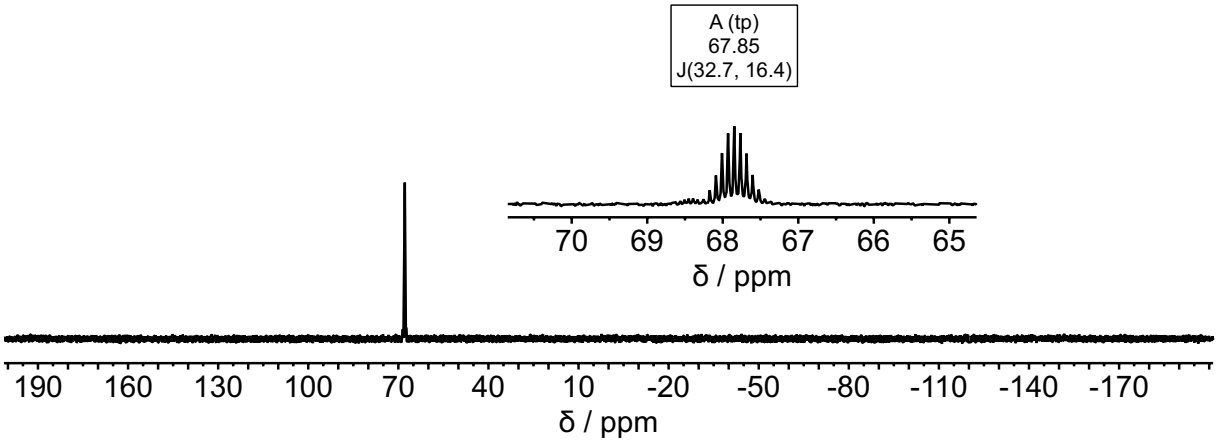


**Figure S34.** $^{31}P$ NMR spectrum of $Bis_2GaSP^tBu_2{\cdot}CO_2$ (**GaSP**·$CO_2$) in $C_6D_6$ (202 MHz, 298K).

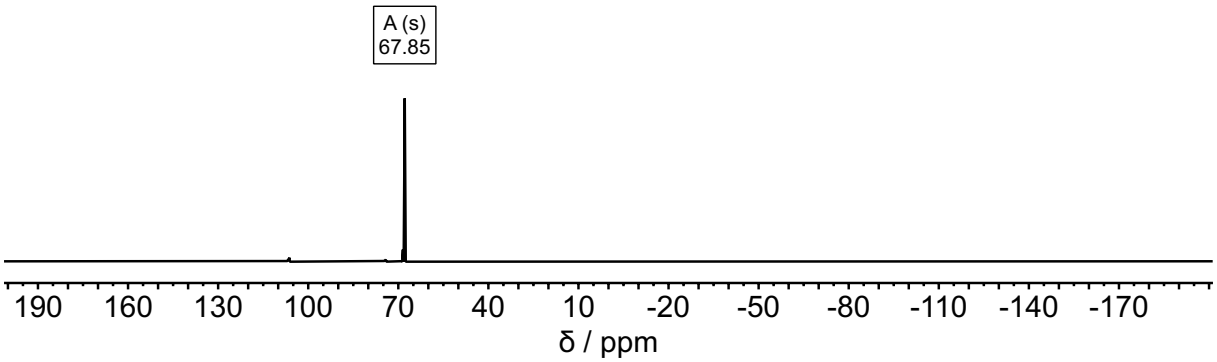


**Figure S35.** $^{31}P\{^1H\}$ NMR spectrum of $Bis_2GaSP^tBu_2{\cdot}CO_2$ (**GaSP**·$CO_2$) in $C_6D_6$ (202 MHz, 298K).

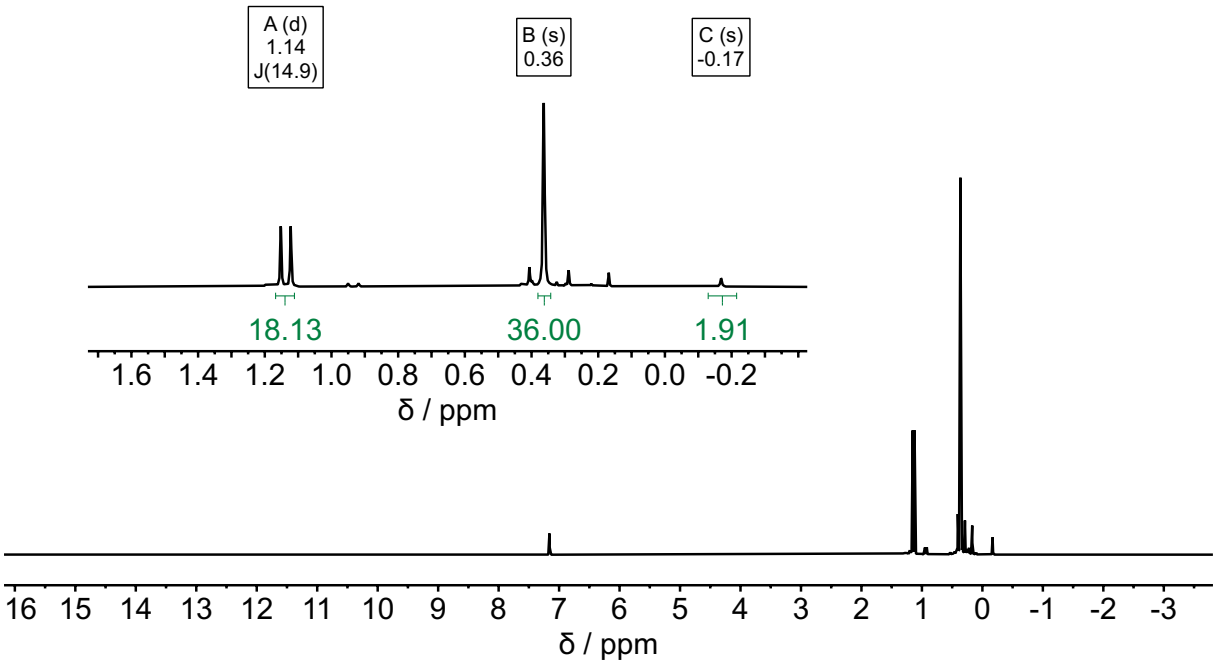


**Figure S36.** $^1H$ NMR spectrum of $Bis_2GaOP^tBu_2{\cdot}CS_2$ (**GaOP**·$CS_2$) in $C_6D_6$ (500 MHz, 298K).

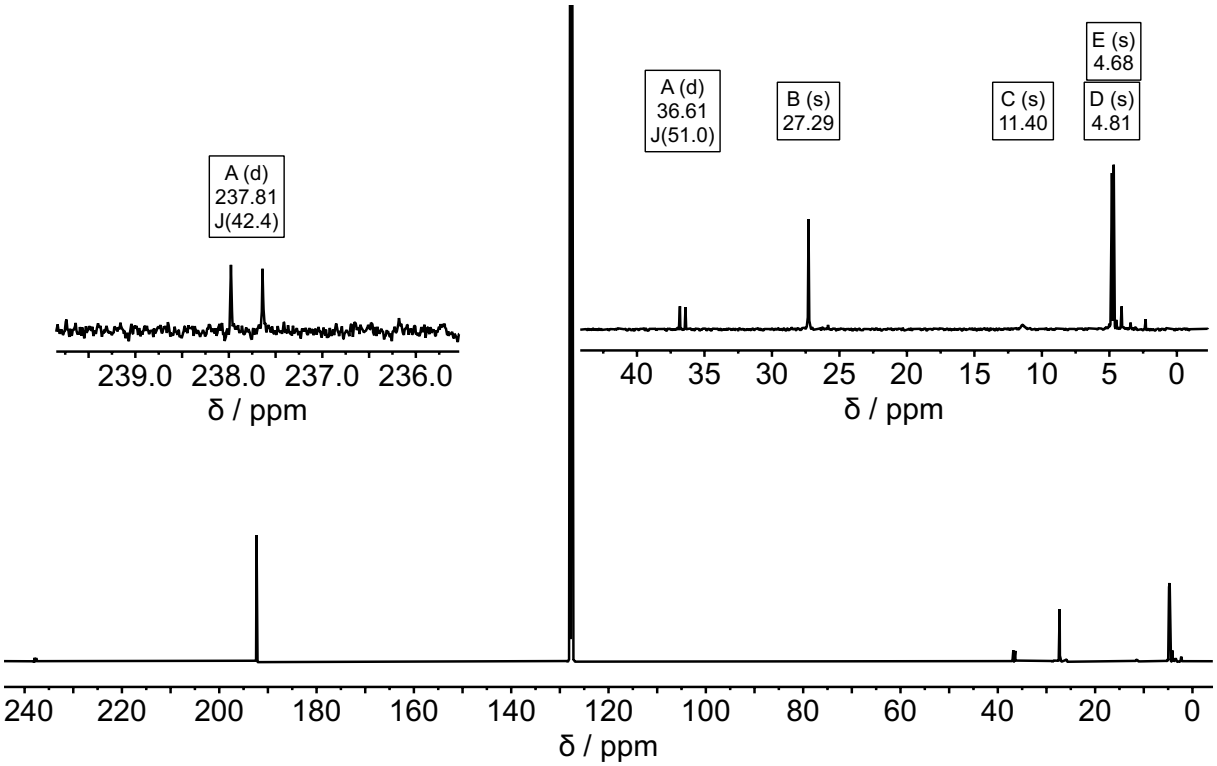


**Figure S37.** $^{13}C\{^{1}H\}$ NMR spectrum of $Bis_2GaOP^tBu_2{\cdot}CS_2$ (**GaOP**·$CS_2$) in $C_6D_6$ (126 MHz, 298K).

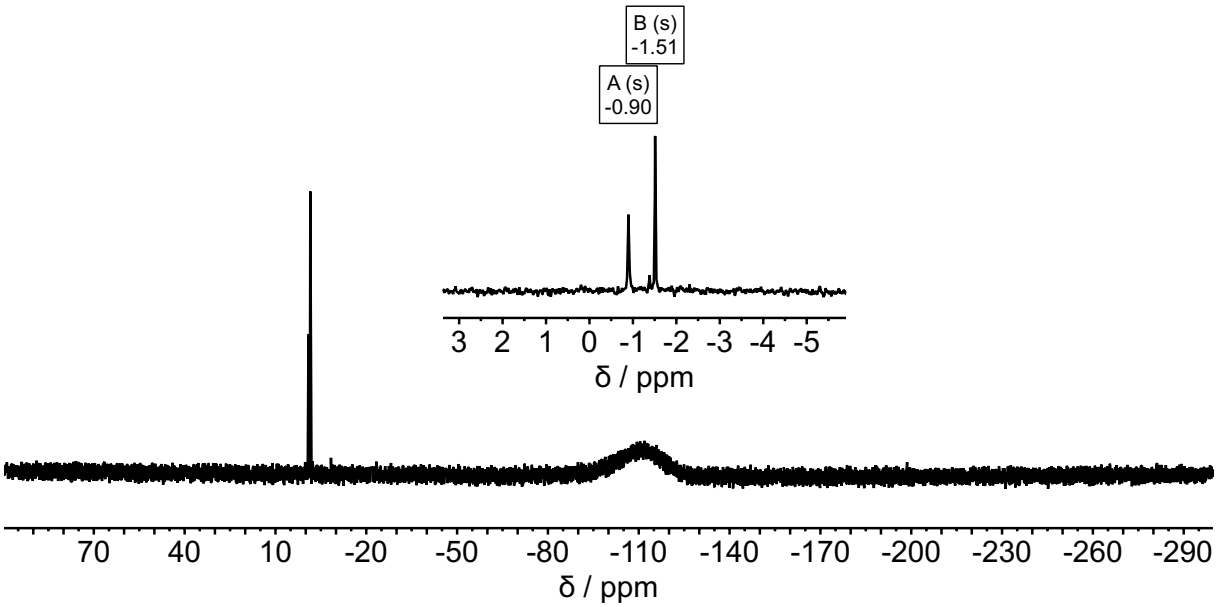


**Figure S38.** $^{29}Si\{^{1}H\}$ NMR spectrum of $Bis_2GaOP^tBu_2{\cdot}CS_2$ (**GaOP**·$CS_2$) in $C_6D_6$ (99 MHz, 298K).

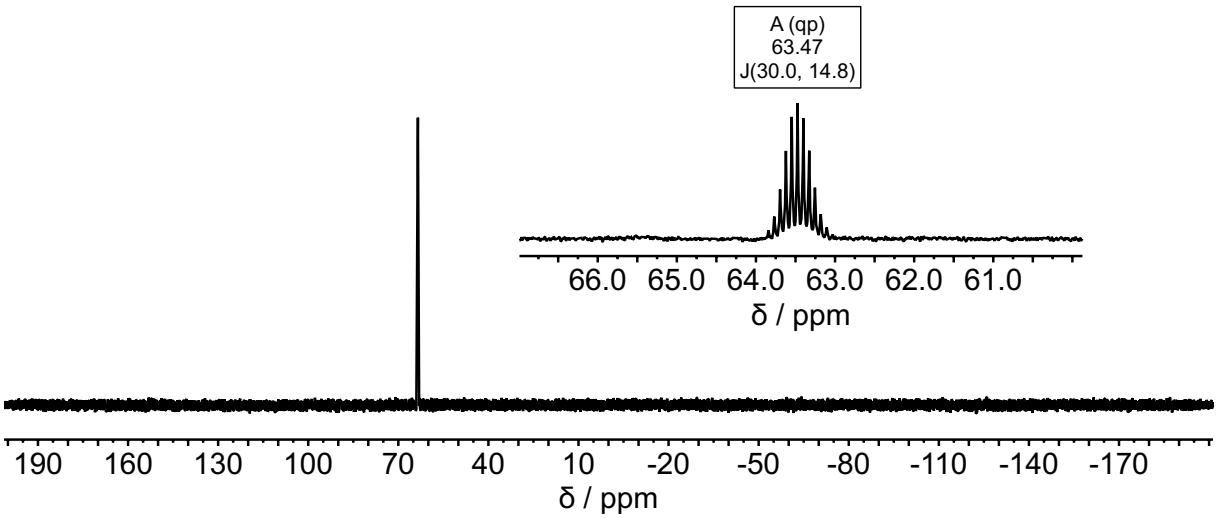


**Figure S39.** $^{31}P$ NMR spectrum of $Bis_2GaOP^tBu_2{\cdot}CS_2$ (**GaOP**·$CS_2$) in $C_6D_6$ (202 MHz, 298K).

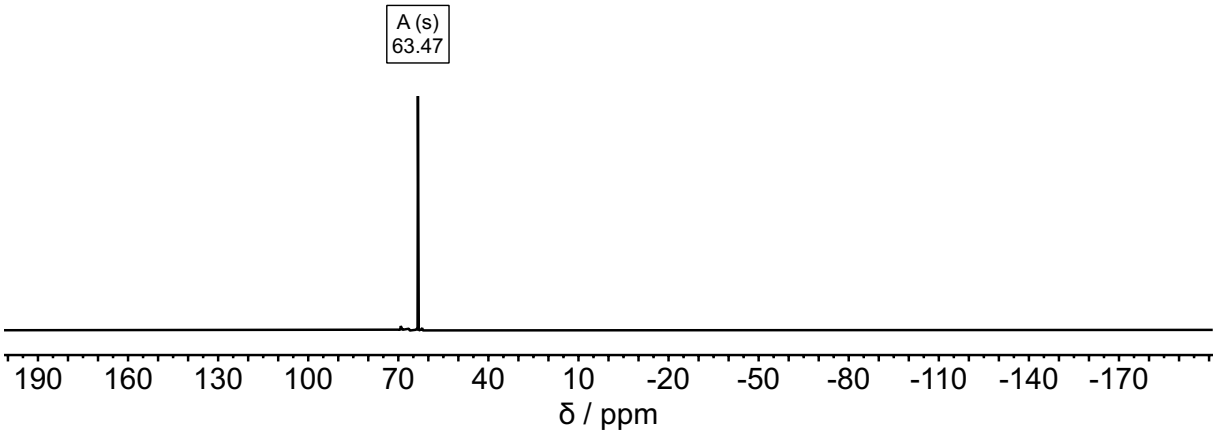


**Figure S40.** $^{31}P\{^1H\}$ NMR spectrum of $Bis_2GaOP^tBu_2{\cdot}CS_2$ (**GaOP**·$CS_2$) in $C_6D_6$ (202 MHz, 298K).

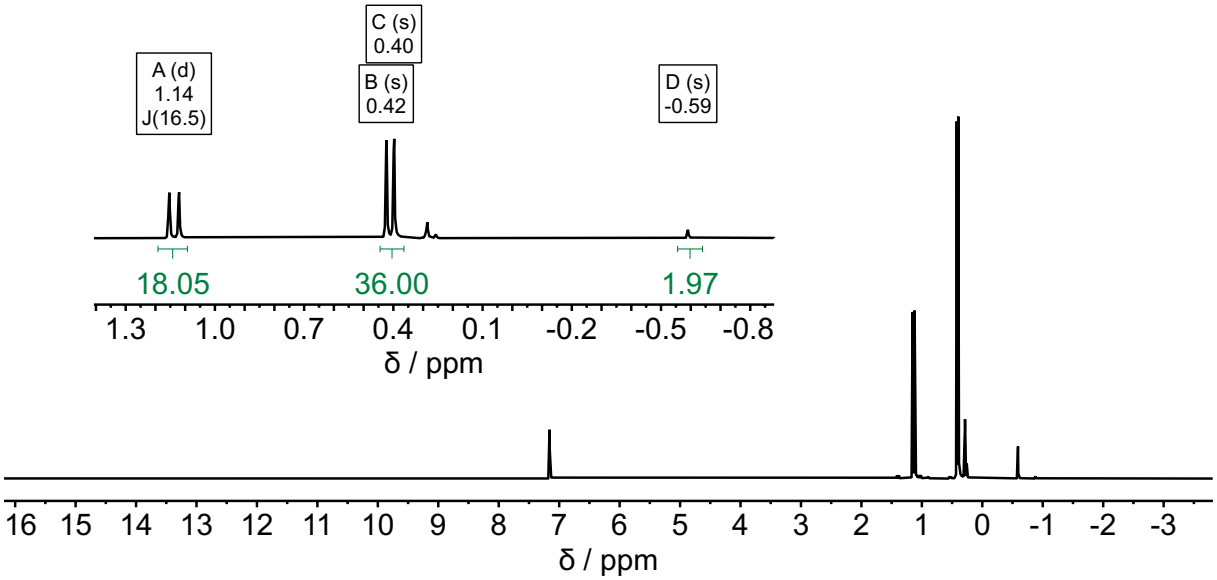


**Figure S41.** $^1H$ NMR spectrum of $Bis_2AlSP^tBu_2{\cdot}CS_2$ (**AlSP**·$CS_2$) in $C_6D_6$ (500 MHz, 298K).

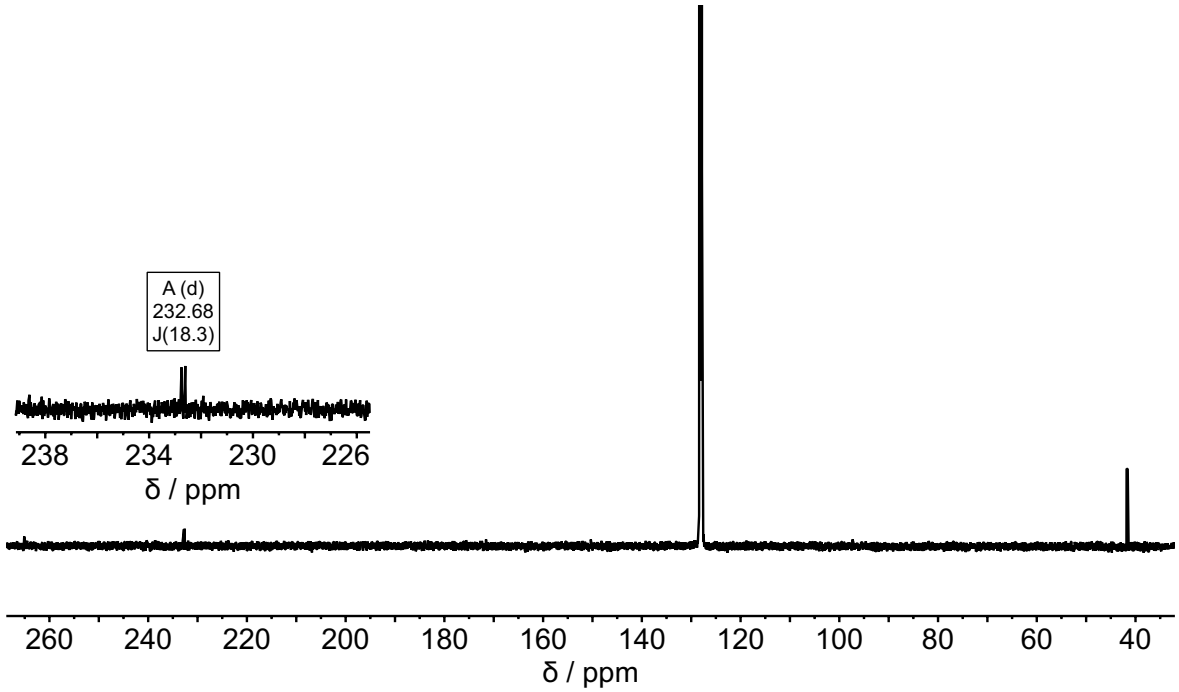


**Figure S42.** Excerpt of $^{13}C\{^{1}H\}$ NMR spectrum of $Bis_2AlSP^tBu_2{\cdot}CS_2$ (**AlSP**·$CS_2$) in $C_6D_6$ (126 MHz, 298K) in the range between 270 – 30 ppm.

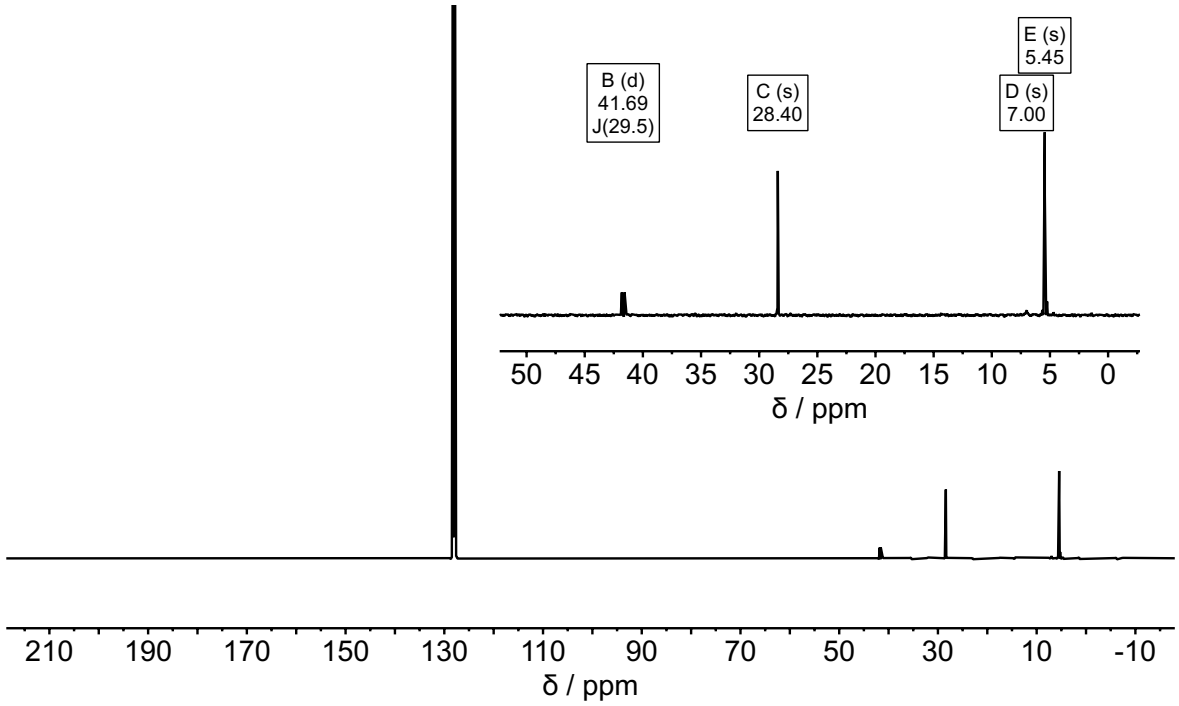


**Figure S43.** Excerpt of $^{13}C\{^{1}H\}$ NMR spectrum of $Bis_2AlSP^tBu_2{\cdot}CS_2$ (**AlSP**·$CS_2$) in $C_6D_6$ (126 MHz, 298K) in the range between 220 – −20 ppm.

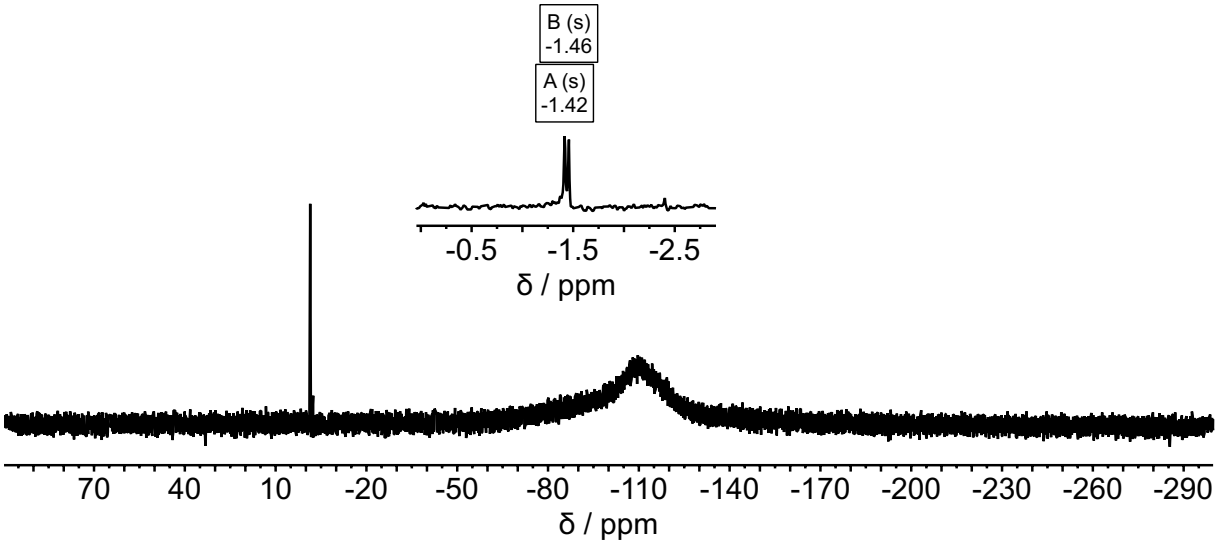


**Figure S44.** $^{29}Si\{^{1}H\}$ NMR spectrum of $Bis_2AlSP^tBu_2{\cdot}CS_2$ (**AlSP**·$CS_2$) in $C_6D_6$ (99 MHz, 298K).

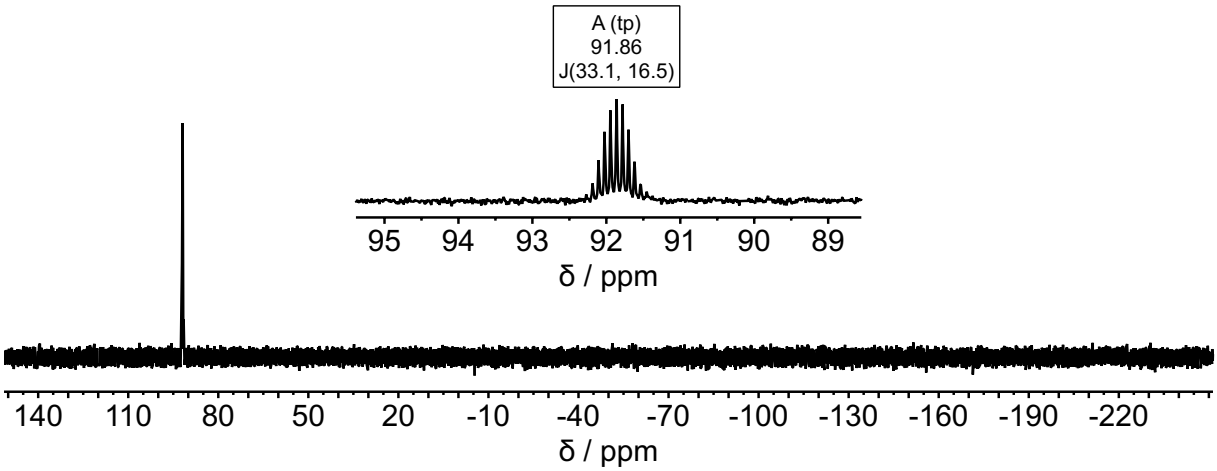


**Figure S45.** $^{31}P$ NMR spectrum of $Bis_2AlSP^tBu_2{\cdot}CS_2$ (**AlSP**·$CS_2$) in $C_6D_6$ (202 MHz, 298K).

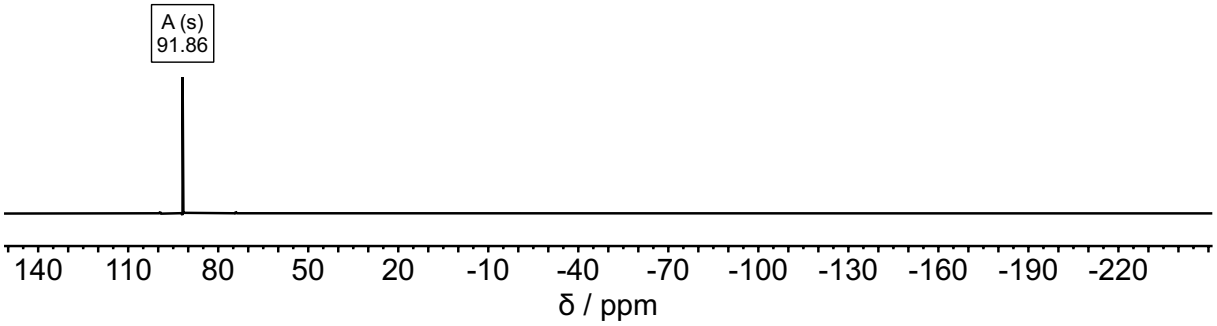


**Figure S46.** $^{31}P\{^{1}H\}$ NMR spectrum of $Bis_2AlSP^tBu_2{\cdot}CS_2$ (**AlSP**·$CS_2$) in $C_6D_6$ (202 MHz, 298K).

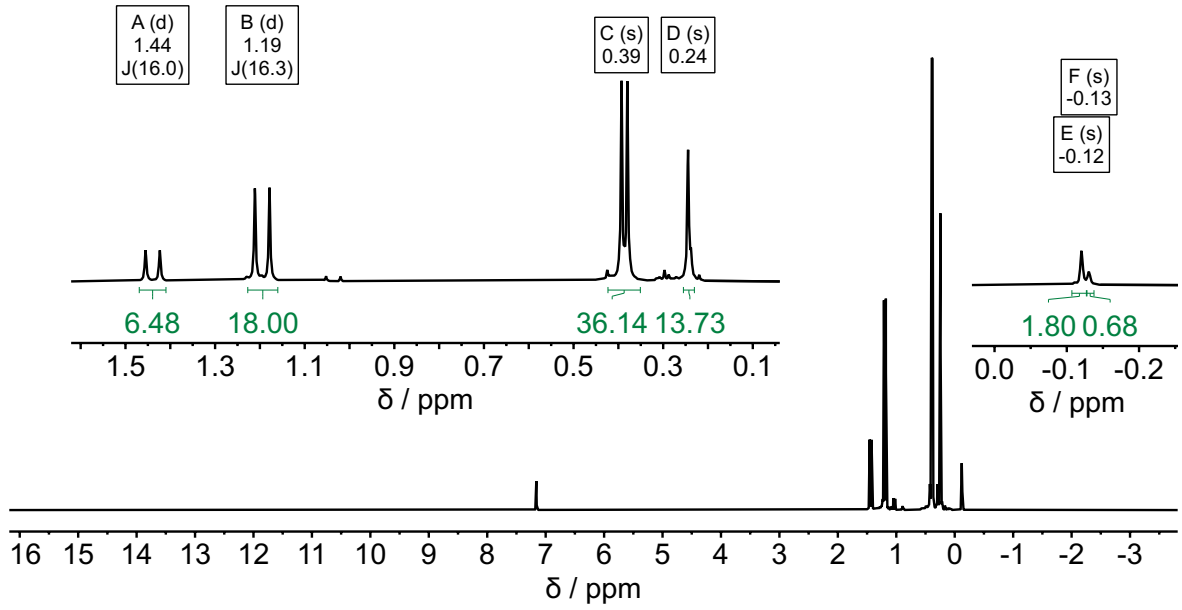


**Figure S47.** $^{1}$H NMR spectrum of $Bis_2GaSP^tBu_2{\cdot}CS_2$ (**GaSP**·$CS_2$) mixture in $C_6D_6$ (500 MHz, 298K).

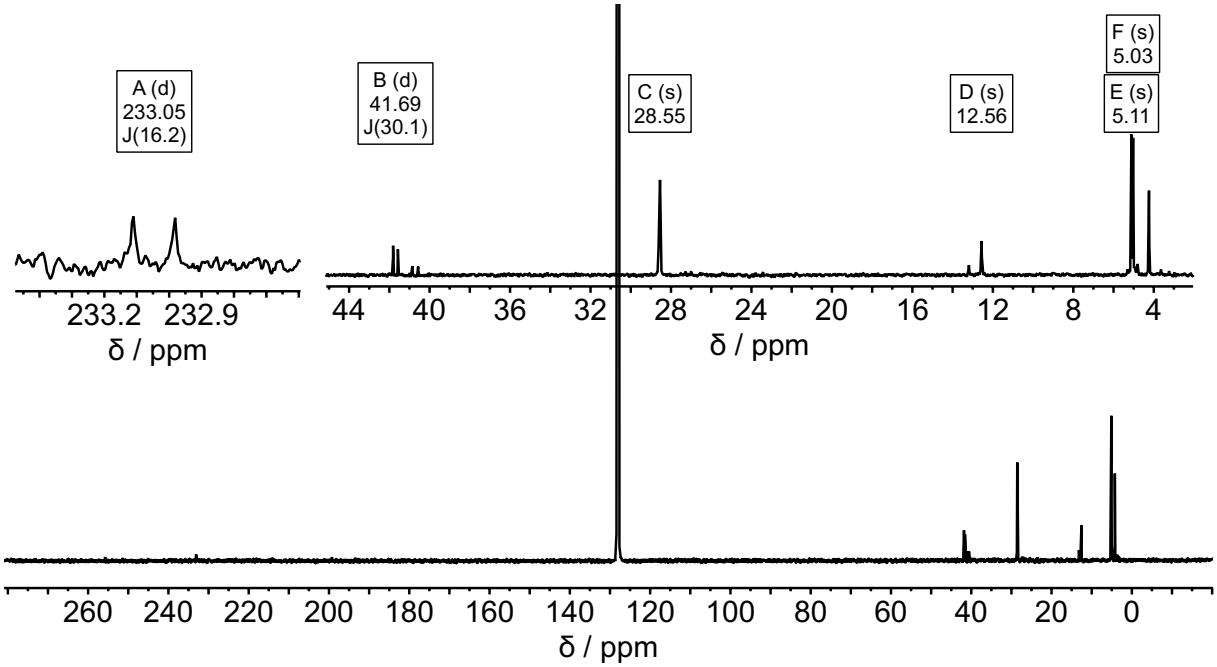


**Figure S48.** $^{13}C\{^{1}H\}$ NMR spectrum of $Bis_2GaSP^tBu_2{\cdot}CS_2$ (**GaSP**·$CS_2$) mixture in $C_6D_6$ (126 MHz, 298K). Only the signals for the 'classical' adduct with Ga–S–C–P connectivity are shown.

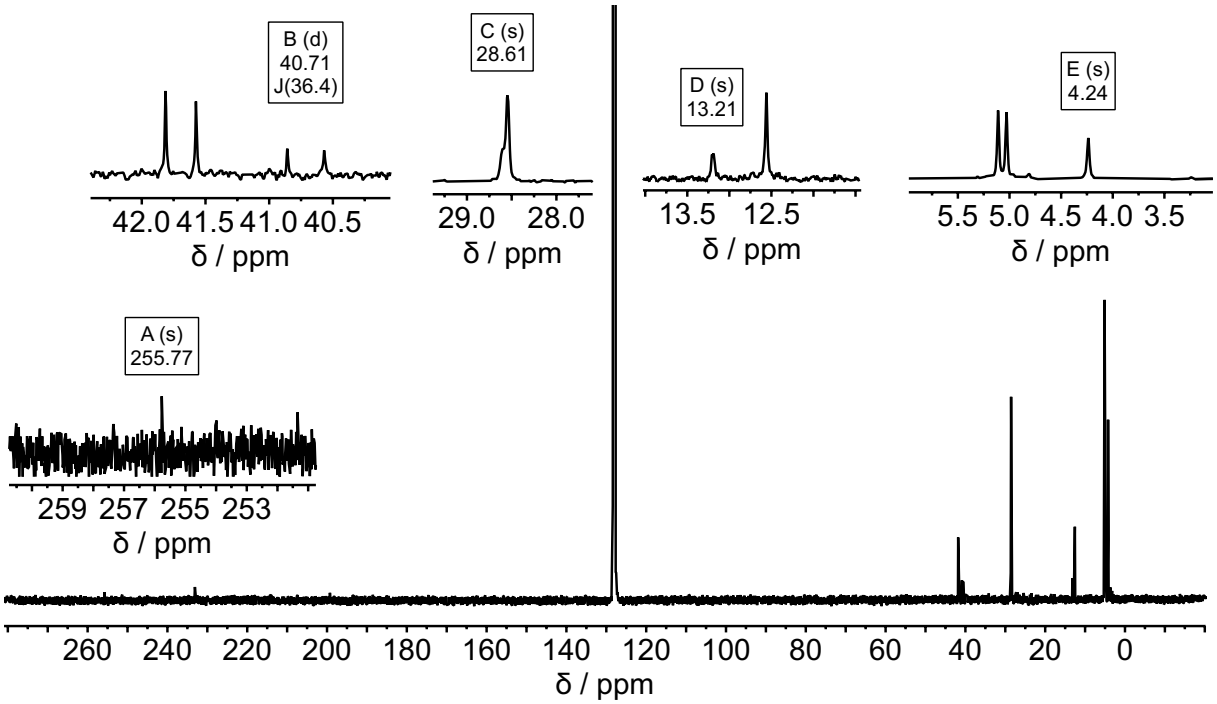


**Figure S49.** $^{13}C\{^{1}H\}$ NMR spectrum of $Bis_2GaSP^tBu_2{\cdot}CS_2$ (**GaSP**·$CS_2$) mixture in $C_6D_6$ (126 MHz, 298K). Only the signals for the 'inverted' adduct with Ga–C–S–P connectivity are shown.

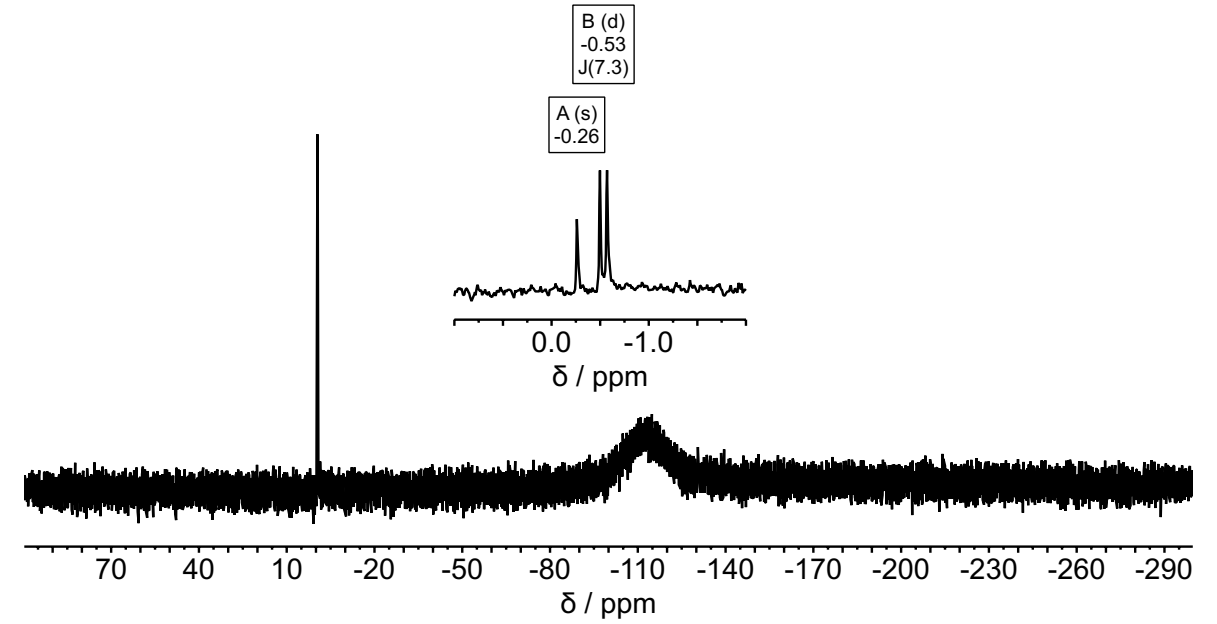


**Figure S50.** $^{29}Si\{^{1}H\}$ NMR spectrum of $Bis_2GaSP^tBu_2{\cdot}CS_2$ (**GaSP**·$CS_2$) mixture in $C_6D_6$ (99 MHz, 298K).

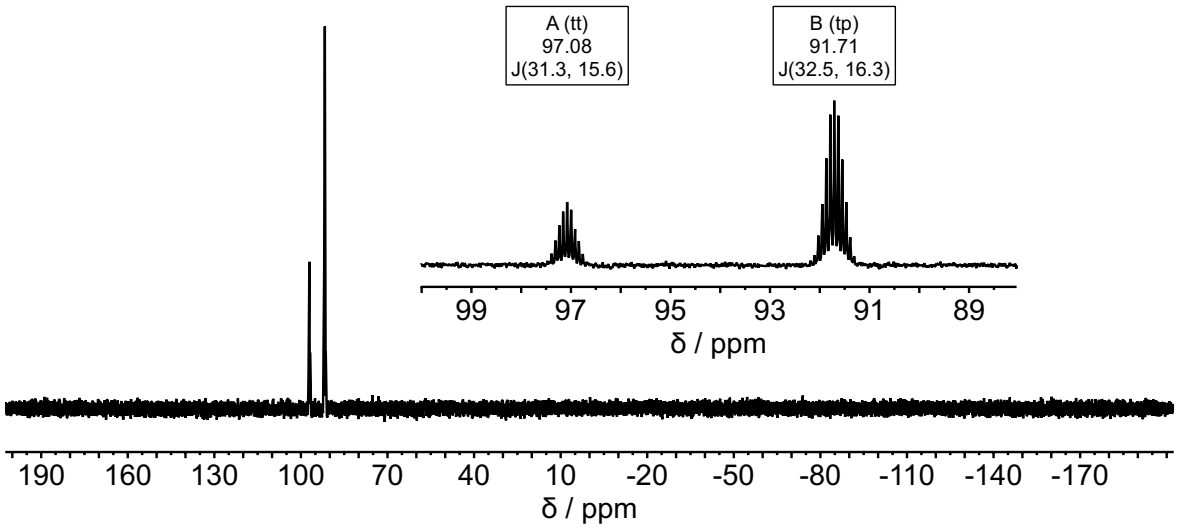


**Figure S51.** $^{31}P$ NMR spectrum of $Bis_2GaSP^tBu_2{\cdot}CS_2$ (**GaSP**$\cdot CS_2$) mixture in $C_6D_6$ (202 MHz, 298K).

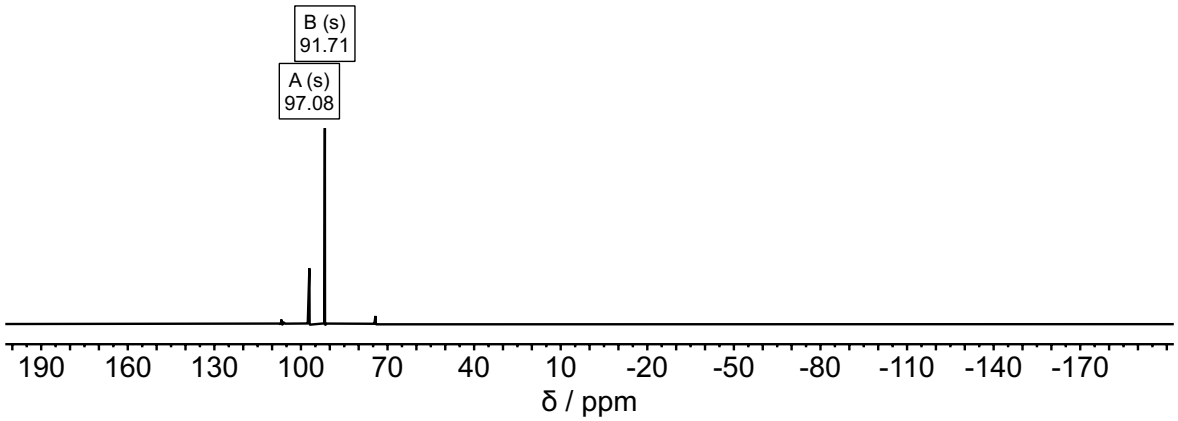


**Figure S52.** $^{31}P\{^1H\}$ NMR spectrum of $Bis_2GaSP^tBu_2{\cdot}CS_2$ (**GaSP**$\cdot CS_2$) mixture in $C_6D_6$ (202 MHz, 298K).

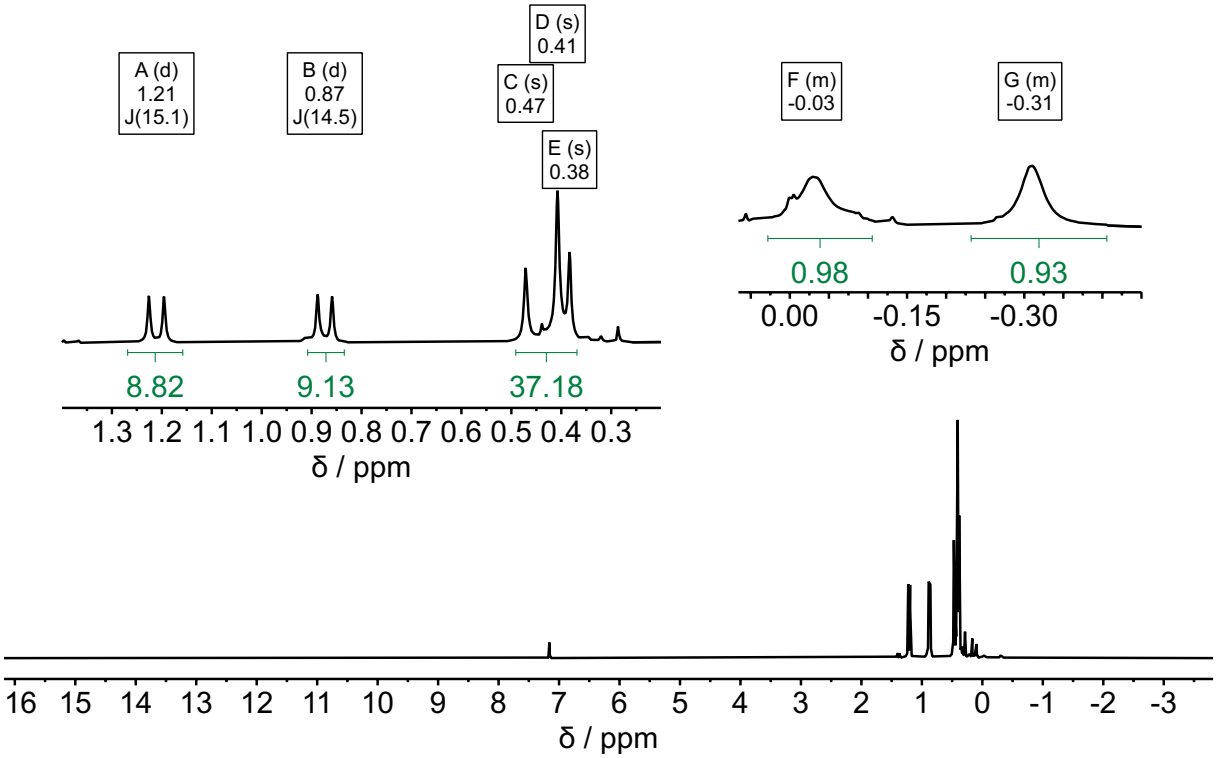


**Figure S53.** $^{1}$H NMR spectrum of $Bis_2GaOP^tBu_2{\cdot}SO_2$ (**GaOP**·$SO_2$) in $C_6D_6$ (500 MHz, 298K).

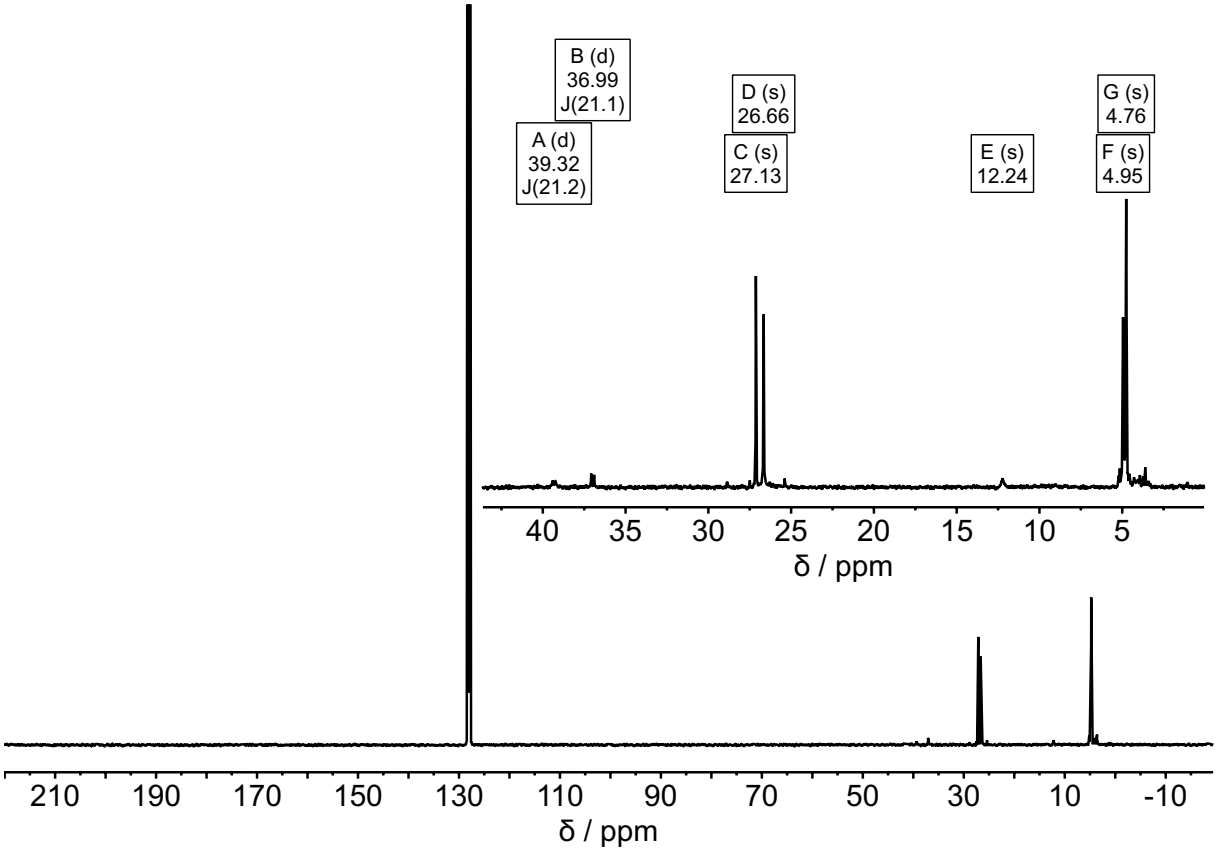


**Figure S54.** $^{13}C\{^{1}H\}$ NMR spectrum of $Bis_2GaOP^tBu_2{\cdot}SO_2$ (**GaOP**·$SO_2$) in $C_6D_6$ (126 MHz, 298K).

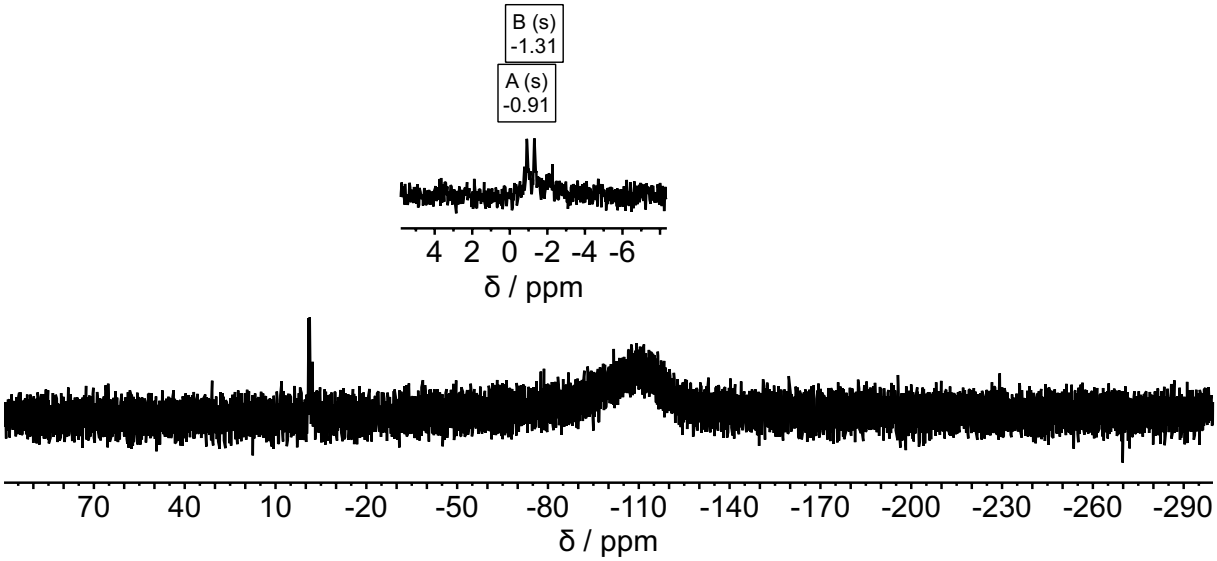


**Figure S55.** $^{29}Si\{^{1}H\}$ NMR spectrum of $Bis_2GaOP^tBu_2{\cdot}SO_2$ (**GaOP**$\cdot SO_2$) in $C_6D_6$ (99 MHz, 298K).

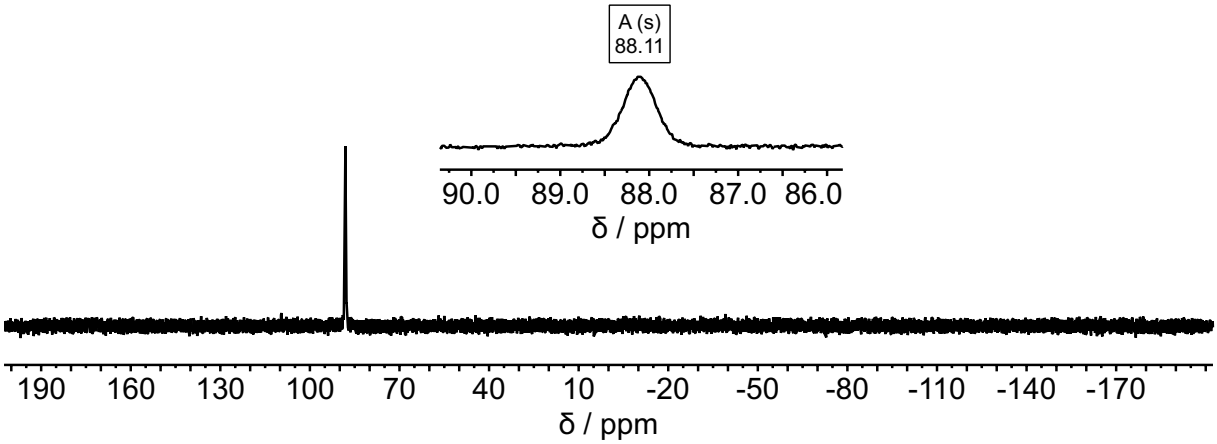


**Figure S56.** $^{31}P$ NMR spectrum of $Bis_2GaOP^tBu_2{\cdot}SO_2$ (**GaOP**$\cdot SO_2$) in $C_6D_6$ (202 MHz, 298K).

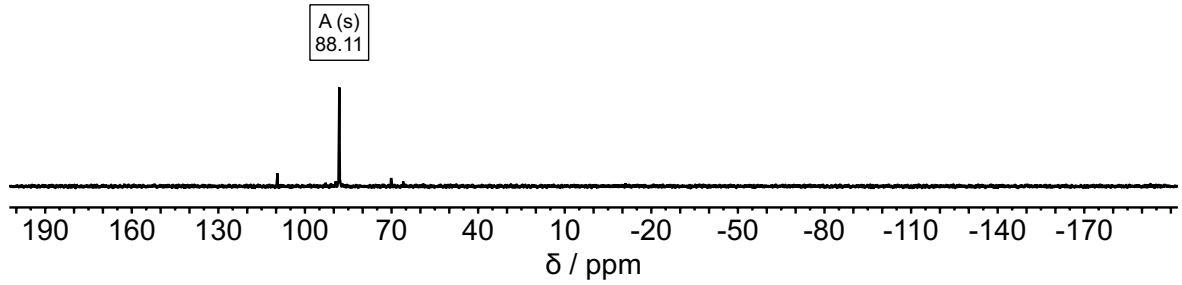


**Figure S57.** $^{31}P\{^{1}H\}$ NMR spectrum of $Bis_2GaOP^tBu_2{\cdot}SO_2$ (**GaOP**$\cdot SO_2$) in $C_6D_6$ (202 MHz, 298K).

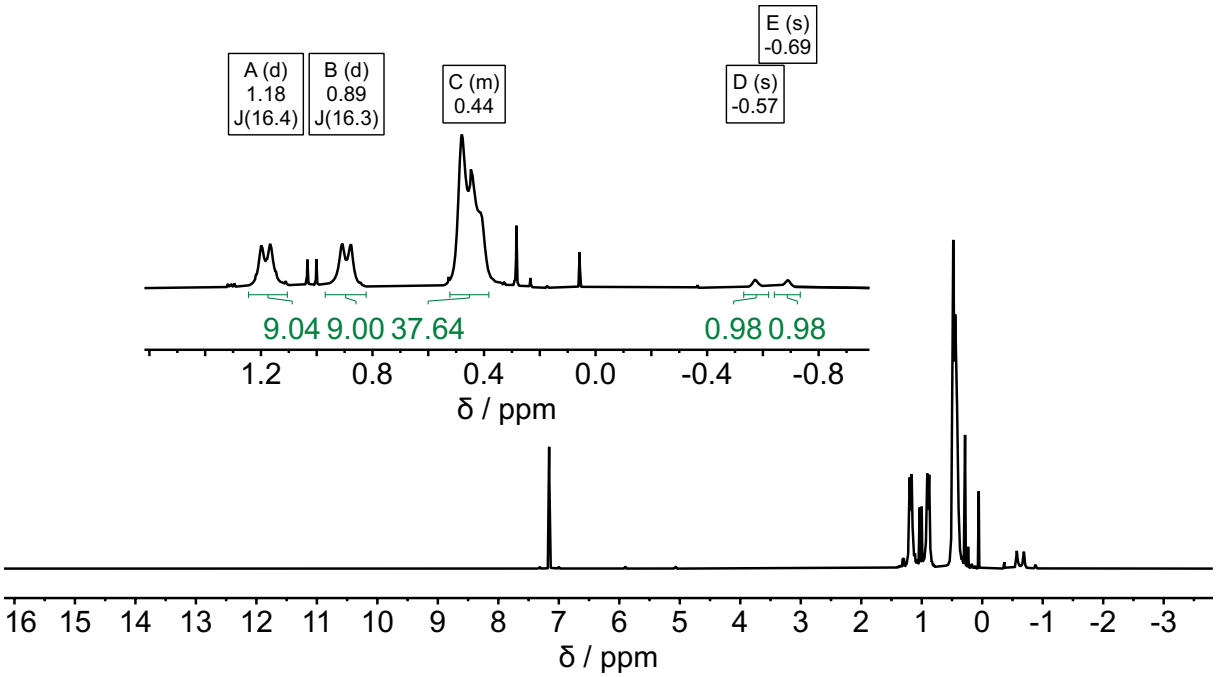


**Figure S58.** $^{1}H$ NMR spectrum of $Bis_2AlSP^tBu_2{\cdot}SO_2$ (**AlSP**·$SO_2$) in $C_6D_6$ (500 MHz, 298K).

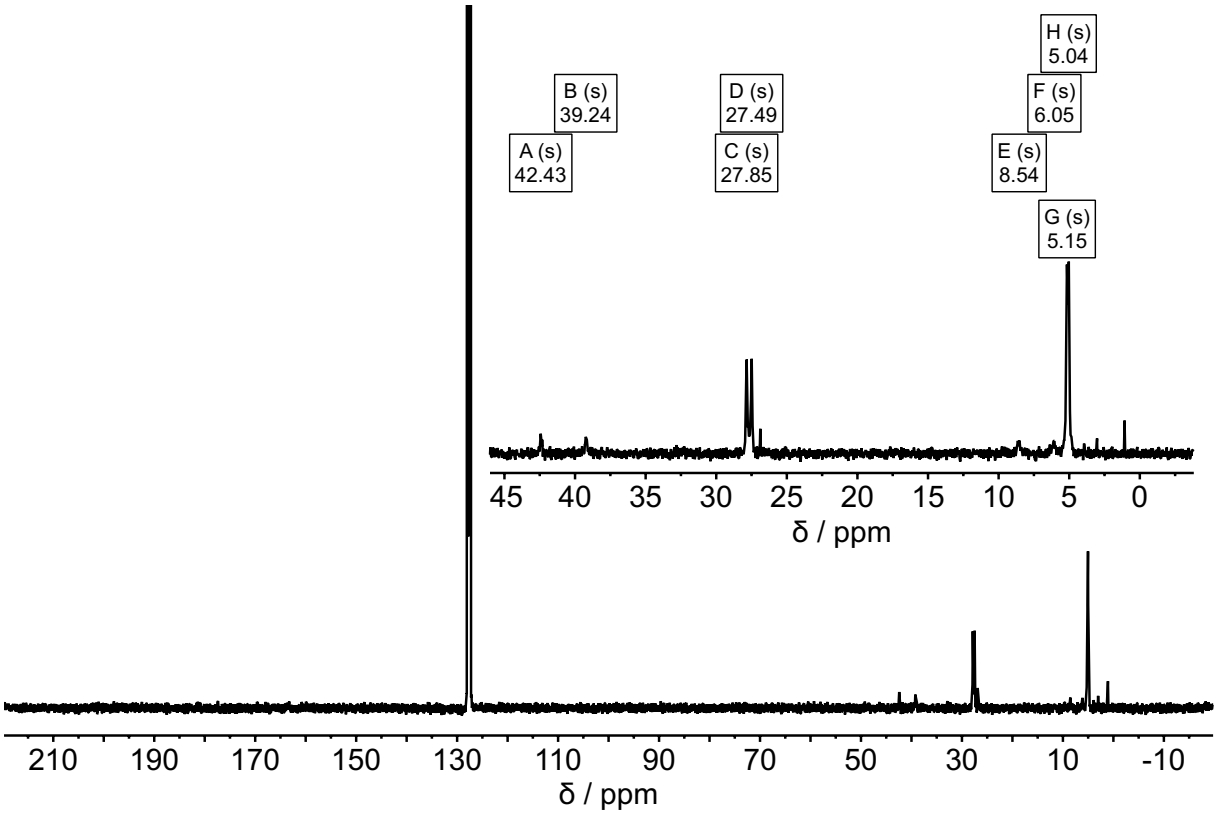


**Figure S59.** $^{13}C\{^{1}H\}$ NMR spectrum of $Bis_2AlSP^tBu_2{\cdot}SO_2$ (**AlSP**·$SO_2$) in $C_6D_6$ (126 MHz, 298K).

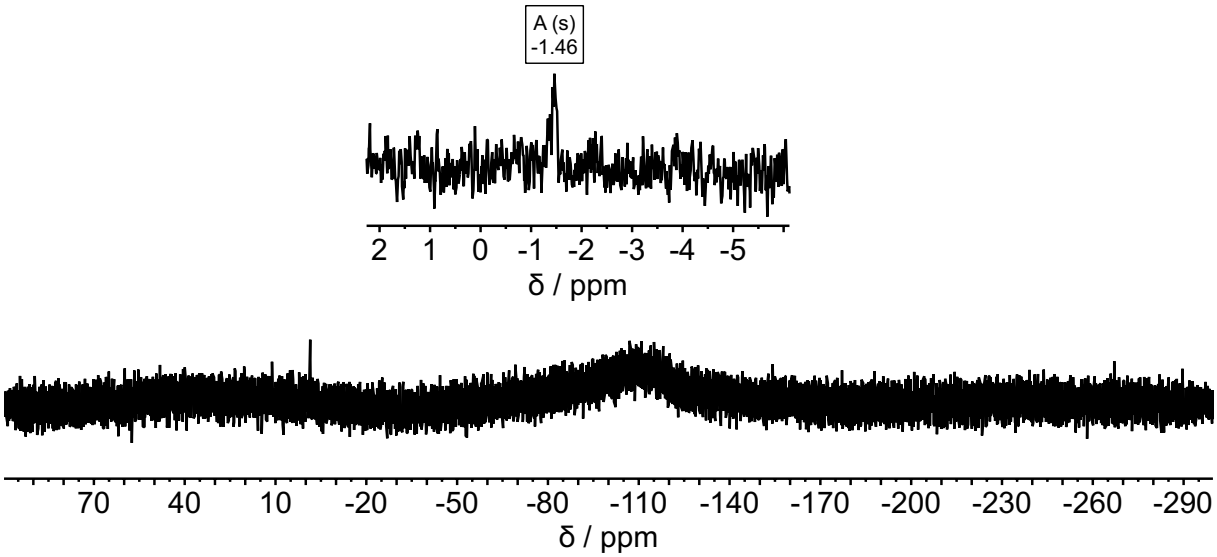


**Figure S60.** $^{29}Si\{^{1}H\}$ NMR spectrum of $Bis_2AlSP^tBu_2{\cdot}SO_2$ (**AlSP**·$SO_2$) in $C_6D_6$ (99 MHz, 298K).

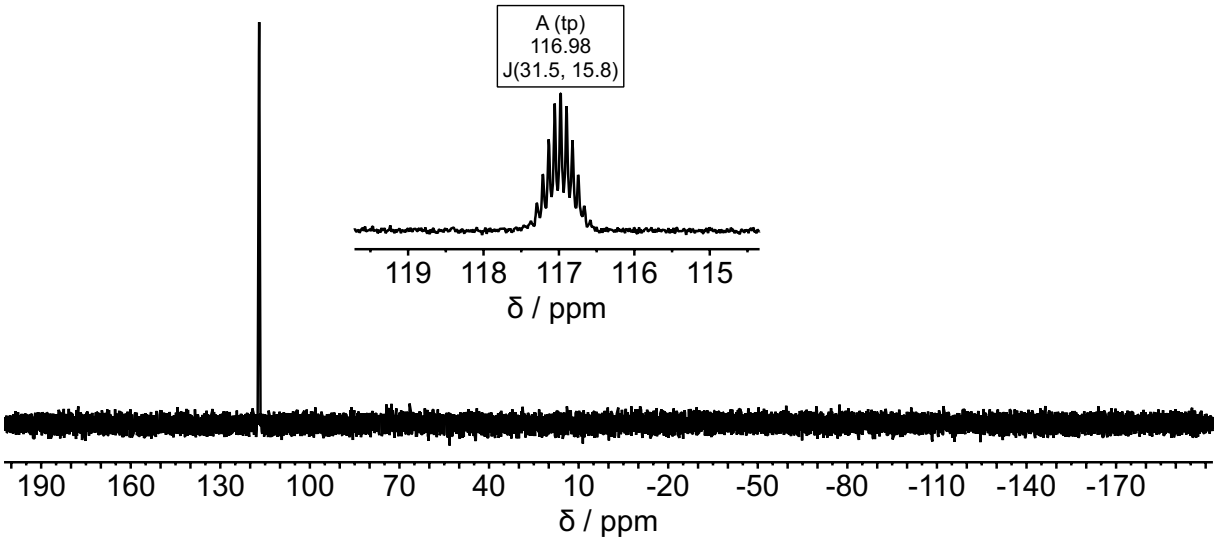


**Figure S61.** $^{31}P$ NMR spectrum of $Bis_2AlSP^tBu_2{\cdot}SO_2$ (**AlSP**·$SO_2$) in $C_6D_6$ (202 MHz, 298K).

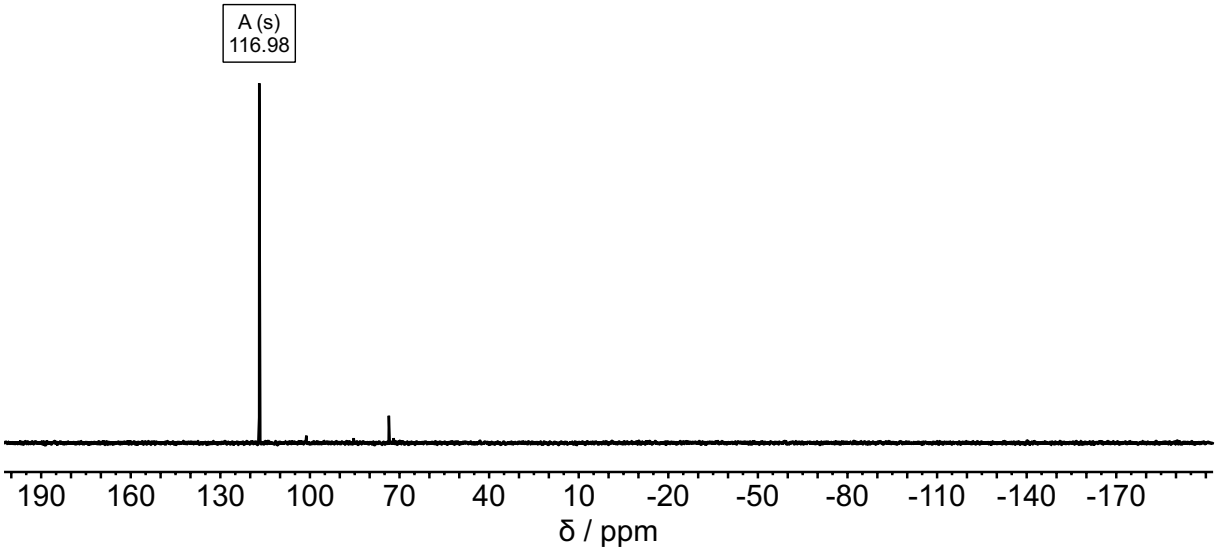


**Figure S62.** $^{31}P\{^{1}H\}$ NMR spectrum of $Bis_2AlSP^tBu_2{\cdot}SO_2$ (**AlSP**·$SO_2$) in $C_6D_6$ (202 MHz, 298K).

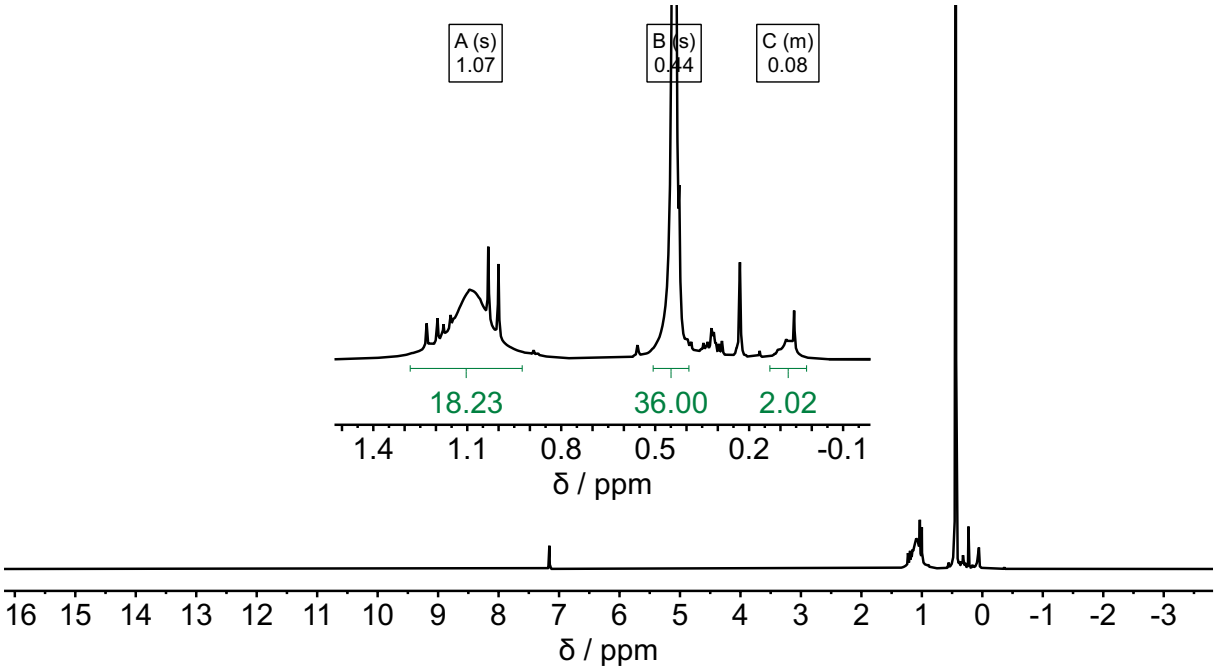


**Figure S63.** $^{1}$H NMR spectrum of Bis$_2$GaSP$^t$Bu$_2$·SO$_2$ (**GaSP**·SO$_2$) in C$_6$D$_6$ (500 MHz, 298K).

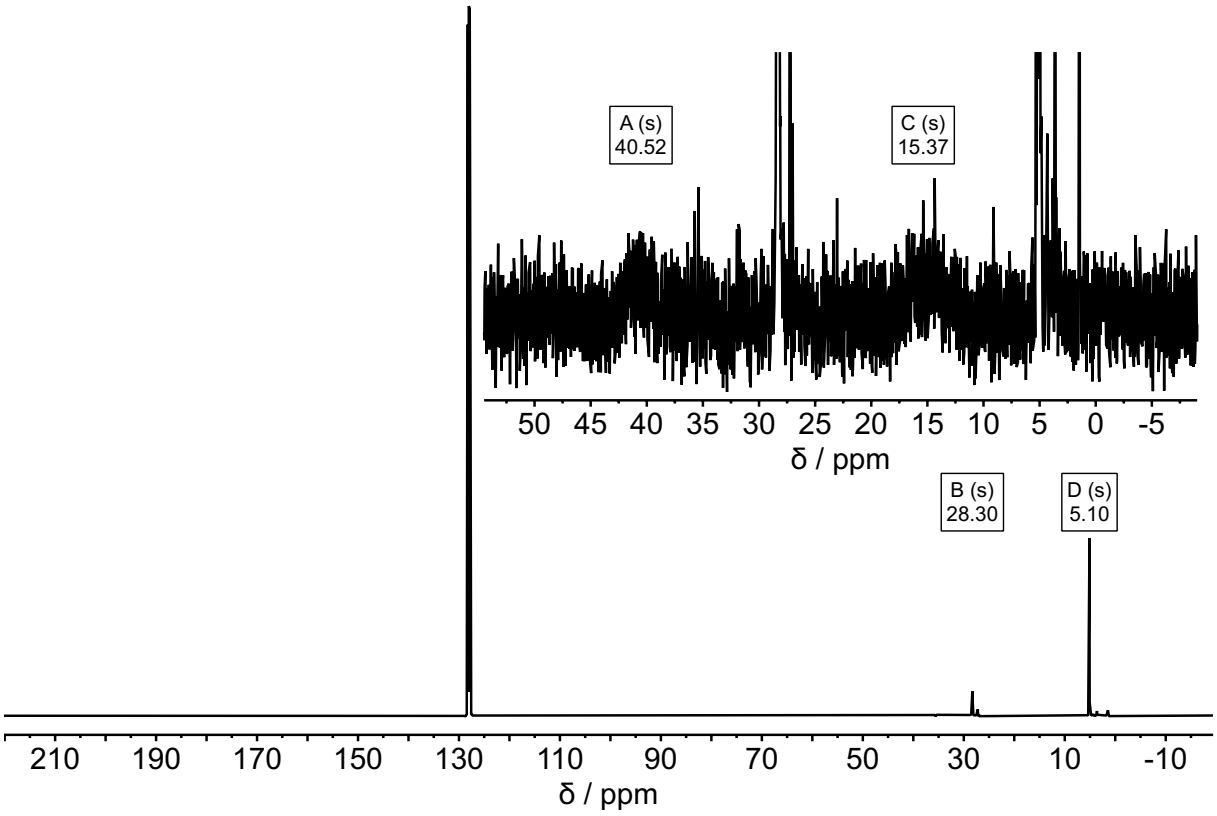


**Figure S64.** $^{13}$C{$^{1}$H} NMR spectrum of Bis$_2$GaSP$^t$Bu$_2$·SO$_2$ (**GaSP**·SO$_2$) in C$_6$D$_6$ (126 MHz, 298K).

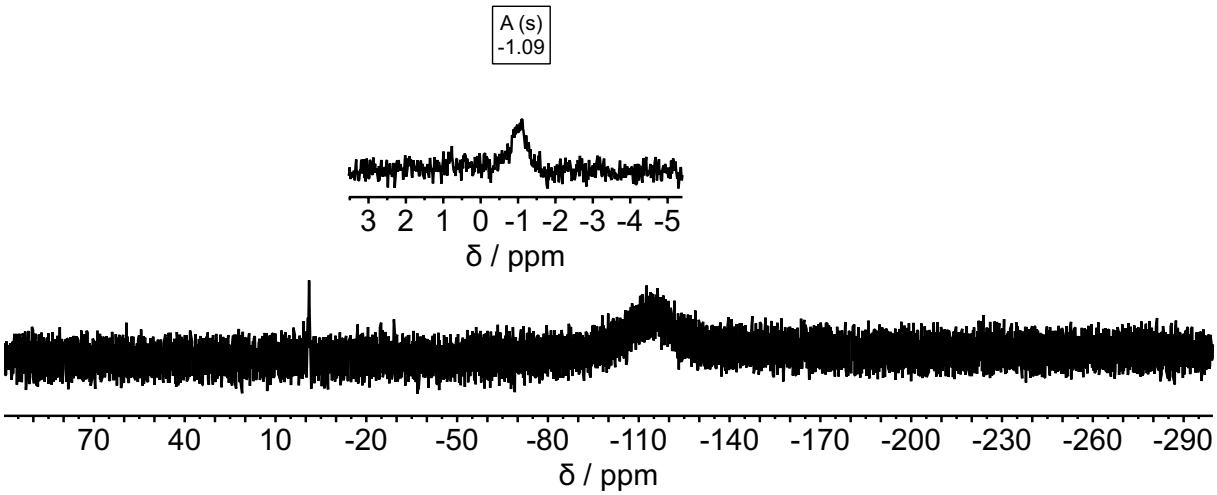


**Figure S65.** $^{29}Si\{^{1}H\}$ NMR spectrum of $Bis_2GaSP^tBu_2{\cdot}SO_2$ (**GaSP**·$SO_2$) in $C_6D_6$ (99 MHz, 298K).

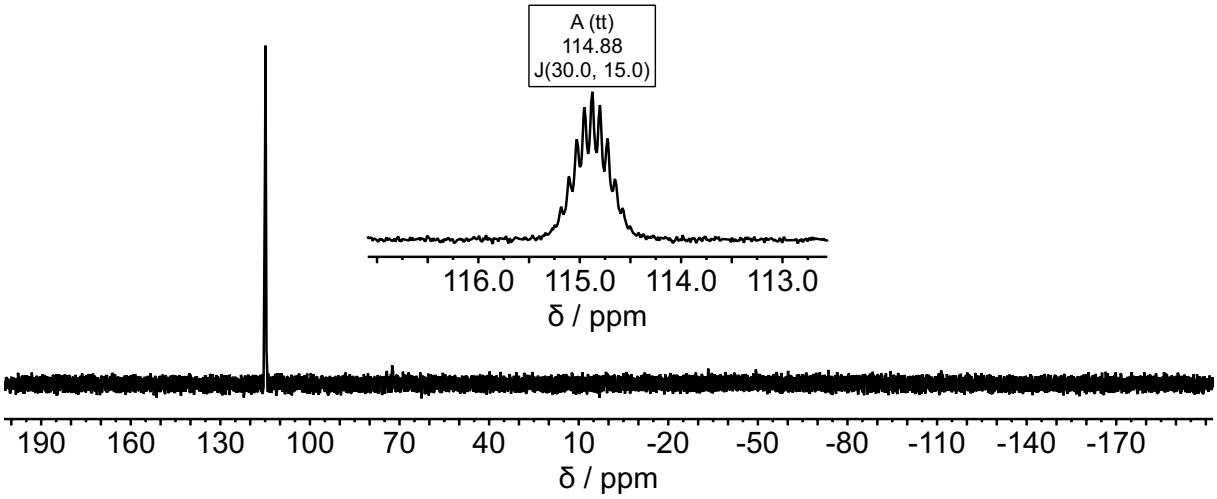


**Figure S66.** $^{31}P$ NMR spectrum of $Bis_2GaSP^tBu_2{\cdot}SO_2$ (**GaSP**·$SO_2$) in $C_6D_6$ (202 MHz, 298K).

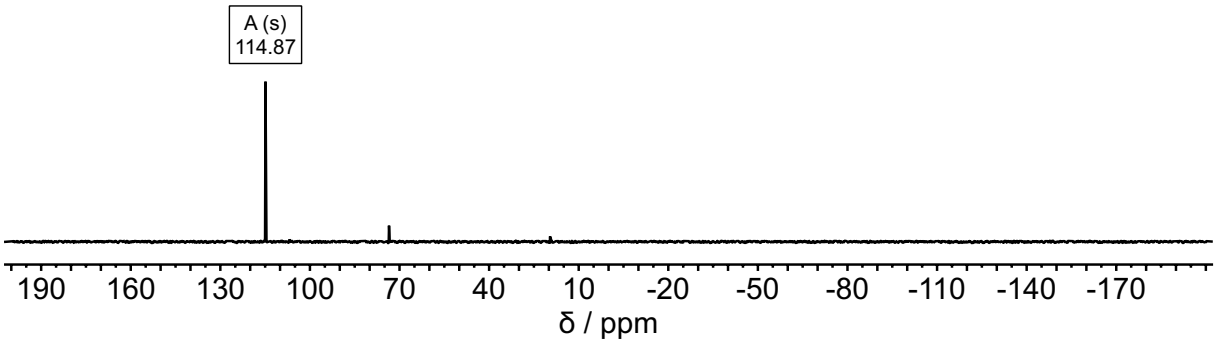


**Figure S67.** $^{31}P\{^{1}H\}$ NMR spectrum of $Bis_2GaSP^tBu_2{\cdot}SO_2$ (**GaSP**·$SO_2$) in $C_6D_6$ (202 MHz, 298K).

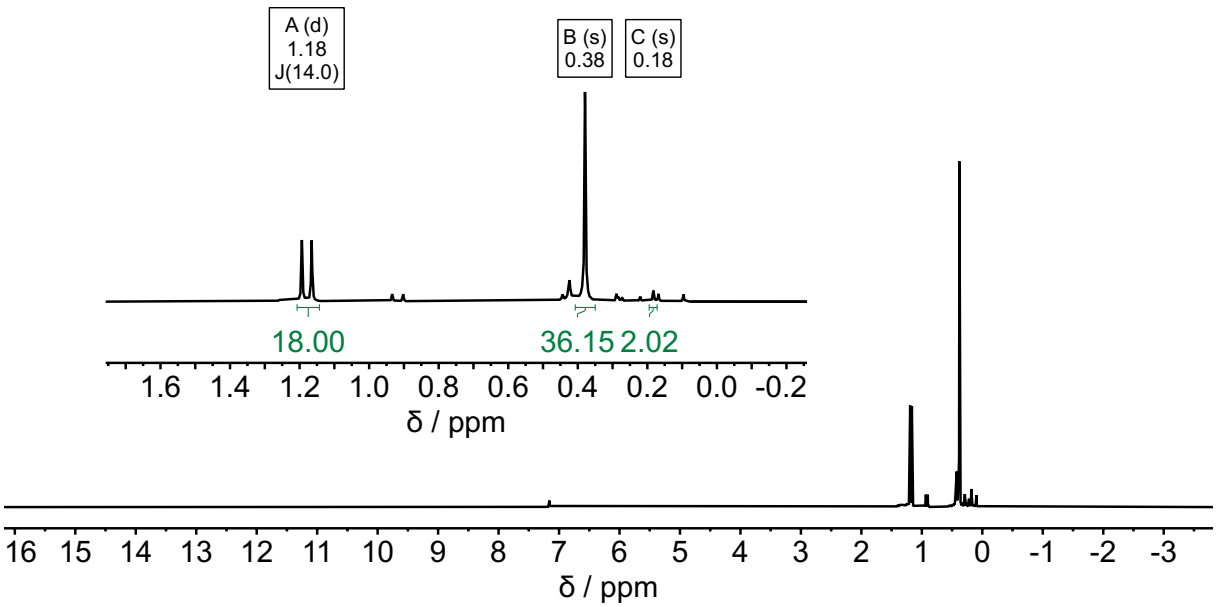


**Figure S68.** $^{1}$H NMR spectrum of Bis$_2$GaOP$^t$Bu$_2$·O (**GaOP**·O) in $C_6D_6$ (500 MHz, 298K).

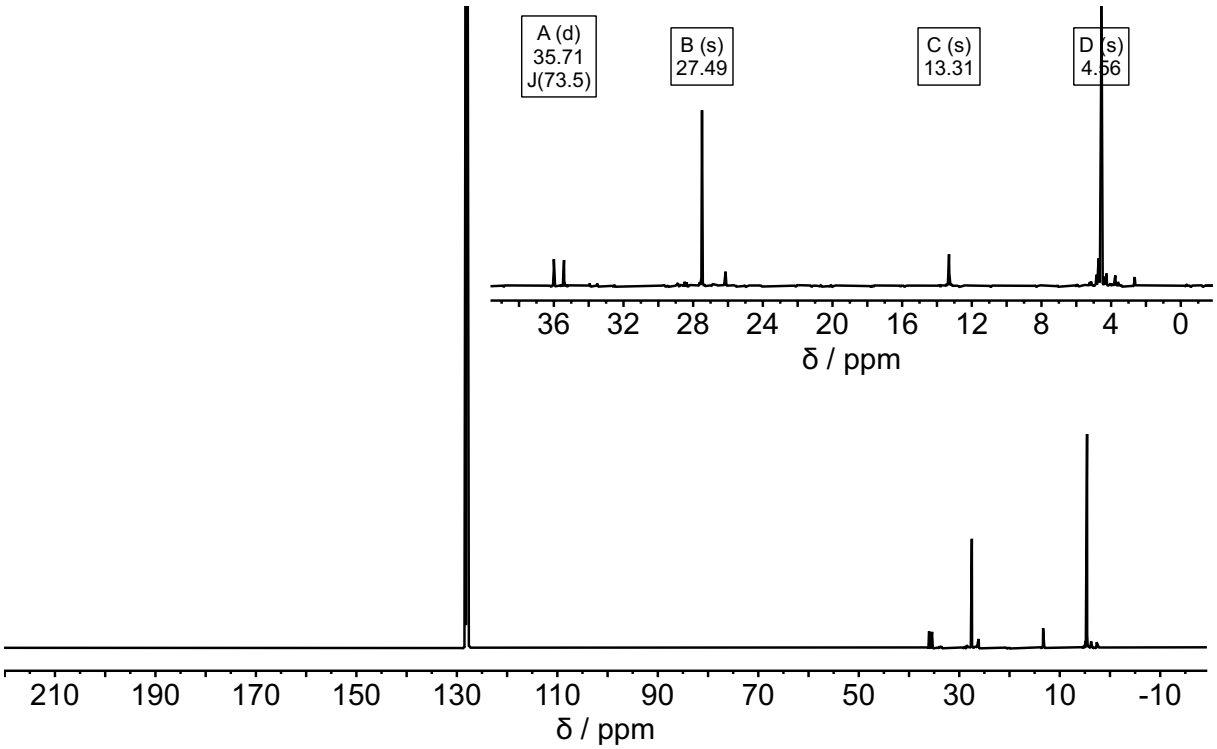


**Figure S69.** $^{13}$C{$^{1}$H} NMR spectrum of Bis$_2$GaOP$^t$Bu$_2$·O (**GaOP**·O) in $C_6D_6$ (126 MHz, 298K).

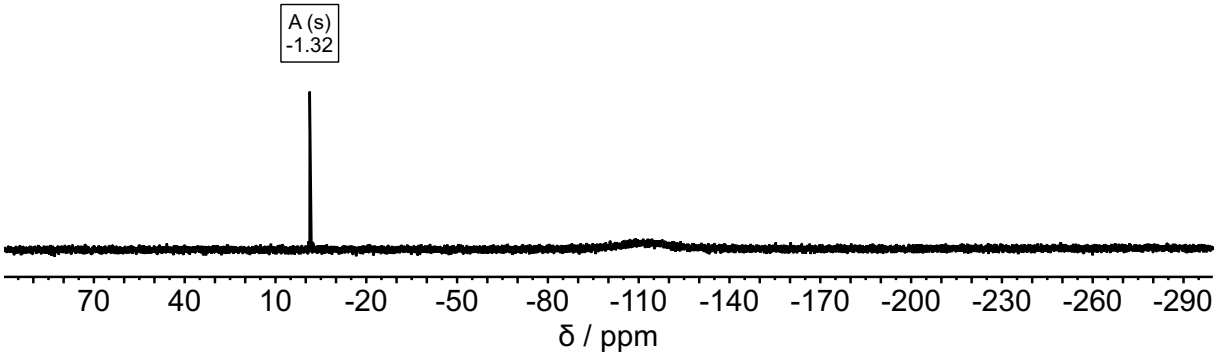


**Figure S70.** $^{29}$Si{$^{1}$H} NMR spectrum of Bis$_2$GaOP$^t$Bu$_2$·O (**GaOP**·O) in $C_6D_6$ (99 MHz, 298K).

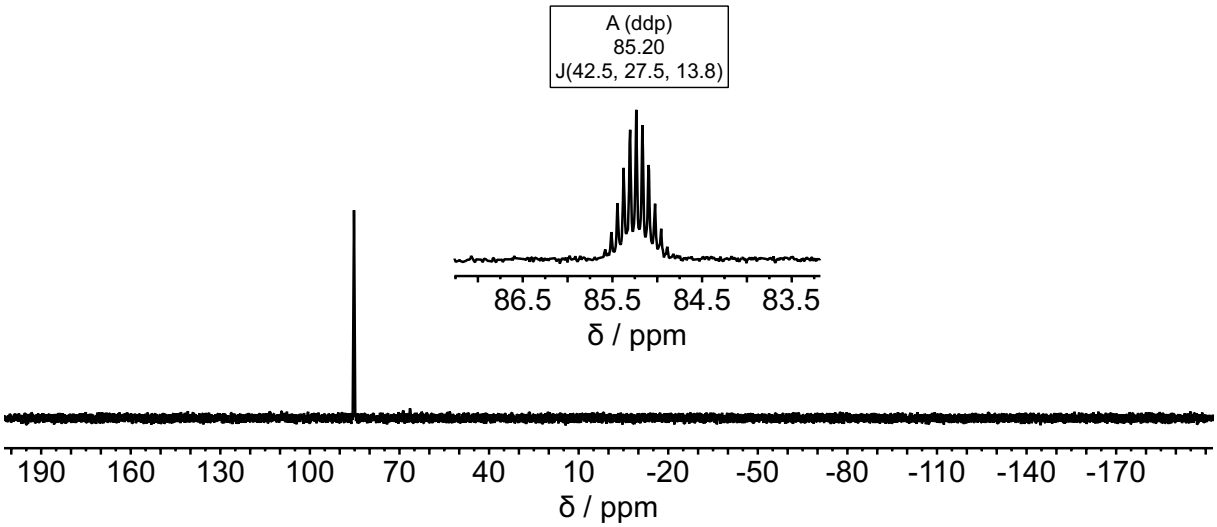


**Figure S71.** $^{31}P$ NMR spectrum of $Bis_2GaOP^tBu_2{\cdot}O$ (**GaOP**·O) in $C_6D_6$ (202 MHz, 298K).

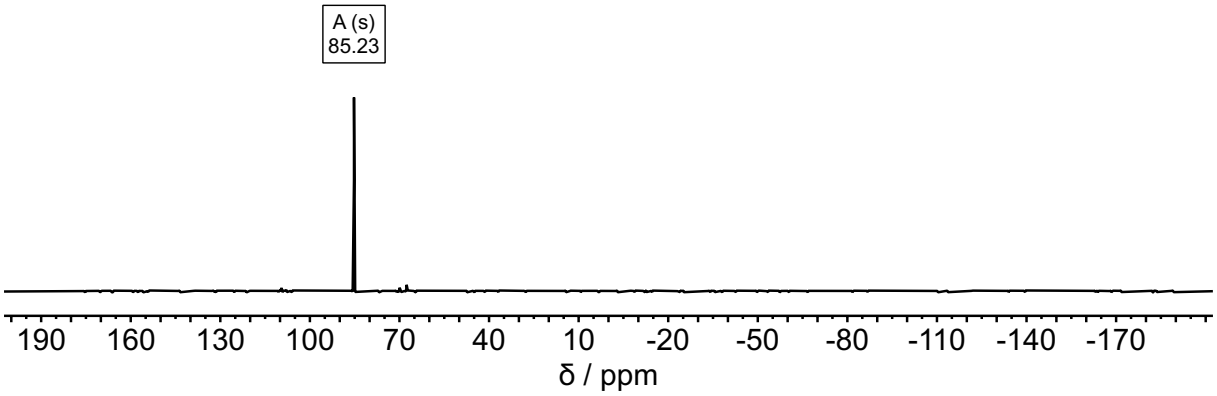


**Figure S72.** $^{31}P\{^1H\}$ NMR spectrum of $Bis_2GaOP^tBu_2{\cdot}O$ (**GaOP**·O) in $C_6D_6$ (202 MHz, 298K).

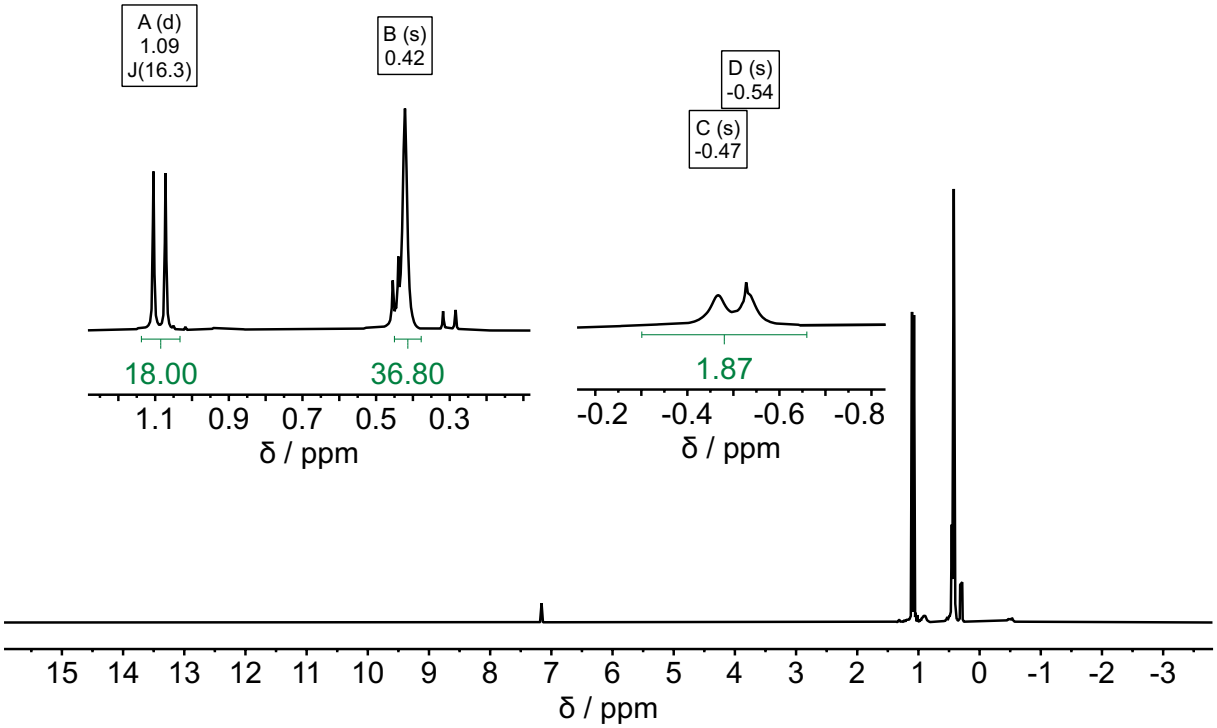


**Figure S73.** $^1H$ NMR spectrum of $Bis_2AlSP^tBu_2{\cdot}O$ (**AlSP**·O) in $C_6D_6$ (500 MHz, 298K).

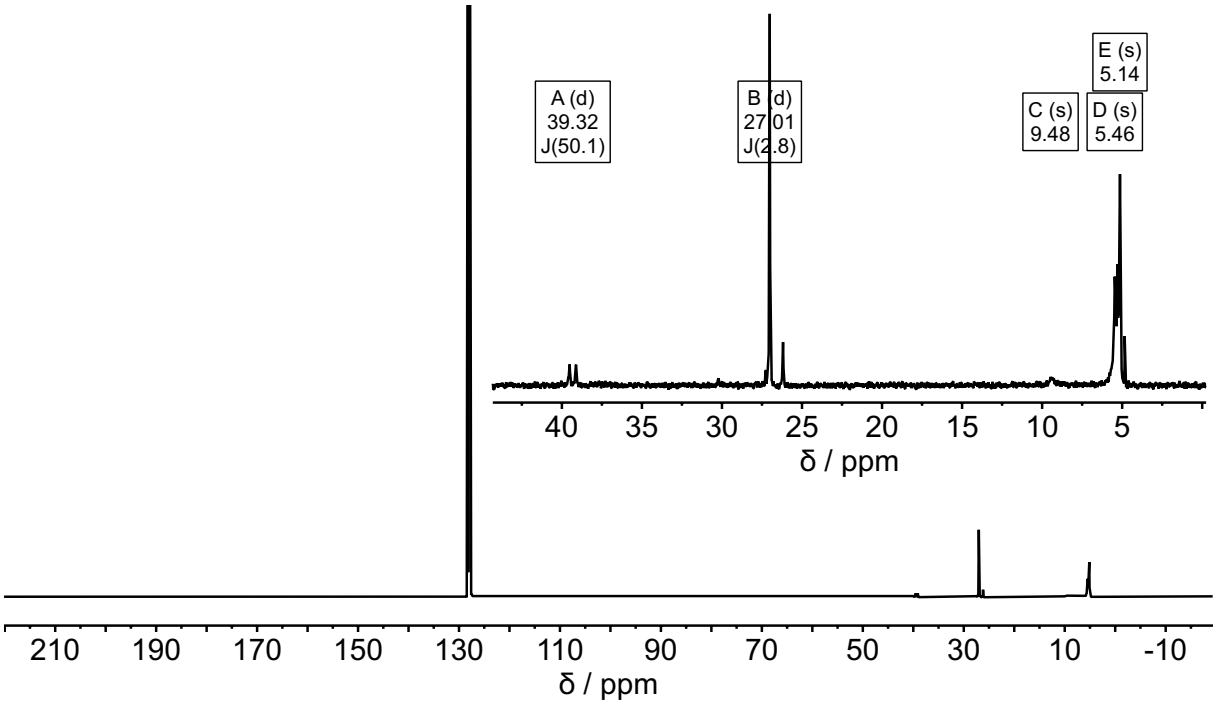


**Figure S74.** $^{13}C\{^{1}H\}$ NMR spectrum of $Bis_2AlSP^tBu_2{\cdot}O$ (**AlSP**·O) in $C_6D_6$ (126 MHz, 298K).

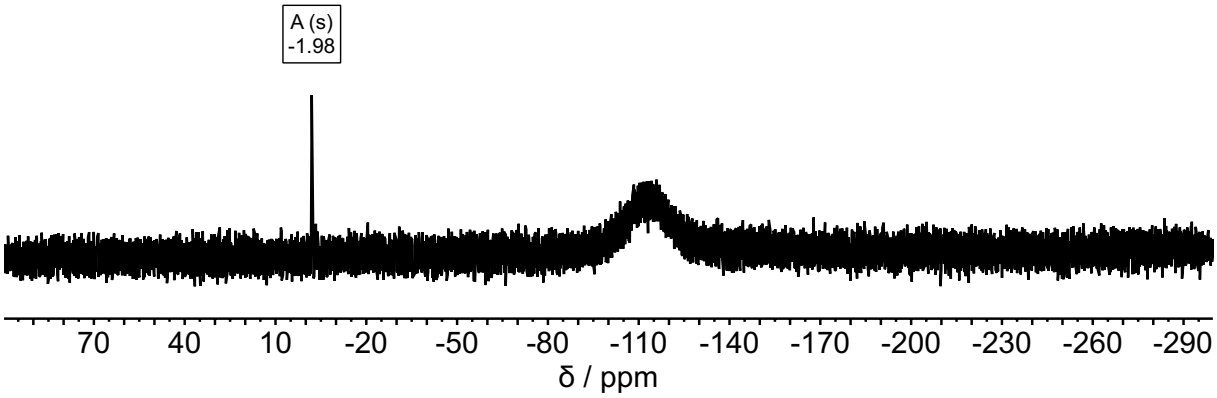


**Figure S75.** $^{29}Si\{^{1}H\}$ NMR spectrum of $Bis_2AlSP^tBu_2{\cdot}O$ (**AlSP**·O) in $C_6D_6$ (99 MHz, 298K).

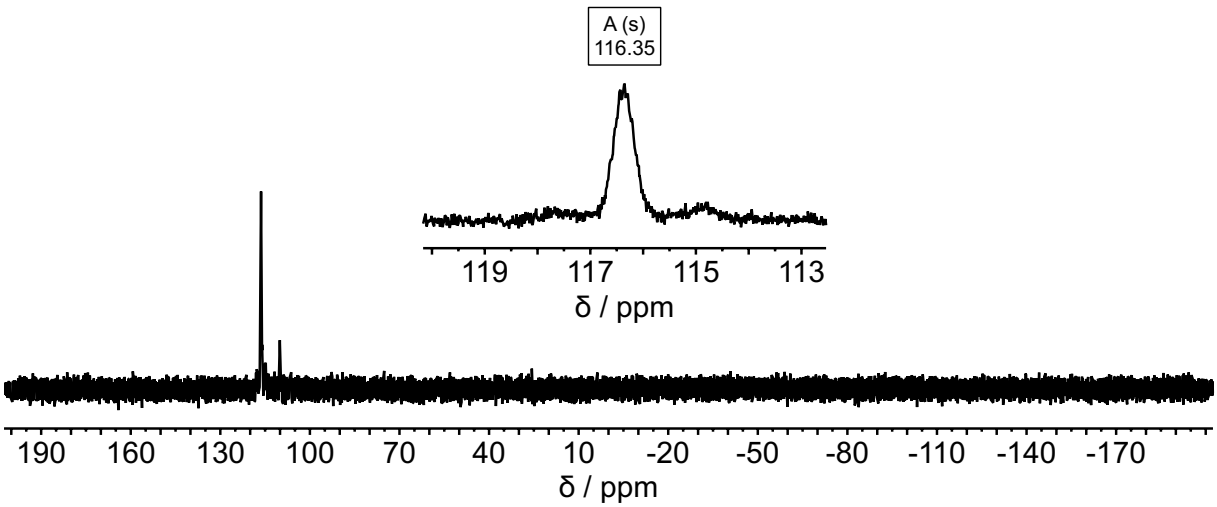


**Figure S76.** $^{31}P$ NMR spectrum of $Bis_2AlSP^tBu_2{\cdot}O$ (**AlSP**·O) in $C_6D_6$ (202 MHz, 298K).

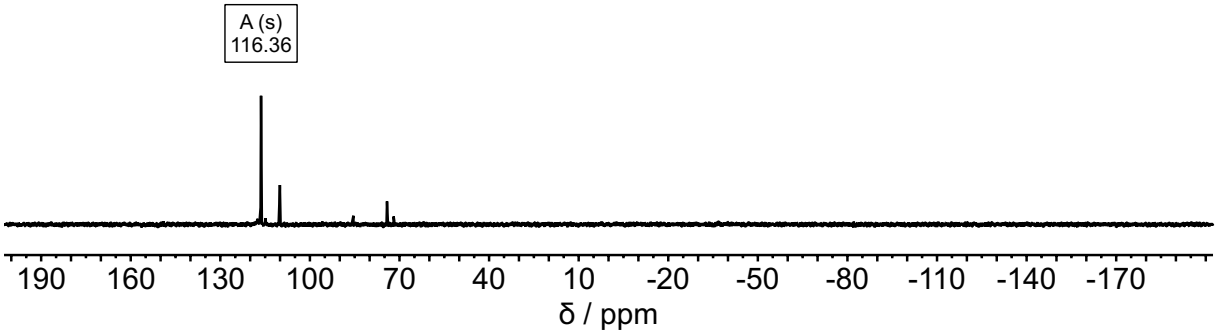


**Figure S77.** $^{31}P\{^{1}H\}$ NMR spectrum of $Bis_2AlSP^tBu_2{\cdot}O$ (**AlSP**·O) in $C_6D_6$ (202 MHz, 298K).

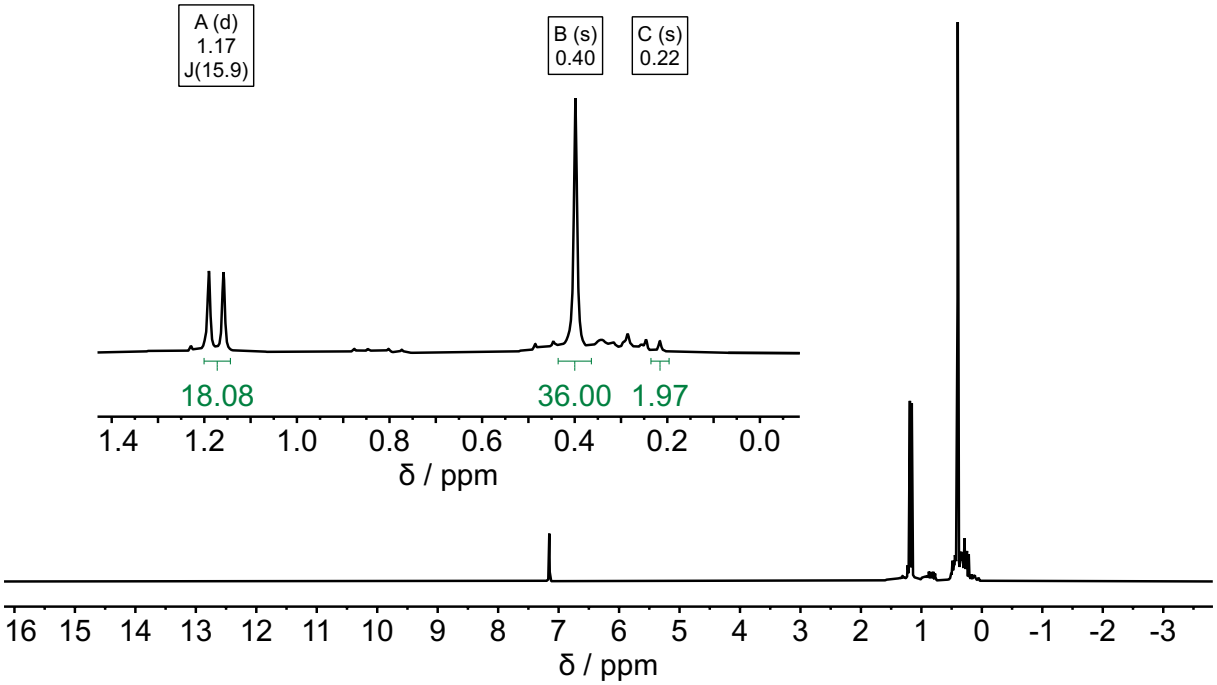


**Figure S78.** $^{1}H$ NMR spectrum of $Bis_2GaOP^tBu_2{\cdot}S$ (**GaOP**·S) in $C_6D_6$ (500 MHz, 298K).

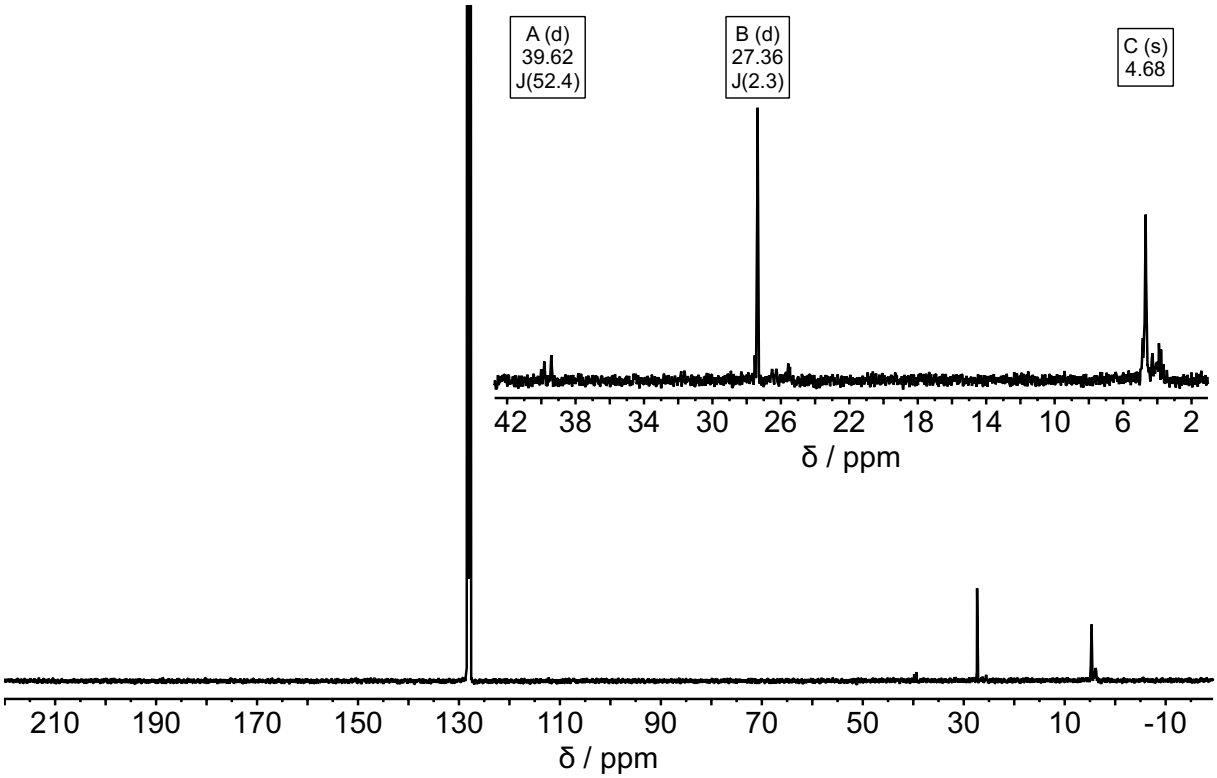


**Figure S79.** $^{13}C\{^{1}H\}$ NMR spectrum of $Bis_2GaOP^tBu_2{\cdot}S$ (**GaOP**·S) in $C_6D_6$ (126 MHz, 298K).

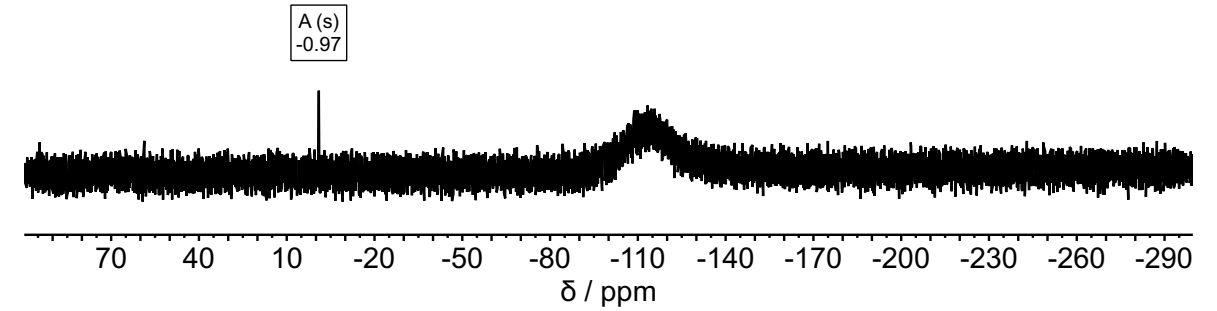


**Figure S80.** $^{29}Si\{^{1}H\}$ NMR spectrum of $Bis_2GaOP^tBu_2{\cdot}S$ (**GaOP**·S) in $C_6D_6$ (99 MHz, 298K).

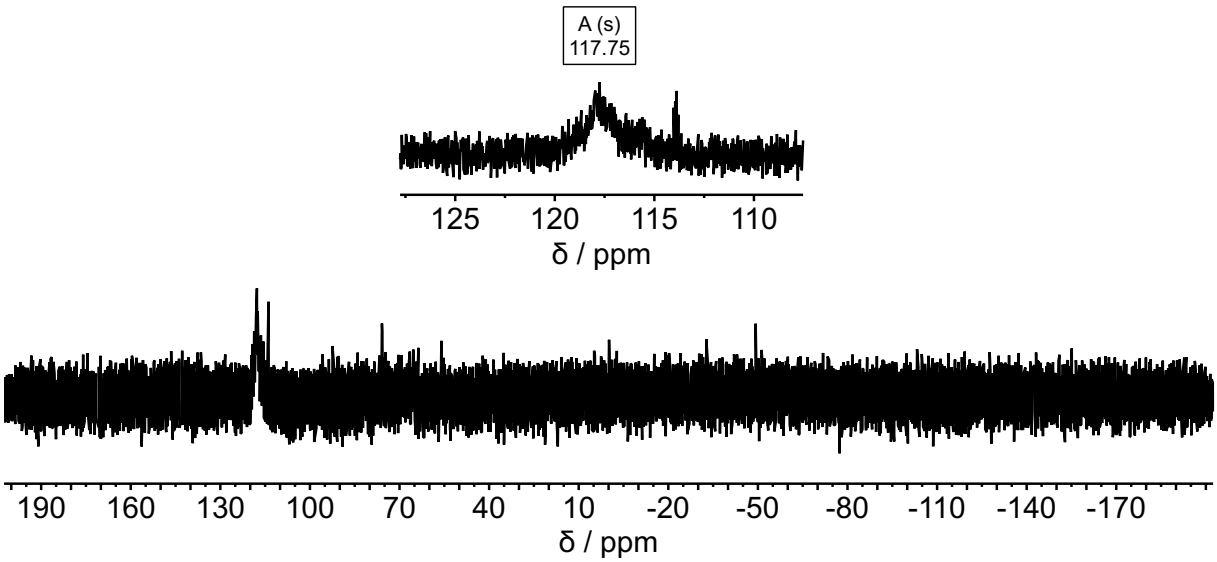


**Figure S81.** $^{31}P$ NMR spectrum of $Bis_2GaOP^tBu_2{\cdot}S$ (**GaOP**·S) in $C_6D_6$ (202 MHz, 298K).

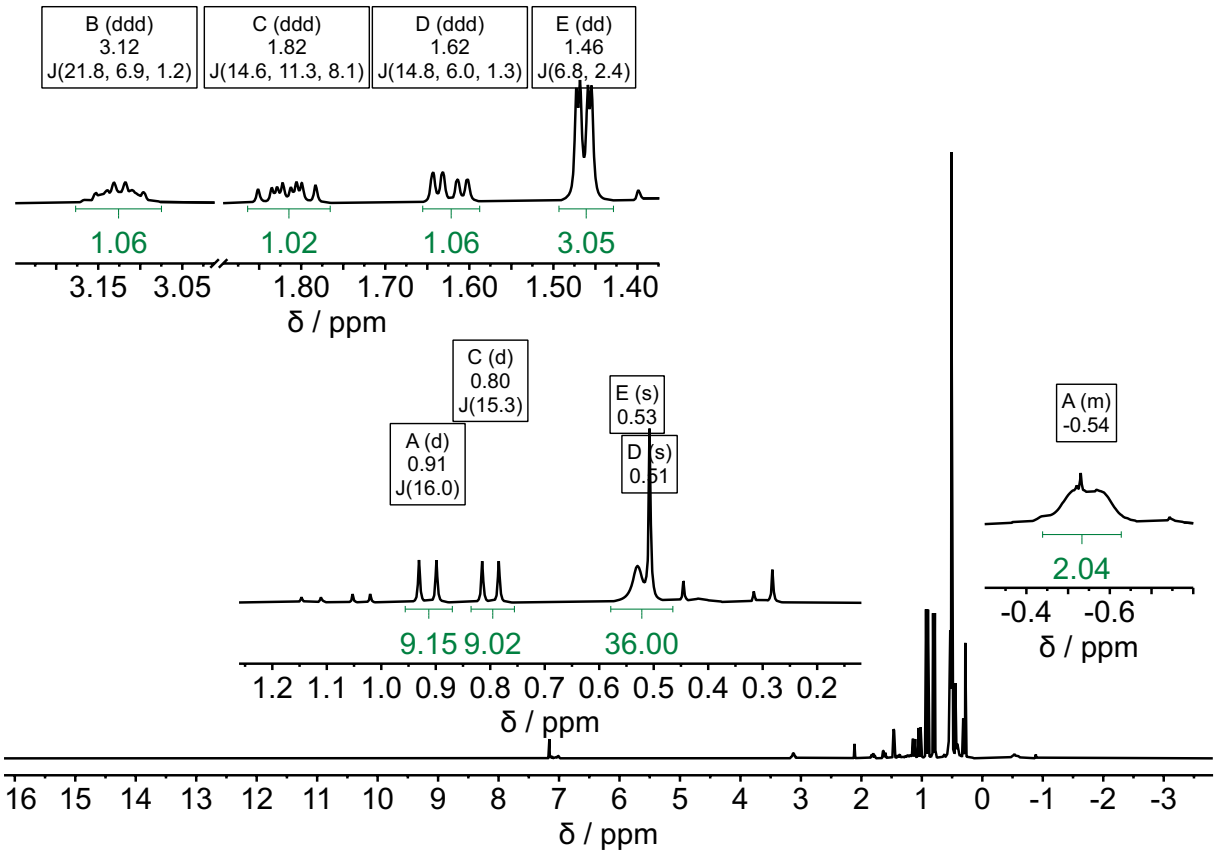


**Figure S82.** $^{1}H$ NMR spectrum $Bis_2AlSP^tBu_2{\cdot}SC_3H_6$ (**AlSP**·$SC_3H_6$) in $C_6D_6$ (500 MHz, 298K).

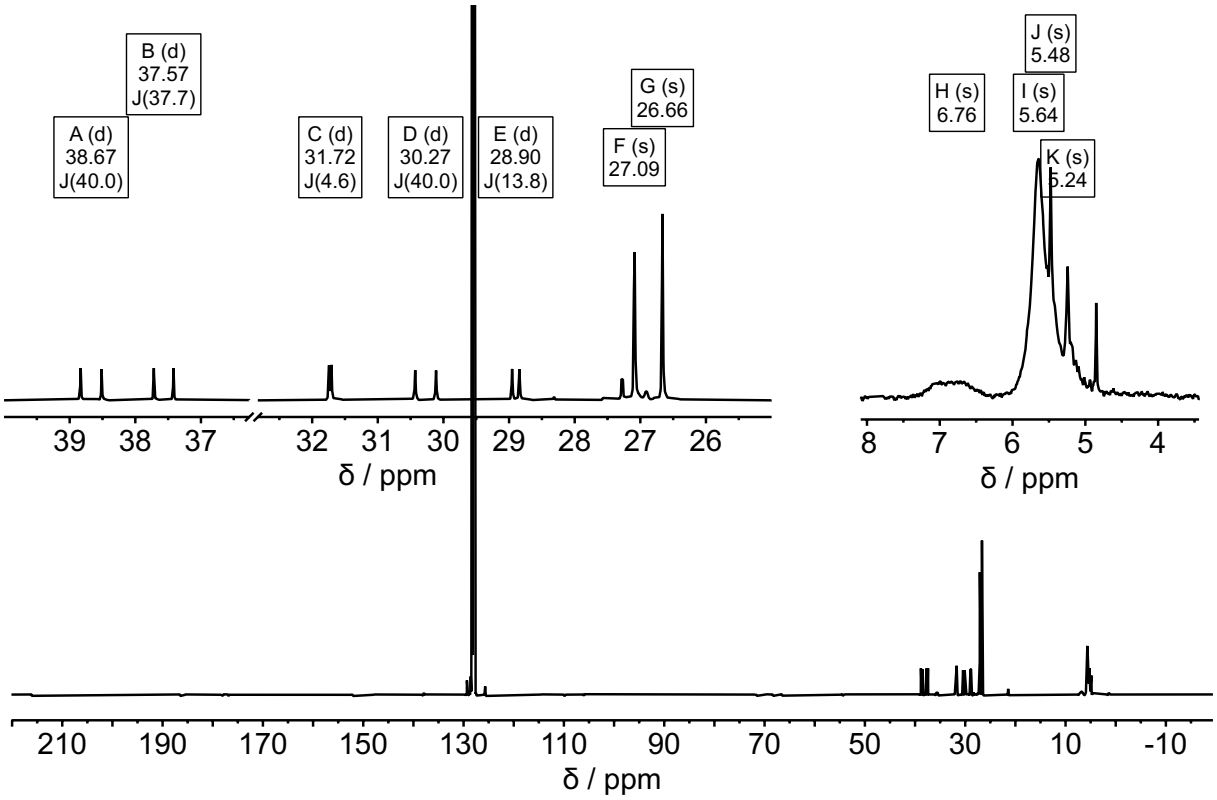


**Figure S83.** $^{13}C\{^{1}H\}$ NMR spectrum of $Bis_2AlSP^tBu_2{\cdot}SC_3H_6$ (**AlSP**·$SC_3H_6$) in $C_6D_6$ (126 MHz, 298K).

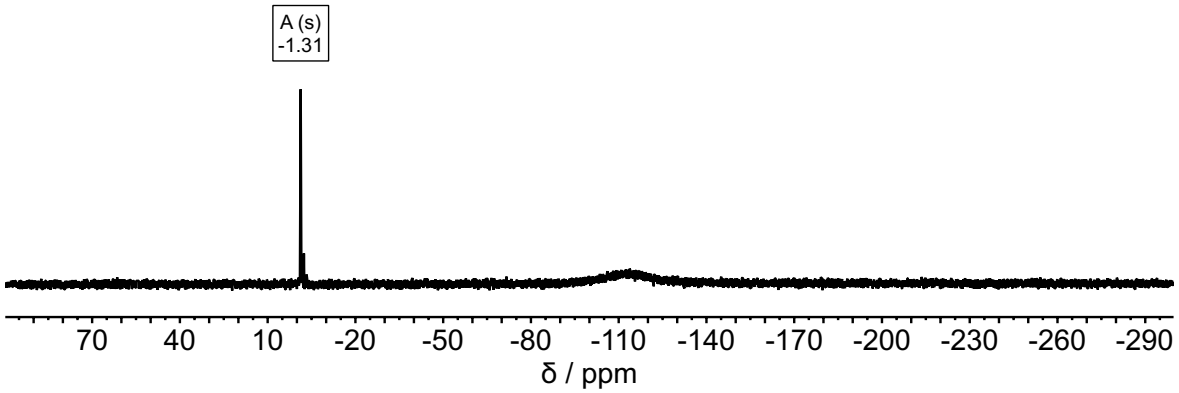


**Figure S84.** $^{29}Si\{^{1}H\}$ NMR spectrum of $Bis_2AlSP^tBu_2{\cdot}SC_3H_6$ (**AlSP**·$SC_3H_6$) in $C_6D_6$ (99 MHz, 298K).

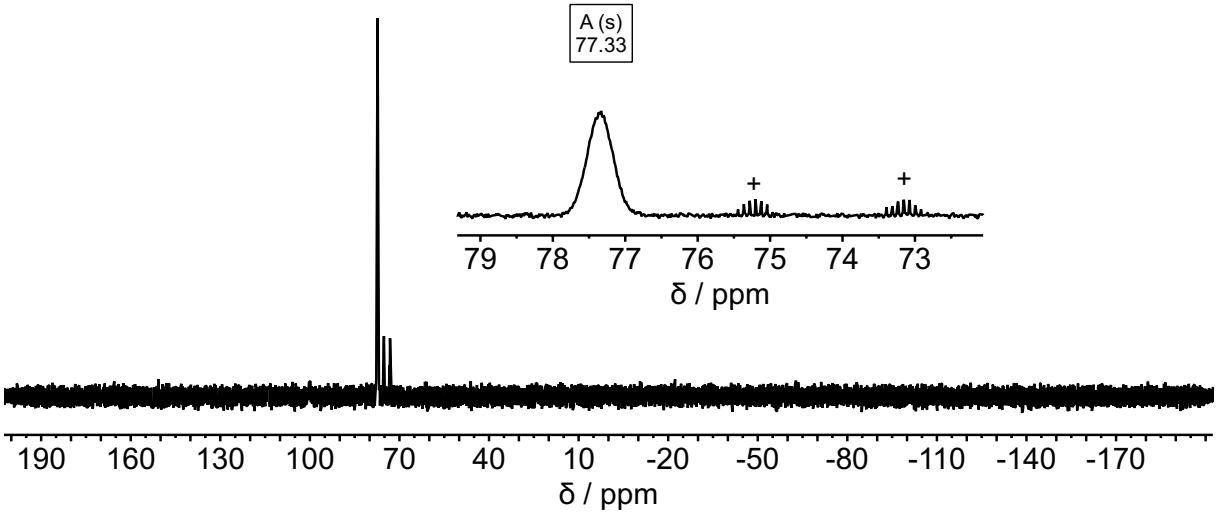


**Figure S85.** $^{31}P$ NMR spectrum of $Bis_2AlSP^tBu_2{\cdot}SC_3H_6$ (**AlSP**·$SC_3H_6$) in $C_6D_6$ (202 MHz, 298K). The signal denoted with + results from partial hydrolysis ($^tBu_2P(S)H$).

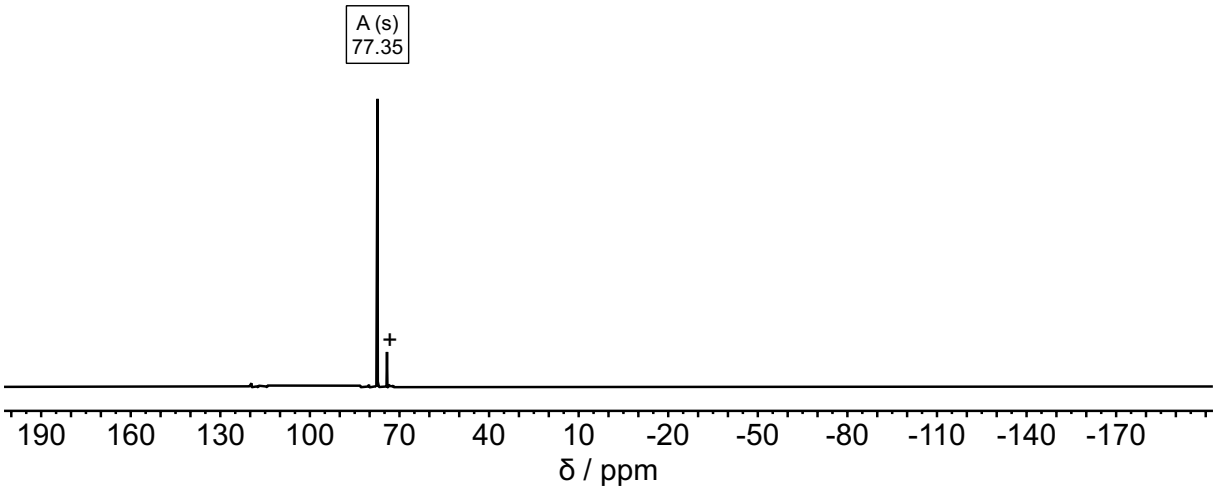


**Figure S86.** $^{31}P\{^{1}H\}$ NMR spectrum of $Bis_2AlSP^tBu_2{\cdot}SC_3H_6$ (**AlSP**·$SC_3H_6$) in $C_6D_6$ (202 MHz, 298K). The signal denoted with + results from partial hydrolysis ($^tBu_2P(S)H$).

## Crystallographic data

Single crystals were examined on a Rigaku Supernova diffractometer. The crystals were kept at 100.0(1) K during data collection. All structures were solved with the ShelXT[4]. Using Olex2[5], the structures of **AlSP**, **GaSP**, **GaOP**·$CO_2$, **AlSP**·$CO_2$, **GaOP**·$CS_2$, **GaSP**·$CS_2$, **GaOP**·$SO_2$, **AlSP**·O, **GaOP**·S and **GaSP**·S were refined with the ShelXL[6] refinement package using Least Squares minimization. For **AlSP**·HBr, **AlSP**·$CS_2$, **AlSP**·$SO_2$, **GaSP**·$SO_2$ and **AlSP**·$SC_3H_6$ the structures were refined with the olex2.refine[7] refinement package using Gauss-Newton minimisation and NoSphereA2,[8] an implementation of NOn-SPHERical Atom-form-factors in Olex2.

Details of the X-ray investigations are given in Tables S1–S4. CCDC 2503479–2503493 contain the supplementary crystallographic data for this paper. These data can be obtained free of charge from The Cambridge Crystallographic Data Centre *via* https://www.ccdc.cam.ac.uk/structures/.

**Table S1.** Crystallographic data for compounds **AlSP**, **GaSP**, **AlSP**·HBr, and **GaOP**·$CO_2$.

| Compound | **AlSP** | **GaSP** | **AlSP**·HBr | **GaOP**·$CO_2$ |
|---|---|---|---|---|
| Empirical formula | $C_{22}H_{56}AlPSSi_4$ | $C_{22}H_{56}GaPSSi_4$ | $C_{25}H_{60}AlBrPSSi_4$ | $C_{23}H_{56}GaO_3PSi_4$ |
| $M$ [g mol$^{-1}$] | 523.03 | 565.77 | 643.022 | 593.72 |
| $T$ [K] | 100.0(1) | 100.0(1) | 100.0(1) | 100.0(1) |
| $\lambda$ [Å] | 1.54184 (Cu K$\alpha$) | 0.71073 (Mo K$\alpha$) | 0.71073 (Mo K$\alpha$) | 0.71073 (Mo K$\alpha$) |
| Crystal size | 0.5×0.22×0.15 | 0.36×0.23×0.12 | 0.68×0.26×0.18 | 0.45×0.25×0.15 |
| Crystal system | triclinic | triclinic | triclinic | monoclinic |
| Space group | $P\bar{1}$ | $P\bar{1}$ | $P\bar{1}$ | $P2_1/c$ |
| $a$ [Å] | 9.3597(2) | 9.4107(2) | 11.4899(3) | 11.7399(11) |
| $b$ [Å] | 13.3329(3) | 13.3305(4) | 12.8148(4) | 28.1763(17) |
| $c$ [Å] | 13.8931(2) | 13.9075(4) | 13.9414(4) | 11.8292(9) |
| $\alpha$ [°] | 106.425(2) | 107.069(2) | 97.116(2) | 90 |
| $\beta$ [°] | 97.765(2) | 97.760(2) | 92.578(2) | 118.553(10) |
| $\gamma$ [°] | 91.828(2) | 90.634(2) | 115.830(3) | 90 |
| *Volume* [Å$^3$] | 1643.26(6) | 1650.19(8)) | 1822.14(10) | 3437.0(5) |
| $Z$ | 2 | 2 | 2 | 4 |
| $\rho_{calc}$ [g cm$^{-3}$] | 1.057 | 1.139 | 1.172 | 1.147 |
| $\mu$ [mm$^{-1}$] | 3.038 | 1.099 | 1.401 | 1.006 |
| $F$(000) [$e$] | 576.0 | 612.0 | 691.0 | 1280.0 |
| 2$\theta$ range [°] | 6.71–153.154 | 7.044–73.4 | 3.96–57.4 | 5.784–65.698 |
| Index ranges | −11 ≤ $h$ ≤ 11, −16 ≤ $k$ ≤ 16, −17 ≤ $l$ ≤ 17 | −15 ≤ $h$ ≤ 15, −21 ≤ $k$ ≤ 22, −23 ≤ $l$ ≤ 23 | −17 ≤ $h$ ≤ 18, −19 ≤ $k$ ≤ 19, −21 ≤ $l$ ≤ 21 | −14 ≤ $h$ ≤ 17, −40 ≤ $k$ ≤ 38, −17 ≤ $l$ ≤ 16 |
| Refl. collected | 36904 | 120880 | 47733 | 49252 |
| Independent refl. | 6836 | 15842 | 9414 | 11541 |
| $R_{int}$ / $R_{sigma}$ | 0.0313/0.0185 | 0.0622/0.0426 | 0.0467/0.0495 | 0.0347/0.0336 |
| Data / restraints / parameters | 6836/36/339 | 15842/636/480 | 9414/84/348 | 11541/272/395 |
| GooF on $F^2$ | 1.137 | 1.115 | 1.030 | 1.027 |
| $R_1$ / w$R_2$ [$I > 2\sigma(I)$] | 0.0480/0.1266 | 0.0626/0.1265 | 0.0279/0.0602 | 0.0587/0.1293 |
| $R_{int}$ (all data) / w$R_2$ | 0.0504/0.1282 | 0.0856/0.1396 | 0.0362/0.0635 | 0.0793/0.1413 |
| $\rho_{fin}$ (max/min) [$e$ Å$^{-3}$] | 0.96/−0.56 | 1.17/−1.49 | 0.55/−0.45 | 1.77/−1.39 |
| CCDC | 2503479 | 2503480 | 2503481 | 2503482 |

[**AlSP**] Disorder of both tert-Bu groups bonded to P1 over two sites in ratio 56:44 and 53:47; [**GaSP**] Disorder of all trimethylsilyl- and tert-butyl groups over two sites; ratio 66:34; [**AlSP**·HBr] Disorder of the benzene molecule (C23-25) over two sites; ratio 70:30; [**GaOP**·$CO_2$] Disorder Si1, Si2, Si4, C2 to C6, C8 to C14 over two sites in ratio 67:33. Suitable constraints and restraints were applied.

**Table S2.** Crystallographic data for compounds **AlSP**·$CO_2$, **GaOP**·$CS_2$, **AlSP**·$CS_2$, and **GaSP**·$CS_2$.

| Compound | **AlSP**·$CO_2$ | **GaOP**·$CS_2$ | **AlSP**·$CS_2$ | **GaSP**·$CS_2$ |
|---|---|---|---|---|
| Empirical formula | $C_{32}H_{65}AlO_2PSSi_4$ | $C_{23}H_{56}GaOPS_2Si_4$ | $C_{23}H_{56}AlPS_3Si_4$ | $C_{23}H_{56}GaPS_3Si_4$ |
| $M$ [g mol$^{-1}$] | 684.21 | 625.84 | 599.196 | 641.90 |
| $T$ [K] | 100.0(1) | 100.0(1) | 100.0(1) | 100.0(1) |
| $\lambda$ [Å] | 1.54184 (Cu K$\alpha$) | 0.71073 (Mo K$\alpha$) | 1.54184 (Cu K$\alpha$) | 0.71073 (Mo K$\alpha$) |
| Crystal size | 0.25×0.17×0.16 | 0.32×0.28×0.07 | 0.58×0.32×0.19 | 0.39×0.3×0.21 |
| Crystal system | monoclinic | monoclinic | monoclinic | monoclinic |
| Space group | $P2_1/n$ | $C2/c$ | $C2/c$ | $C2/c$ |
| $a$ [Å] | 12.1936(2) | 20.4227(5) | 20.7333(1) | 20.7104(2) |
| $b$ [Å] | 23.2523(3) | 11.8217(3) | 11.8416(1) | 11.88290(10) |
| $c$ [Å] | 15.3726(2) | 27.8550(7) | 28.2218(1) | 28.2287(3) |
| $\alpha$ [°] | 90 | 90 | 90 | 90 |
| $\beta$ [°] | 107.8720(10) | 92.925(2) | 90.657(1) | 90.6200(10) |
| $\gamma$ [°] | 90 | 90 | 90 | 90 |
| *Volume* [Å$^3$] | 4148.26(10) | 6716.3(3) | 6928.43(7) | 6946.67(12) |
| $Z$ | 4 | 8 | 8 | 8 |
| $\rho_{calc}$ [g cm$^{-3}$] | 1.096 | 1.238 | 1.149 | 1.228 |
| $\mu$ [mm$^{-1}$] | 2.553 | 1.149 | 4.041 | 1.168 |
| $F$(000) [$e$] | 1492.0 | 2688.0 | 2632.3 | 2752.0 |
| 2$\theta$ range [°] | 7.138–152.3 | 5.854–69.556 | 6.26–152.16 | 6.826–60.066 |
| Index ranges | −15 ≤ $h$ ≤ 15, −29 ≤ $k$ ≤ 29, −19 ≤ $l$ ≤ 19 | −26 ≤ $h$ ≤ 31, −18 ≤ $k$ ≤ 18, −43 ≤ $l$ ≤ 42 | −26 ≤ $h$ ≤ 26, −14 ≤ $k$ ≤ 14, −35 ≤ $l$ ≤ 35 | −29 ≤ $h$ ≤ 29, −16 ≤ $k$ ≤ 16, −39 ≤ $l$ ≤ 39 |
| Refl. collected | 77529 | 52139 | 124642 | 323588 |
| Independent refl. | 8612 | 13480 | 7188 | 10152 |
| $R_{int}$ / $R_{sigma}$ | 0.0790/0.0332 | 0.0325/0.0316 | 0.0776/0.0237 | 0.0420/0.0105 |
| Data / restraints / parameters | 8612/0/461 | 13480/0/307 | 7188/0/457 | 10152/0/307 |
| GooF on $F^2$ | 1.048 | 1.060 | 1.047 | 1.132 |
| $R_1$ / w$R_2$ [$I > 2\sigma(I)$] | 0.0468/0.1236 | 0.0281/0.0626 | 0.0305/0.0798 | 0.0254/0.0612 |
| $R_{int}$ (all data) / w$R_2$ | 0.0530/0.1310 | 0.0338/0.0649 | 0.0307/0.0801 | 0.0270/0.0620 |
| $\rho_{fin}$ (max/min) [$e$ Å$^{-3}$] | 0.60/−0.32 | 0.54/−0.34 | 0.76/−0.25 | 1.27/−0.38 |
| CCDC | 2503483 | 2503484 | 2503485 | 2503486 |

[**AlSP**·$CO_2$] Disorder of one bis(trimethylsilyl)methyl group and the sulfur atom over two sites; ratio 67:33.

**Table S3.** Crystallographic data for compounds **GaOP**·$SO_2$, **AlSP**·$SO_2$, and **GaSP**·$SO_2$.

| Compound | **GaOP**·$SO_2$ | **AlSP**·$SO_2$ | **GaSP**·$SO_2$ |
|---|---|---|---|
| Empirical formula | $C_{22}H_{56}GaO_3PSSi_4$ | $C_{22}H_{56}AlO_2PS_2Si_4$ | $C_{22}H_{56}GaO_2PS_2Si_4$ |
| $M$ [g mol$^{-1}$] | 613.77 | 587.118 | 629.859 |
| $T$ [K] | 100.0(1) | 100.0(1) | 100.0(1) |
| $\lambda$ [Å] | 0.71073 (Mo K$\alpha$) | 1.54184 (Cu K$\alpha$) | 0.71073 (Mo K$\alpha$) |
| Crystal size | 0.67×0.38×0.17 | 0.37×0.17×0.12 | 0.25×0.17×0.09 |
| Crystal system | monoclinic | monoclinic | monoclinic |
| Space group | $P2_1/c$ | $P2_1/n$ | $P2_1/n$ |
| $a$ [Å] | 14.9783(5) | 17.00365(7) | 16.9878(5) |
| $b$ [Å] | 11.9478(5) | 11.56562(3) | 11.5830(3) |
| $c$ [Å] | 19.4795(7) | 17.31949(6) | 17.3586(4) |
| $\alpha$ [°] | 90 | 90 | 90 |
| $\beta$ [°] | 101.560(3) | 97.8697(3) | 97.744(2) |
| $\gamma$ [°] | 90 | 90 | 90 |
| *Volume* [Å$^3$] | 3415.3(2) | 3373.94(2) | 3384.50(15) |
| $Z$ | 4 | 4 | 4 |
| $\rho_{calc}$ [g cm$^{-3}$] | 1.194 | 1.156 | 1.236 |
| $\mu$ [mm$^{-1}$] | 1.074 | 3.622 | 1.143 |
| $F$(000) [$e$] | 1320.0 | 1291.1 | 1356.3 |
| 2$\theta$ range [°] | 6.502–66.492 | 7.84–152.16 | 6.62–60.06 |
| Index ranges | −22 ≤ $h$ ≤ 22, −15 ≤ $k$ ≤ 17, −29 ≤ $l$ ≤ 28 | −19 ≤ $h$ ≤ 21, −14 ≤ $k$ ≤ 14, −21 ≤ $l$ ≤ 21 | −26 ≤ $h$ ≤ 26, −17 ≤ $k$ ≤ 18, −28 ≤ $l$ ≤ 27 |
| Refl. collected | 43689 | 124076 | 96998 |
| Independent refl. | 12070 | 7025 | 9897 |
| $R_{int}$ / $R_{sigma}$ | 0.0328/0.0349 | 0.0257/0.0088 | 0.0567/0.0427 |
| Data / restraints / parameters | 12070/207/369 | 7025/0/513 | 9897/0/457 |
| GooF on $F^2$ | 1.026 | 1.007 | 1.045 |
| $R_1$ / w$R_2$ [$I > 2\sigma(I)$] | 0.0322/0.0756 | 0.0161/0.0360 | 0.0232/0.0428 |
| $R_{int}$ (all data) / w$R_2$ | 0.0447/0.0816 | 0.0162/0.0361 | 0.0322/0.0462 |
| $\rho_{fin}$ (max/min) [$e$ Å$^{-3}$] | 0.75/−0.42 | 0.20/−0.15 | 0.55/−0.34 |
| CCDC | 2503487 | 2503488 | 2503489 |

[**GaOP**·$SO_2$] Disorder of one trimethylsilyl group (Si1, C2-4) over two sites; ratio 58:42. Disorder of S1 and O2/3 over two sites; ratio 81:19.

**Table S4.** Crystallographic data for compounds **AlSP**·O, **GaOP**·S, **AlSP**·$SC_3H_6$, and **GaSP**·S.

| Compound | **AlSP**·O | **GaOP**·S | **AlSP**·$SC_3H_6$ | **GaSP**·S |
|---|---|---|---|---|
| Empirical formula | $C_{22}H_{56}AlO_{1.2}PS_{0.99}Si_4$ | $C_{22}H_{56}GaOPSSi_4$ | $C_{25}H_{62}AlPS_2Si_4$ | $C_{22}H_{56}GaPS_2Si_4$ |
| $M$ [g mol$^{-1}$] | 541.77 | 581.77 | 597.20 | 597.83 |
| $T$ [K] | 100.0(1) | 100.0(1) | 100.0(1) | 100.0(1) |
| $\lambda$ [Å] | 1.54184 (Cu K$\alpha$) | 0.71073 (Mo K$\alpha$) | 0.71073 (Mo K$\alpha$) | 0.71073 (Mo K$\alpha$) |
| Crystal size | 0.179×0.081×0.046 | 0.39×0.19×0.07 | 0.67×0.31×0.24 | 0.33×0.17×0.1 |
| Crystal system | monoclinic | tetragonal | triclinic | monoclinic |
| Space group | $C2/c$ | $P4_12_12$ | $P\bar{1}$ | $Cc$ |
| $a$ [Å] | 16.7077(4) | 11.7907(1) | 12.1972(3) | 17.2488(6) |
| $b$ [Å] | 16.4890(3) | 11.7907(1) | 17.2090(4) | 17.0657(7) |
| $c$ [Å] | 24.1502(4) | 47.9511(9) | 18.0410(3) | 23.2928(9) |
| $\alpha$ [°] | 90 | 90 | 83.294(2) | 90 |
| $\beta$ [°] | 93.764(2) | 90 | 86.526(2) | 94.614(3) |
| $\gamma$ [°] | 90 | 90 | 76.911(2) | 90 |
| *Volume* [Å$^3$] | 6638.9(2) | 6666.2(2) | 3660.9(2) | 6834.3(5) |
| $Z$ | 8 | 8 | 4 | 8 |
| $\rho_{calc}$ [g cm$^{-3}$] | 1.084 | 1.159 | 1.084 | 1.162 |
| $\mu$ [mm$^{-1}$] | 3.043 | 1.092 | 0.357 | 1.124 |
| $F$(000) [$e$] | 2379.0 | 2512.0 | 1315.3 | 2576.0 |
| 2$\theta$ range [°] | 7.336–152.518 | 6.88–56.554 | 3.74–59.14 | 6.728–57.4 |
| Index ranges | −21 ≤ $h$ ≤ 20, −20 ≤ $k$ ≤ 20, −30 ≤ $l$ ≤ 30 | −15 ≤ $h$ ≤ 15, −15 ≤ $k$ ≤ 15, −63 ≤ $l$ ≤ 63 | −18 ≤ $h$ ≤ 19, −26 ≤ $k$ ≤ 26, −28 ≤ $l$ ≤ 28 | −23 ≤ $h$ ≤ 23, −23 ≤ $k$ ≤ 23, −31 ≤ $l$ ≤ 31 |
| Refl. collected | 57080 | 129842 | 95073 | 80965 |
| Independent refl. | 8751 | 8263 | 20502 | 17649 |
| $R_{int}$ / $R_{sigma}$ | 0.0479/0.0794 | 0.0989/0.0397 | 0.0547/0.0637 | 0.0551/0.0543 |
| Data / restraints / parameters | 8751/592/477 | 8263/534/410 | 20502/402/708 | 17649/1911/1035 |
| GooF on $F^2$ | 1.046 | 1.283 | 1.043 | 1.017 |
| $R_1$ / w$R_2$ [$I > 2\sigma(I)$] | 0.0585/0.1469 | 0.0831/0.1603 | 0.0377/0.0682 | 0.0528/0.1044 |
| $R_{int}$ (all data) / w$R_2$ | 0.0688/0.1527 | 0.0857/0.1615 | 0.0571/0.0764 | 0.0767/0.1156 |
| $\rho_{fin}$ (max/min) [$e$ Å$^{-3}$] | 0.51/−0.43 | 0.69/−1.07 | 0.79/−0.89 | 0.74/−0.71 |
| Flack parameter | – | – | – | 0.486(16) |
| CCDC | 2503490 | 2503491 | 2503492 | 2503493 |

[**AlSP**·O] Twinned crystal; BASF [0.4008(14)], component 2 rotated by 180.0° around [1.00 –0.00 –0.10] (reciprocal) or [1.00 0.00 0.00] (direct). Mixed crystal: Al and P are linked by a) O (O1) and S (S1) (ratio 93:7) on the one site, and b) O (O2), S (S2), and OS (O3/S3) (ratio 9:73:18) on the other site. Rotational disorder of all trimethylsilyl and *tert*-butyl groups over two sites: C2–4, ratio 73:27); C5–7, ratio 59:41; C9–14, ratio 52:48; C16–18 and C20–22, ratio 59:41.

[**GaOP**·S] Racemic twin BASF 0.26(3). Disorder of one complete Bis-group over two sites in ratio 52:48, disorder of one $SiMe_3$-group over two sites in ratio 54:46. Necessary restraints were applied.
[**AlSP**·$SC_3H_6$] Rotational disorder of one *tert*-butyl group (C16–18) over two sites; ratio 53:47. Disorder of one trimethylsilyl group (Si7, C34–36) over two sites; ratio 77:23.
[**GaSP**·S] Refined as an inversion twin, BASF [0.486(16)]. Disorder of Si1/2 and C1-7 over two sites; ratio 65:35. Disorder of Si3/4 and C8-22 over two sites; ratio 57:43. Disorder of Si6-8 and C23–36 over two sites; ratio 82:18. Disorder of C37–44 over two sites; ratio 57:43.

UV/vis spectra

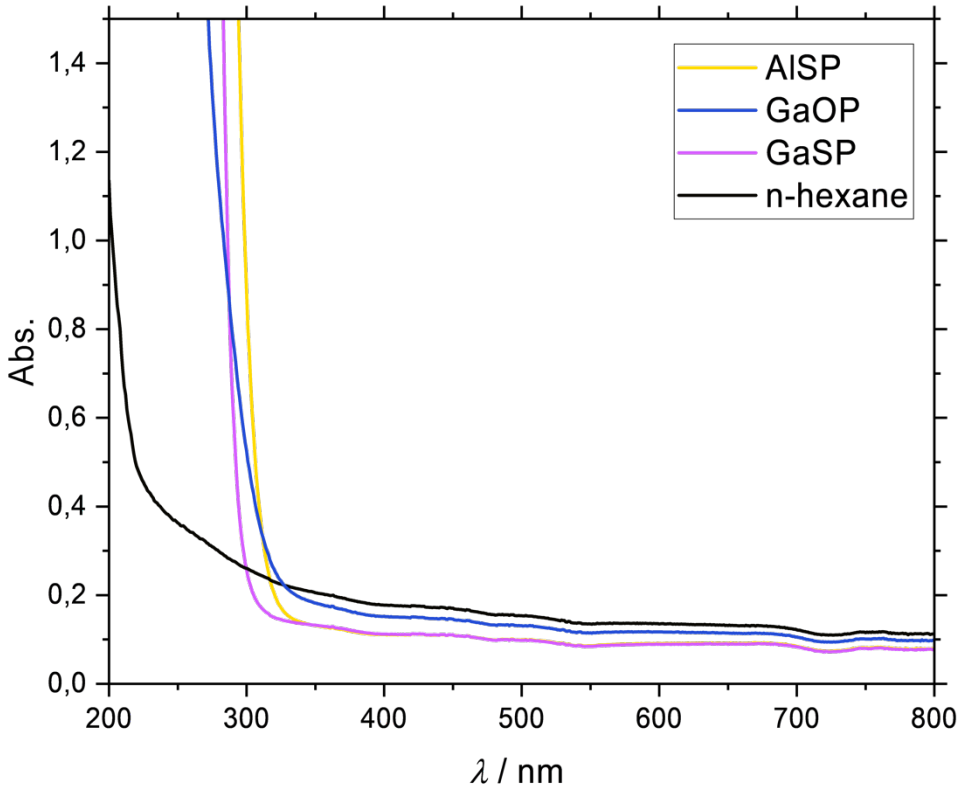


**Figure S87.** UV/vis spectra of the free FLPs in *n*-hexane.

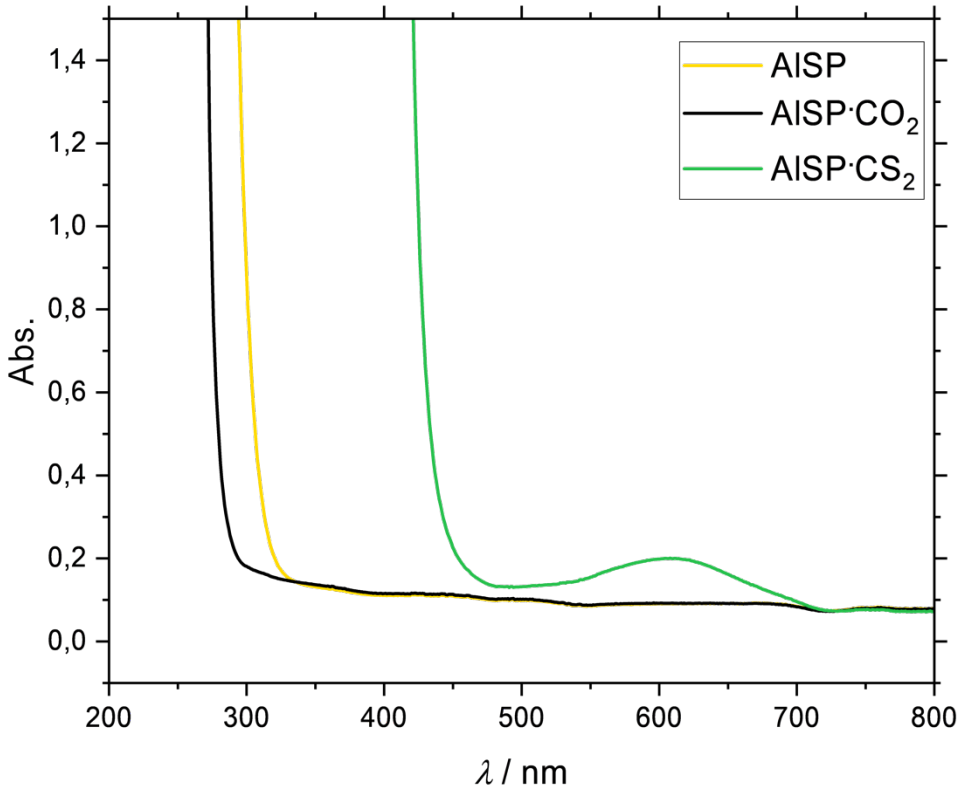


**Figure S88.** UV/vis spectra of **AlSP**, **AlSP**·$CO_2$ and **AlSP**·$CS_2$ in *n*-hexane.

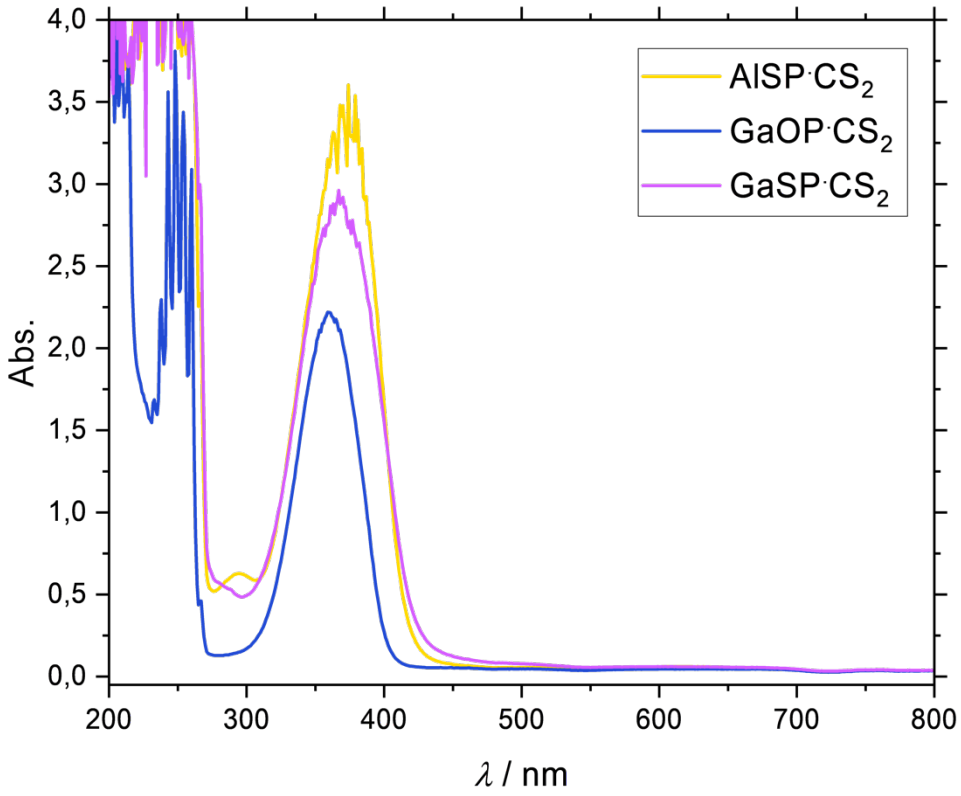


**Figure S89.** UV/vis spectra of **AlSP**·$CS_2$, **GaOP**·$CS_2$ and **GaSP**·$CS_2$ (lower concentration) in *n*-hexane.

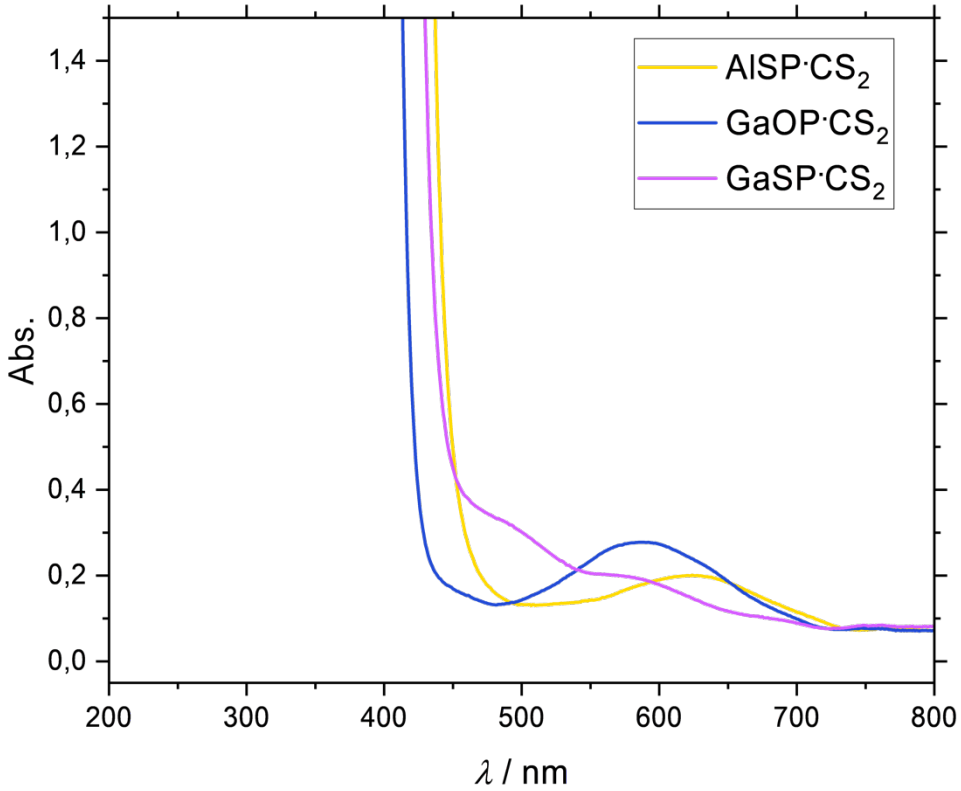


**Figure S90.** UV/vis spectra of **AlSP**·$CS_2$, **GaOP**·$CS_2$ and **GaSP**·$CS_2$ (higher concentration) in *n*-hexane.

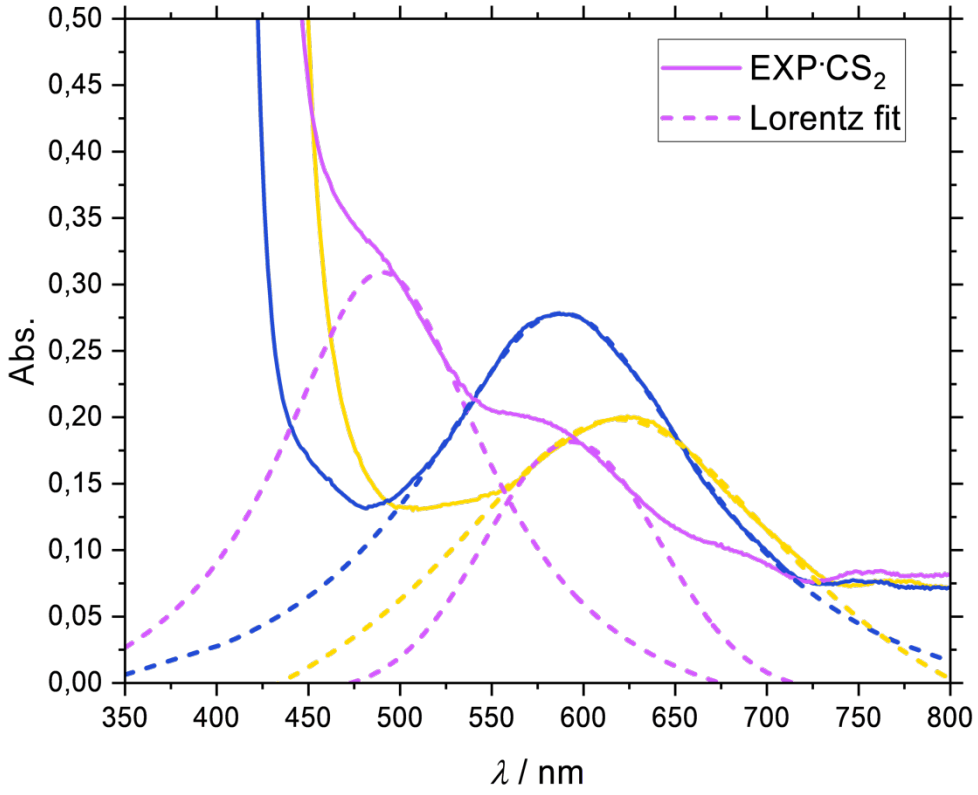


**Figure S91.** UV/vis spectra of **EXP**·$CS_2$ (higher concentration) with fitted curves (dotted) in *n*-hexane.

## Quantum chemical calculations

Calculations have been performed using Orca 6.0.1 software package,[9] unless otherwise stated. Molecular structures of selected studied compounds have been optimised at the PBEh-3c level of theory[10] using restricted Kohn-Sham (RKS) formalism. All species were modelled as isolated molecules. As starting approximations, the geometries from the available experimental crystal structures were taken. Otherwise, they were modelled manually. The target convergence in geometry optimisations has been set to *TightOpt*. Also, in all calculations we used the settings *TightSCF* and *DefGrid3*, as well as the RIJCOSX accelerating approximation.[11] The obtained molecular structures are shown in Figures S92 – S95. In addition, hypothetical isomers (see Figures S96 – S102) of **GaSP**·$CS_2$ have been optimised using the same protocol. In particular, the dimer (**GaSP**·$CS_2$-iso3)$_2$ (Figure S98) has been calculated. The obtained relative energies are collected in Tables S6 and S7. Relative energy of isomer 2 of **GaSP**·$CS_2$ has been checked by optimising structures at higher level of theory, PBE0-D3BJ/def2-TZVP[12–14], resulting in similar value $\Delta E$ = 19.4 kcal/mol.

TD-DFT calculations were performed at the PBE0/def2-TZVP level of theory[12–14] using the TDA approximation. The number of calculated roots was restricted to 40. Selected transitions are listed in Tables S7 – S10. Frontier molecular orbitals are collected in Tables S11 – S14. Simulated UV-Vis spectra are shown in Figures S103 – S106.

Energies of some selected reactions have been computed also at the PBEh-3c level. For obtaining the Gibbs free energies $\Delta G^0_{298}$, frequencies were calculated utilising the Quasi-RRHO approximation[15] with standard settings. The obtained results are listed in Table S5.

**Table S5**. Electronic ($\Delta E$) and Gibbs free energies ($\Delta G^0_{298}$) for selected reactions.[a]

| Reaction | $\Delta E$ [kcal mol$^{-1}$] | $\Delta G^0_{298}$ [kcal mol$^{-1}$] |
|---|---|---|
| **GaOP** + $^t$Bu$_2$P(S)H → **GaSP** + $^t$Bu$_2$P(O)H | −1.9 | −1.3 |
| **GaOP** + **AlSP** → **AlOP** + **GaSP** | −10.0 | −10.2 |
| **GaSP** + $CO_2$ → **GaSP**·$CO_2$ | −15.7 | −0.7 |
| **GaSP** + $CS_2$ → **GaSP**·$CS_2$ | −24.5 | −8.6 |
| **GaSP**·$CS_2$ → **GaSP**·$CS_2$-iso2 | 22.2 | n.c. |
| **GaSP**·$CS_2$ → **GaSP**·$CS_2$-iso3 | 44.3 | n.c. |

[a] n.c. stands for not calculated.

**Table S6**. Relative electronic energies ($\Delta E$) for different isomers of **GaSP**·$CS_2$.

| Reaction | $\Delta E$ [kcal mol$^{-1}$] |
|---|---|
| **GaSP**·$CS_2$ | 0 |
| **GaSP**·$CS_2$-iso2 | 22.2 |
| **GaSP**·$CS_2$-iso3 | 44.3 |
| **GaSP**·$CS_2$-iso4 | 44.8 |
| **GaSP**·$CS_2$-iso5 | 44.1 |
| **GaSP**·$CS_2$-iso6 | 47.5 |
| **GaSP**·$CS_2$-iso7 | 33.6 |

**Table S7**. Relative dimerisation Δ*E* energy of **GaSP**·$CS_2$.

| Reaction | Δ*E* [kcal $mol^{-1}$] |
|---|---|
| (**GaSP**·$CS_2$-iso3)$_2$ | 0 |
| 2 **GaSP**·$CS_2$ | 21.2 |

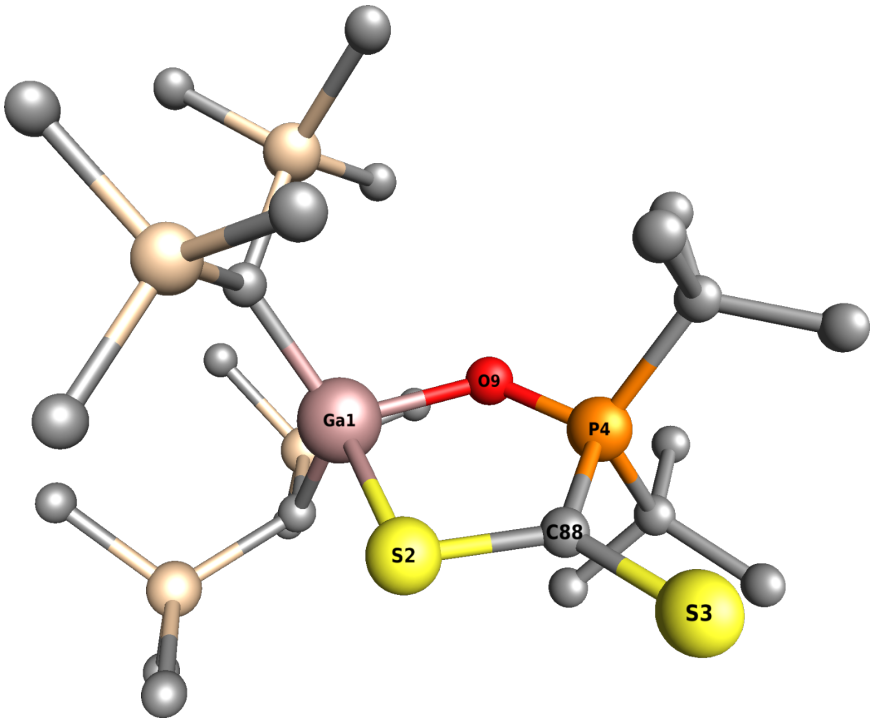


**Figure S92**. Optimised molecular structure of **GaOP**·$CS_2$ (RKS-PBEh-3c). Hydrogen atoms are omitted for clarity. Internal working numeration of selected atoms is shown. Selected equilibrium parameters (Å, degrees) are: r(S2-Ga1)=2.414, r(O9-Ga1)=1.946, r(O9-P4)=1.550, r(C88-S2)=1.693, r(C88-S3)=1.639, r(C88-P4)=1.833, a(S2-Ga1-O9)=87.6, a(Ga1-S2-C88)=103.2, a(Ga1-O9-P4)=125.7, a(O9-P4-C88)=107.5, a(S2-C88-S3)=126.1, a(S2-C88-P4)=115.6, a(S3-C88-P4)=118.3, t(S2-Ga1-O9-P4)=4.7, t(C88-S2-Ga1-O9)=0.4, t(Ga1-S2-C88-S3)=176.5, t(Ga1-S2-C88-P4)=-4.3, t(Ga1-O9-P4-C88)=-7.8, t(O9-P4-C88-S2)=7.3, t(O9-P4-C88-S3)=-173.4, o(S3-C88<S2/P4)=0.6.

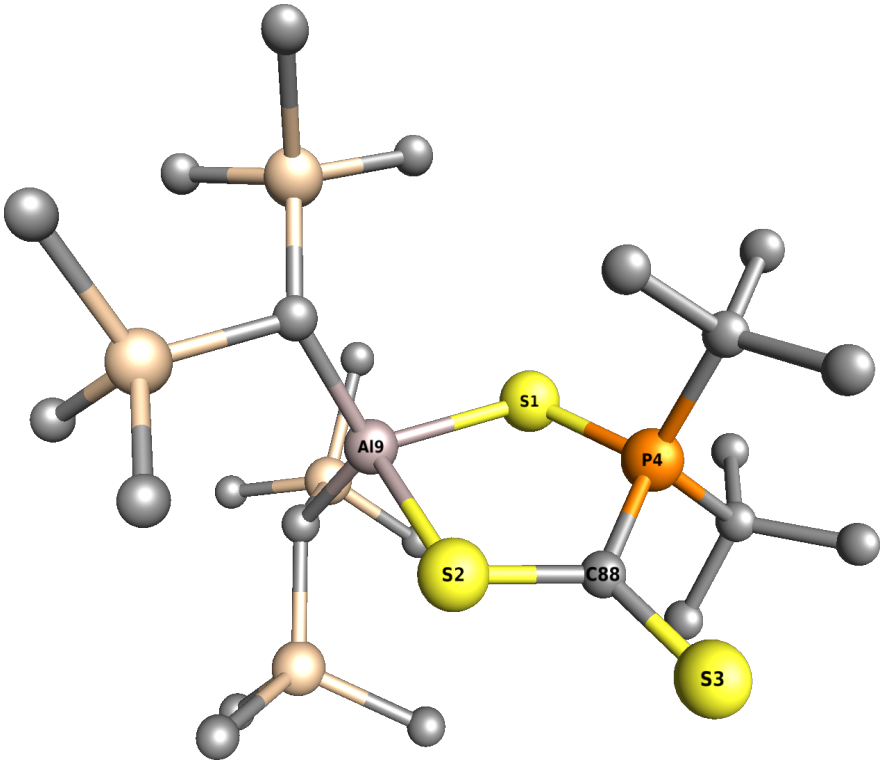


**Figure S93.** Optimised molecular structure of **AlSP**·$CS_2$ (RKS-PBEh-3c). Hydrogen atoms are omitted for clarity. Internal working numeration of selected atoms is shown. Selected equilibrium parameters (Å, degrees) are: r(S1-P4)=2.028, r(Al9-S1)=2.353, r(Al9-S2)=2.372, r(C88-S2)=1.692, r(C88-S3)=1.637, r(C88-P4)=1.845, a(P4-S1-Al9)=104.4, a(S1-P4-C88)=110.3, a(S1-Al9-S2)=93.6, a(Al9-S2-C88)=109.7, a(S2-C88-S3)=124.3, a(S2-C88-P4)=118.9, a(S3-C88-P4)=116.6, t(P4-S1-Al9-S2)=-8.4, t(C88-P4-S1-Al9)=16.1, t(S1-P4-C88-S2)=-19.8, t(S1-P4-C88-S3)=164.7, t(S1-Al9-S2-C88)=-1.3, t(Al9-S2-C88-S3)=-172.1, t(Al9-S2-C88-P4)=12.7, o(S3-C88<S2/P4)=-4.0.

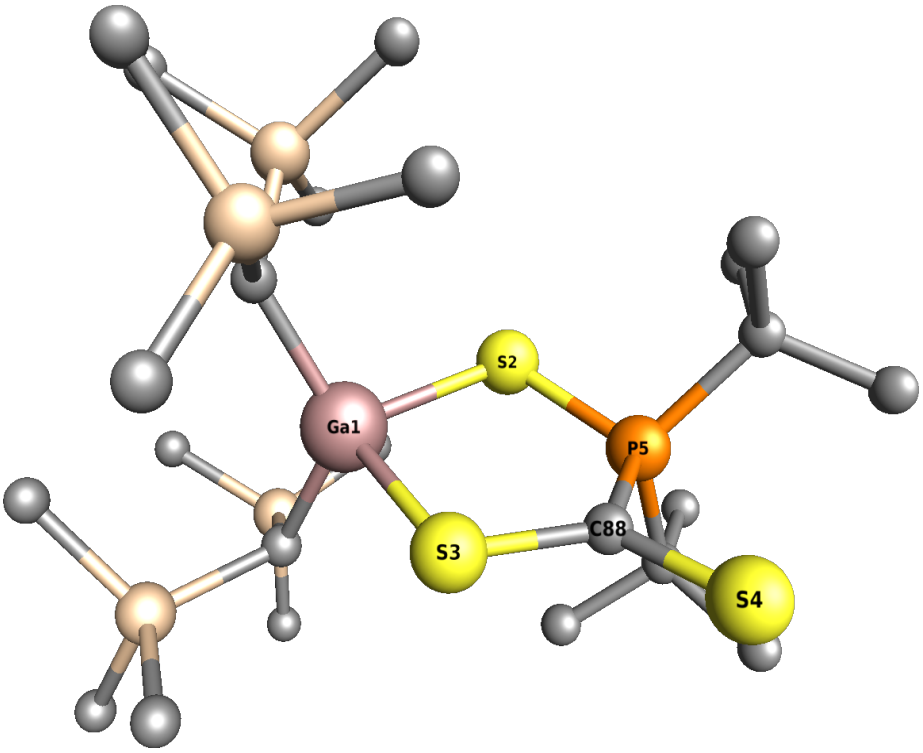


**Figure S94**. Optimised molecular structure of **GaSP**·$CS_2$ (RKS-PBEh-3c). Hydrogen atoms are omitted for clarity. Internal working numeration of selected atoms is shown. Selected equilibrium parameters (Å, degrees) are: r(Ga1-S2)=2.391, r(S3-Ga1)=2.402, r(P5-S2)=2.025, r(C88-S3)=1.689, r(C88-S4)=1.640, r(C88-P5)=1.847, a(S2-Ga1-S3)=92.6, a(Ga1-S2-P5)=104.4, a(Ga1-S3-C88)=109.9, a(S2-P5-C88)=110.7, a(S3-C88-S4)=124.1, a(S3-C88-P5)=119.3, a(S4-C88-P5)=116.4, t(P5-S2-Ga1-S3)=8.8, t(S2-Ga1-S3-C88)=0.8, t(Ga1-S2-P5-C88)=-16.3, t(Ga1-S3-C88-S4)=172.6, t(Ga1-S3-C88-P5)=-12.3, t(S2-P5-C88-S3)=19.7, t(S2-P5-C88-S4)=-164.7, o(S4-C88<S3/P5)=4.0.

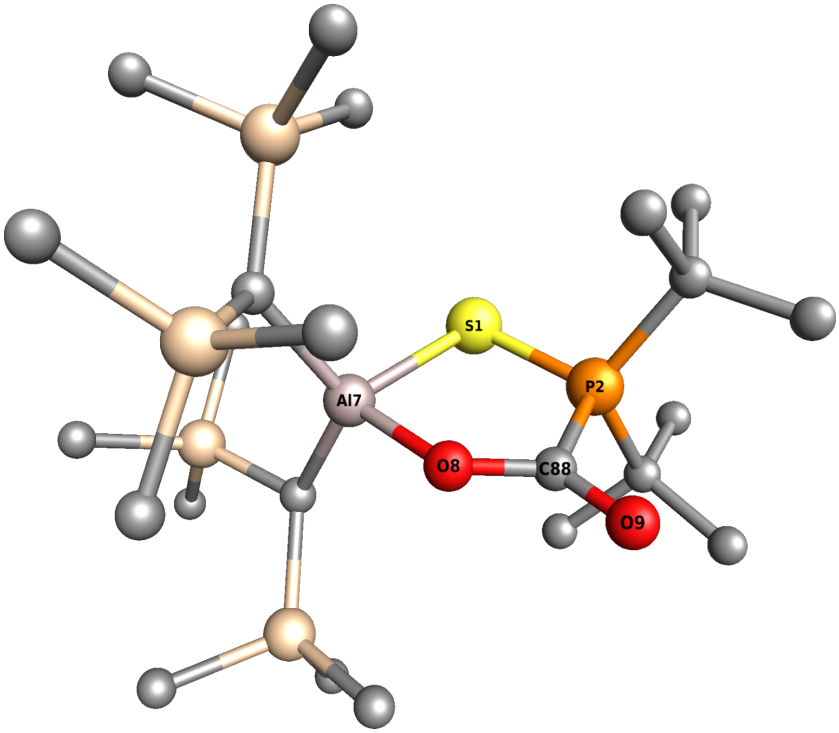


**Figure S95.** Optimised molecular structure of **AlSP**·$CO_2$ (RKS-PBEh-3c). Hydrogen atoms are omitted for clarity. Internal working numeration of selected atoms is shown. Selected equilibrium parameters (Å, degrees) are: r(P2-S1)=2.017, r(Al7-S1)=2.417, r(O8-Al7)=1.826, r(C88-P2)=1.894, r(C88-O8)=1.273, r(C88-O9)=1.203, a(P2-S1-Al7)=94.8, a(S1-P2-C88)=107.1, a(S1-Al7-O8)=92.2, a(Al7-O8-C88)=132.3, a(P2-C88-O8)=113.3, a(P2-C88-O9)=118.0, a(O8-C88-O9)=128.7, t(P2-S1-Al7-O8)=4.6, t(C88-P2-S1-Al7)=-4.2, t(S1-P2-C88-O8)=2.5, t(S1-P2-C88-O9)=-176.3, t(S1-Al7-O8-C88)=-5.0, t(Al7-O8-C88-P2)=2.4, t(Al7-O8-C88-O9)=-179.0, o(O9-C88<P2/O8)=1.1.

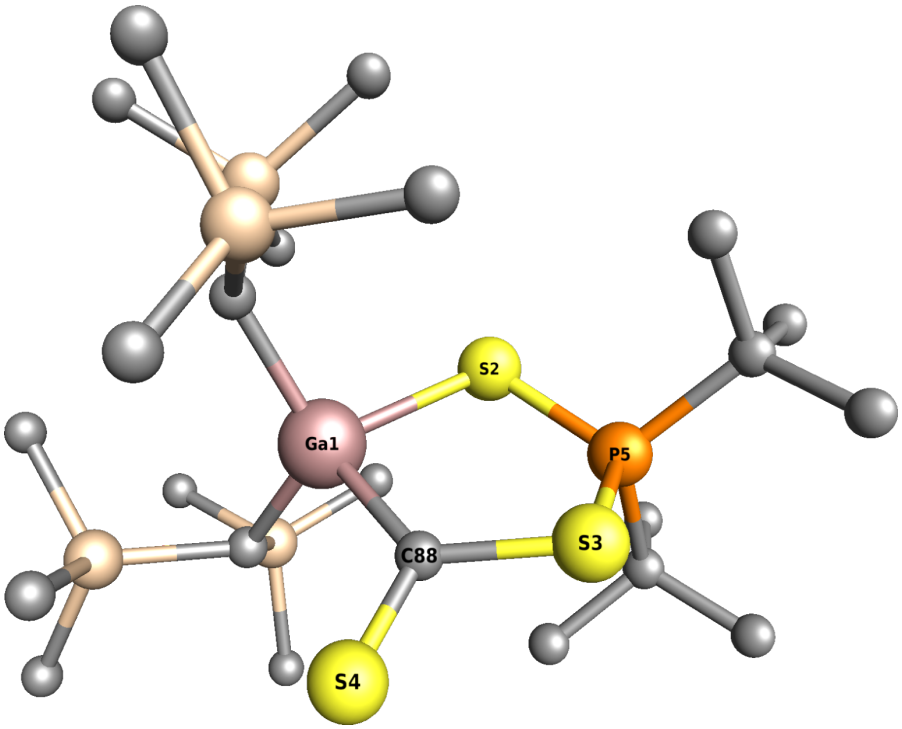


**Figure S96**. Optimised molecular structure of **GaSP**·$CS_2$-iso2 (RKS-PBEh-3c). Hydrogen atoms are omitted for clarity. Internal working numeration of selected atoms is shown. Selected equilibrium parameters (Å, degrees) are: r(S2-Ga1)=2.499, r(P5-S2)=2.003, r(P5-S3)=2.096, r(C88-Ga1)=2.062, r(C88-S3)=1.780, r(C88-S4)=1.621, a(Ga1-S2-P5)=102.3, a(S2-Ga1-C88)=92.7, a(S2-P5-S3)=111.3, a(P5-S3-C88)=102.5, a(Ga1-C88-S3)=124.8, a(Ga1-C88-S4)=120.8, a(S3-C88-S4)=114.3, t(Ga1-S2-P5-S3)=-18.8, t(C88-Ga1-S2-P5)=5.9, t(S2-Ga1-C88-S3)=12.3, t(S2-Ga1-C88-S4)=-170.4, t(S2-P5-S3-C88)=25.9, t(P5-S3-C88-Ga1)=-24.1, t(P5-S3-C88-S4)=158.4, o(S4-C88<Ga1/S3)=-2.3.

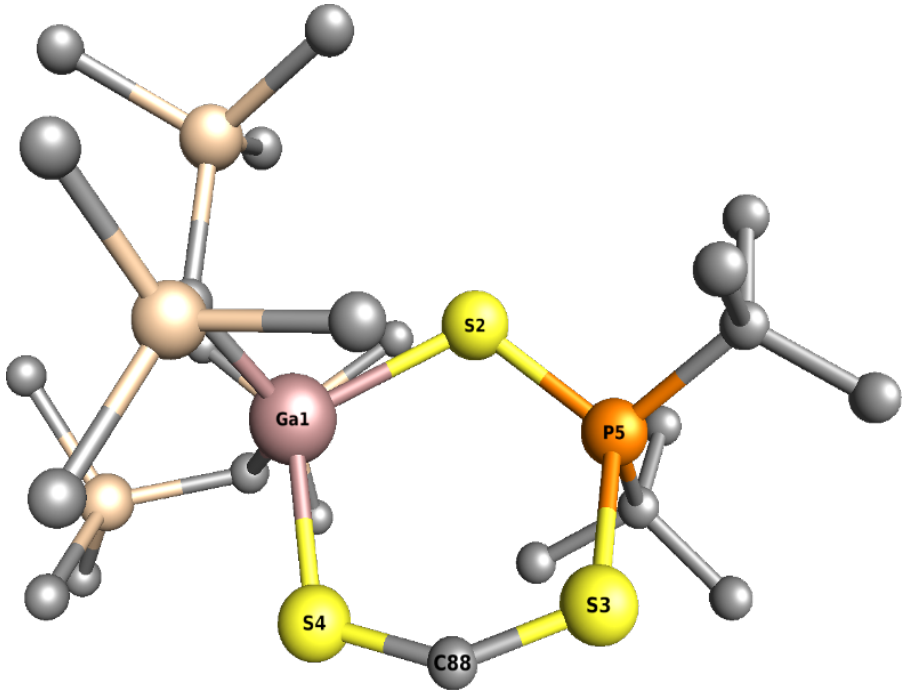


**Figure S97**. Optimised molecular structure of **GaSP**·$CS_2$-iso3 (RKS-PBEh-3c). Hydrogen atoms are omitted for clarity. Internal working numeration of selected atoms is shown. Selected equilibrium parameters (Å, degrees) are: r(S2-Ga1)=2.417, r(S4-Ga1)=2.427, r(P5-S2)=2.031, r(P5-S3)=2.289, r(C88-S3)=1.608, r(C88-S4)=1.634, a(S2-Ga1-S4)=107.1, a(Ga1-S2-P5)=114.3, a(Ga1-S4-C88)=117.7, a(S2-P5-S3)=115.9, a(P5-S3-C88)=116.7, a(S3-C88-S4)=140.2, t(P5-S2-Ga1-S4)=12.6, t(S2-Ga1-S4-C88)=9.2, t(Ga1-S2-P5-S3)=-29.2, t(Ga1-S4-C88-S3)=-15.0, t(S2-P5-S3-C88)=29.0, t(P5-S3-C88-S4)=-4.0.

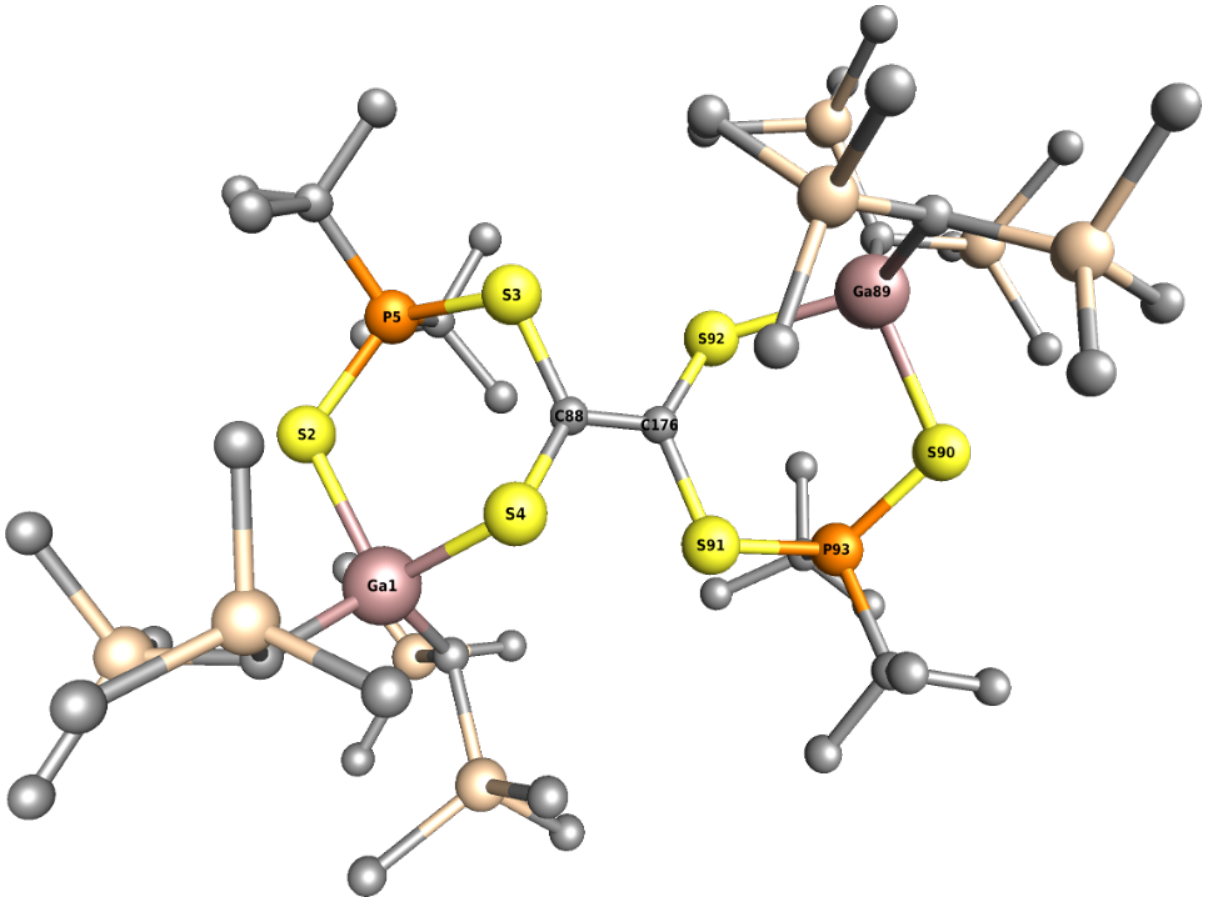


**Figure S98**. Optimised molecular structure of **GaSP**·$CS_2$-iso3 dimer (RKS-PBEh-3c). Hydrogen atoms are omitted for clarity. Internal working numeration of selected atoms is shown. Selected equilibrium parameters (Å, degrees) are: r(S2-Ga1)=2.453, r(S4-Ga1)=2.335, r(P5-S2)=2.019, r(P5-S3)=2.090, r(C88-S3)=1.770, r(C88-S4)=1.743, r(S90-Ga89)=2.431, r(S92-Ga89)=2.373, r(P93-S90)=2.013, r(P93-S91)=2.108, r(C176-C88)=1.354, r(C176-S91)=1.778, r(C176-S92)=1.732, a(S2-Ga1-S4)=100.2, a(Ga1-S2-P5)=116.1, a(Ga1-S4-C88)=108.9, a(S2-P5-S3)=118.1, a(P5-S3-C88)=106.3, a(S3-C88-S4)=118.3, a(S3-C88-C176)=117.9, a(S4-C88-C176)=121.7, a(S90-Ga89-S92)=97.9, a(Ga89-S90-P93)=110.7, a(Ga89-S92-C176)=117.1, a(S90-P93-S91)=117.9, a(P93-S91-C176)=110.0, a(C88-C176-S91)=111.5, a(C88-C176-S92)=124.8, a(S91-C176-S92)=123.7, t(P5-S2-Ga1-S4)=24.8, t(S2-Ga1-S4-C88)=-45.6, t(Ga1-S2-P5-S3)=-25.8, t(Ga1-S4-C88-S3)=82.8, t(Ga1-S4-C88-C176)=-114.1, t(S2-P5-S3-C88)=42.5, t(P5-S3-C88-S4)=-76.9, t(P5-S3-C88-C176)=119.4, t(S3-C88-C176-S91)=173.2, t(S3-C88-C176-S92)=-9.1, t(S4-C88-C176-S91)=10.0, t(S4-C88-C176-S92)=-172.3, t(P93-S90-Ga89-S92)=-2.6, t(S90-Ga89-S92-C176)=52.2, t(Ga89-S90-P93-S91)=-45.1, t(Ga89-S92-C176-C88)=127.0, t(Ga89-S92-C176-S91)=-55.5, t(S90-P93-S91-C176)=54.1, t(P93-S91-C176-C88)=178.2, t(P93-S91-C176-S92)=0.4.

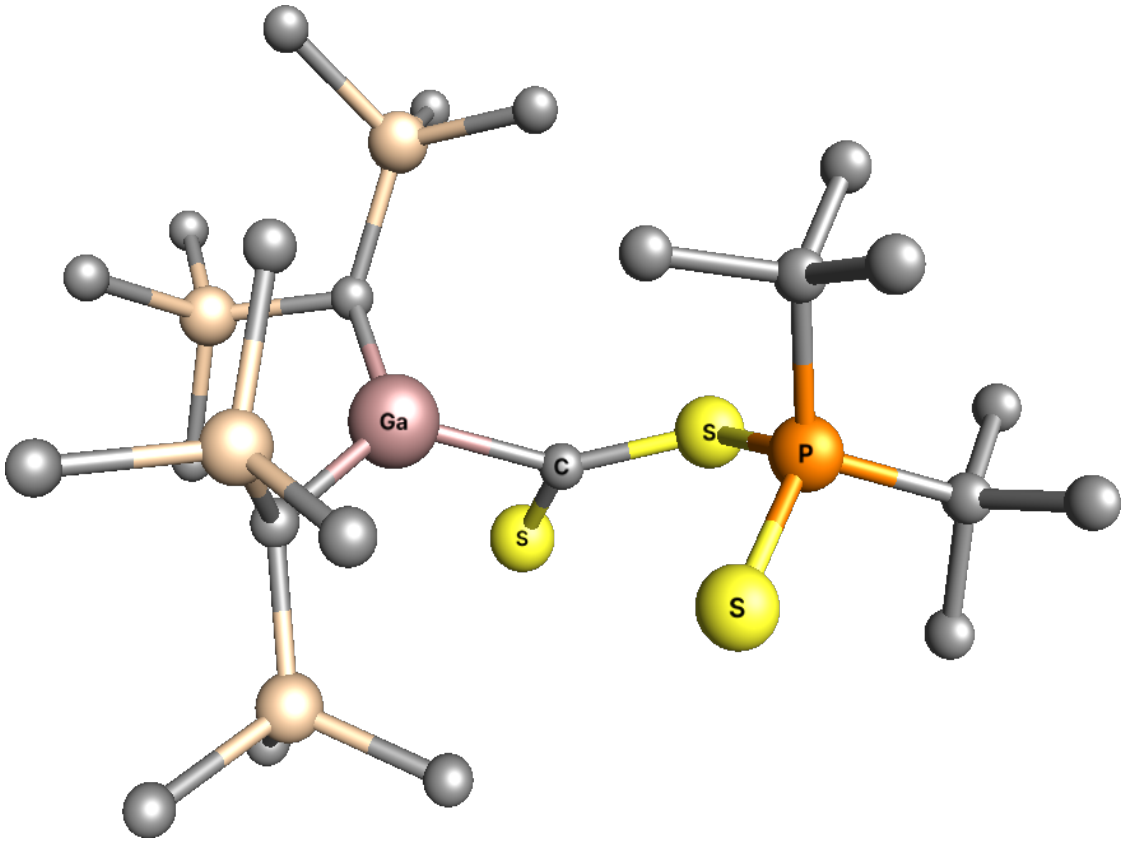


**Figure S99**. Optimised molecular structure of **GaSP**·$CS_2$-iso4 (RKS-PBEh-3c). Hydrogen atoms are omitted for clarity.

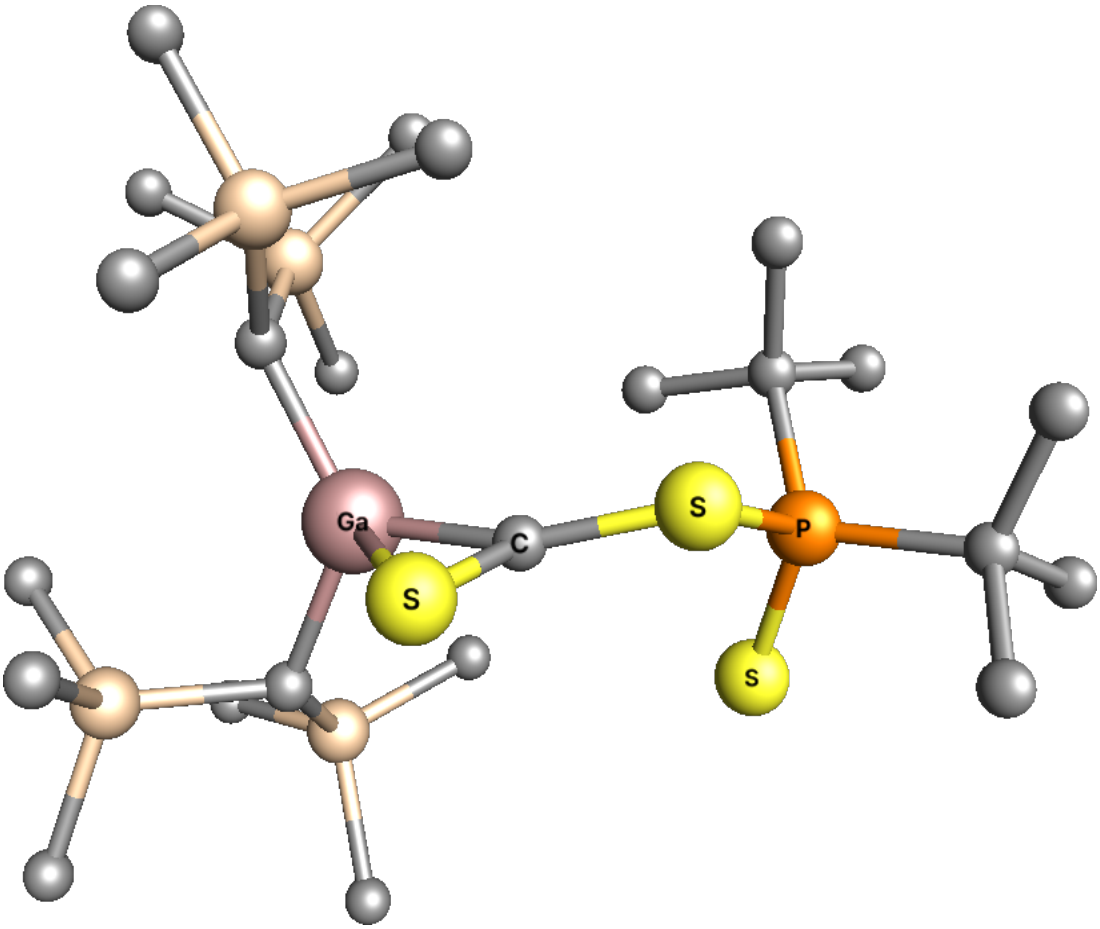


**Figure S100**. Optimised molecular structure of **GaSP**·$CS_2$-iso5 (RKS-PBEh-3c). Hydrogen atoms are omitted for clarity.

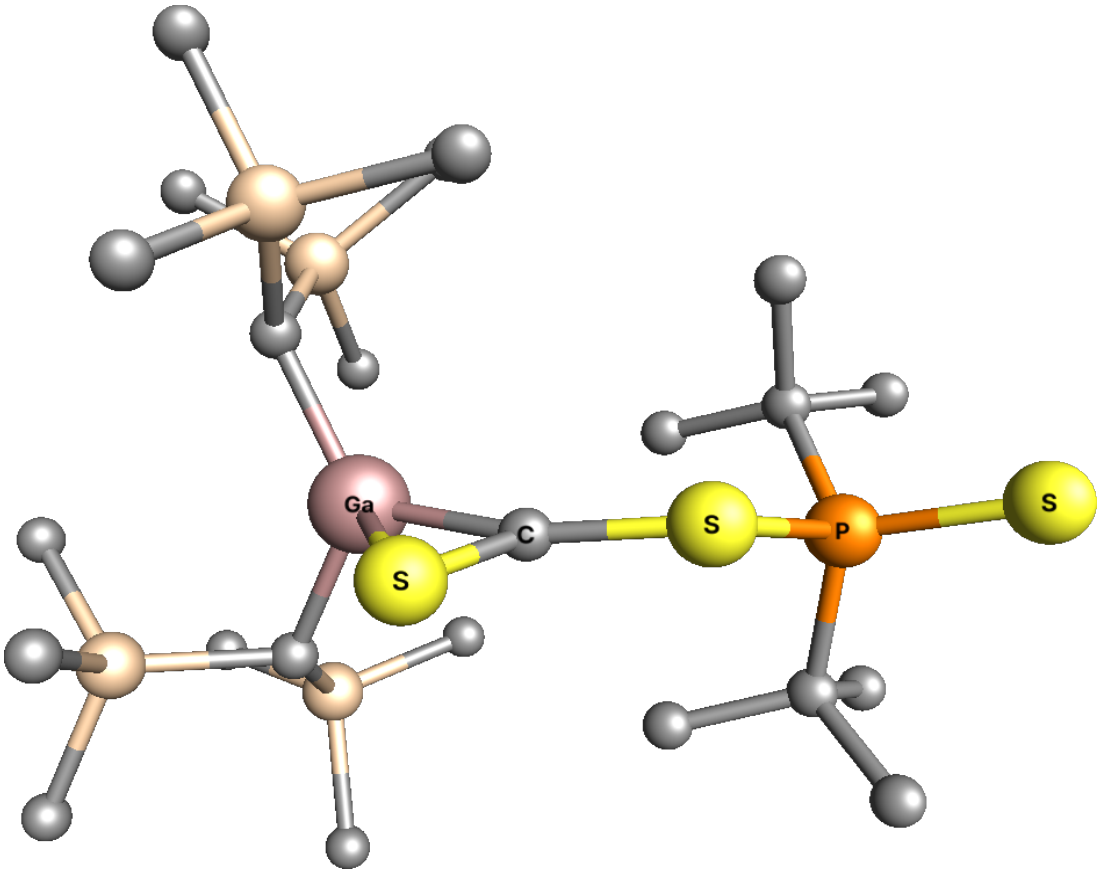


**Figure S101**. Optimised molecular structure of **GaSP**·$CS_2$-iso6 (RKS-PBEh-3c). Hydrogen atoms are omitted for clarity.

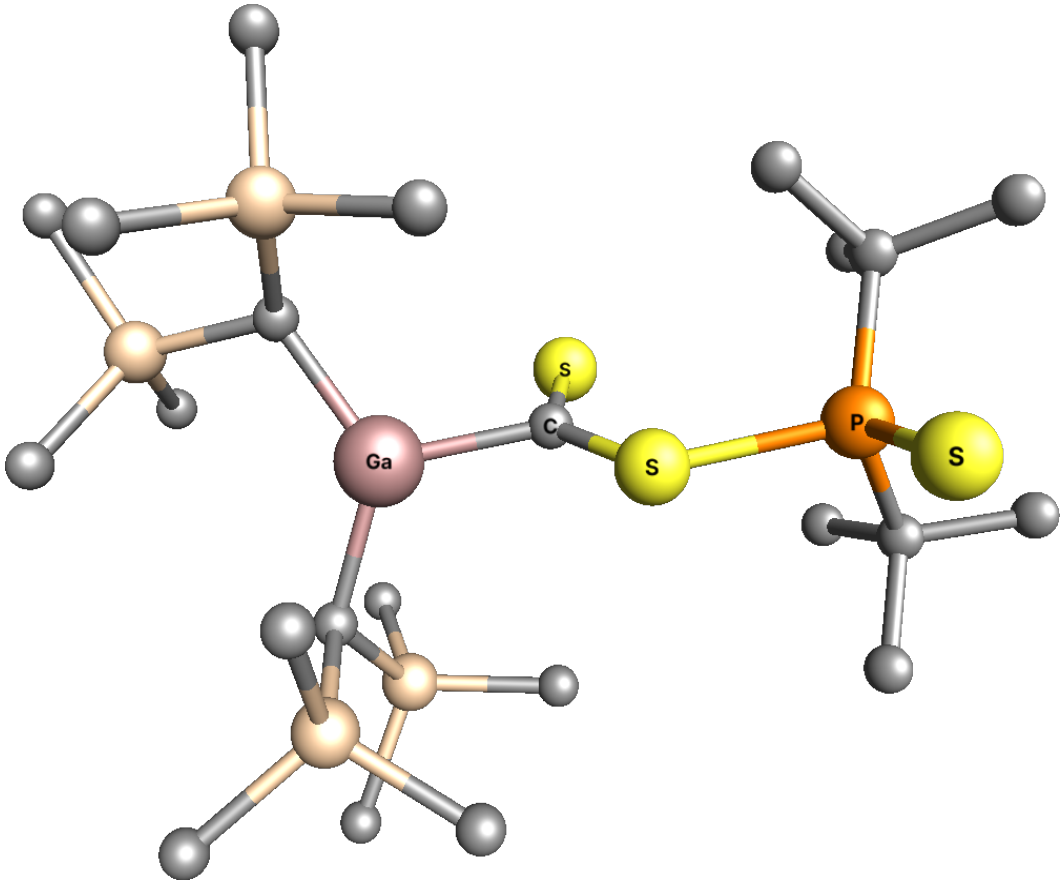


**Figure S102**. Optimised molecular structure of **GaSP**·$CS_2$-iso7 (RKS-PBEh-3c). Hydrogen atoms are omitted for clarity.

**Table S7**. Most important transitions (vertical energy differences) in the TD-DFT calculation of **GaOP**·$CS_2$. Wavelengths $\lambda$ in nm, oscillator strengths *f* via transition electric dipole moments and assignments are listed.

| $\lambda$ | *f* | Assignment |
|---|---|---|
| 531 | 0.00006 | 98 % HOMO → LUMO |
| 287 | 0.18 | 13 % HOMO-4 → LUMO; 60 % HOMO-2 → LUMO; 14 % HOMO-1 → LUMO |
| 200 | 0.10 | 74 % HOMO → LUMO+3 |

**Table S8**. Most important transitions (vertical energy differences) in the TD-DFT calculation of **AlSP**·$CS_2$. Wavelengths $\lambda$ in nm, oscillator strengths *f* via transition electric dipole moments and assignments are listed.

| $\lambda$ | *f* | Assignment |
|---|---|---|
| 537 | 0.0002 | 89 % HOMO → LUMO |
| 289 | 0.06 | 43 % HOMO-7 → LUMO; 24 % HOMO-6 → LUMO; 12 % HOMO-2 → LUMO |
| 215 | 0.06 | 21 % HOMO-16 → LUMO; 54 % HOMO → LUMO+2; 10 % HOMO → LUMO+3 |

**Table S9**. Most important transitions (vertical energy differences) in the TD-DFT calculation of **GaSP**·$CS_2$. Wavelengths $\lambda$ in nm, oscillator strengths *f* via transition electric dipole moments and assignments are listed.

| $\lambda$ | *f* | Assignment |
|---|---|---|
| 538 | 0.0002 | 92 % HOMO → LUMO |
| 284 | 0.09 | 27 % HOMO-6 → LUMO; 25 % HOMO-5 → LUMO; 12 % HOMO-4 → LUMO; 17 % HOMO-2 → LUMO |
| 222 | 0.06 | 16 % HOMO-16 → LUMO; 63 % HOMO → LUMO+2 |

**Table S10**. Most important transitions (vertical energy differences) in the TD-DFT calculation of **AlSP**·$CO_2$. Wavelengths $\lambda$ in nm, oscillator strengths *f* via transition electric dipole moments and assignments are listed.

| $\lambda$ | *f* | Assignment |
|---|---|---|
| 248 | 0.02 | 81 % HOMO → LUMO |
| 223 | 0.04 | 87 % HOMO → LUMO+1 |
| 203 | 0.04 | 23 % HOMO-2 → LUMO+1; 45 % HOMO-1 → LUMO+1 |

**Table S11**. Frontier molecular orbitals (isosurfaces 0.05 a.u.) and respective energies (eV) in PBE0-D3BJ/def2-TZVP calculation of **GaOP**·$CS_2$.

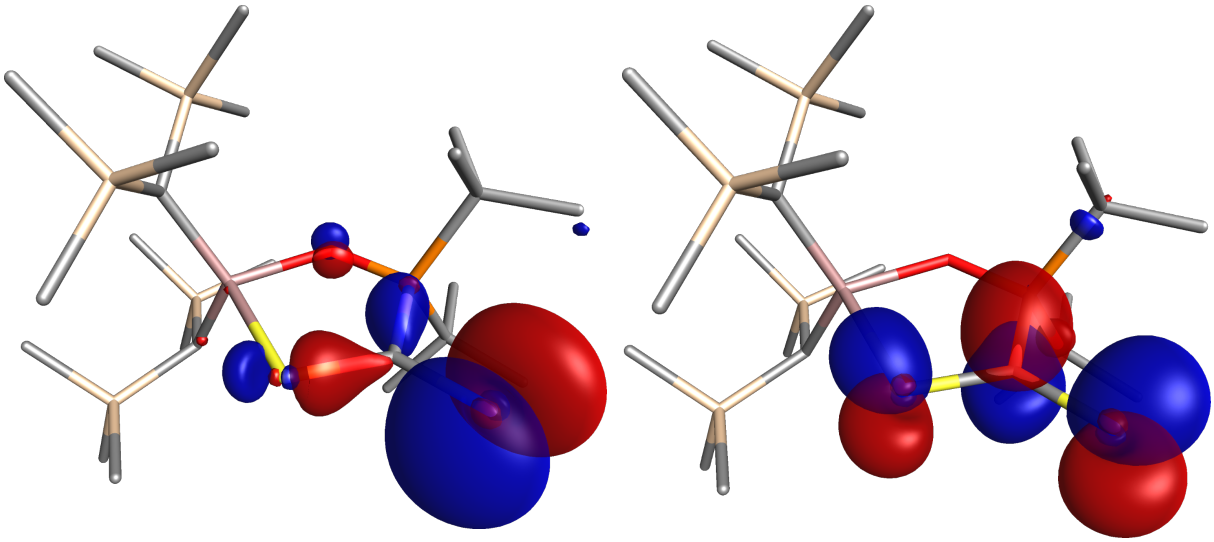

| HOMO (-6.3668) | LUMO (-2.4614) |
|---|---|

**Table S12**. Frontier molecular orbitals (isosurfaces 0.05 a.u.) and respective energies (eV) in PBE0-D3BJ/def2-TZVP calculation of **AlSP**·$CS_2$.

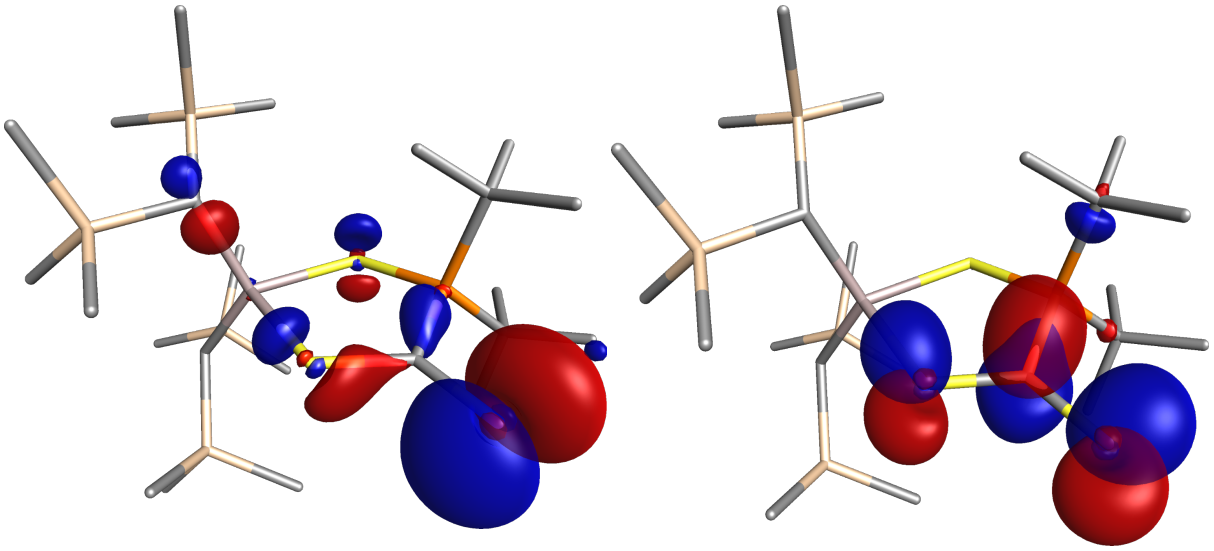

| HOMO (-6.5087) | LUMO (-2.6666) |
|---|---|

**Table S13**. Frontier molecular orbitals (isosurfaces 0.05 a.u.) and respective energies (eV) in PBE0-D3BJ/def2-TZVP calculation of **GaSP**·$CS_2$.

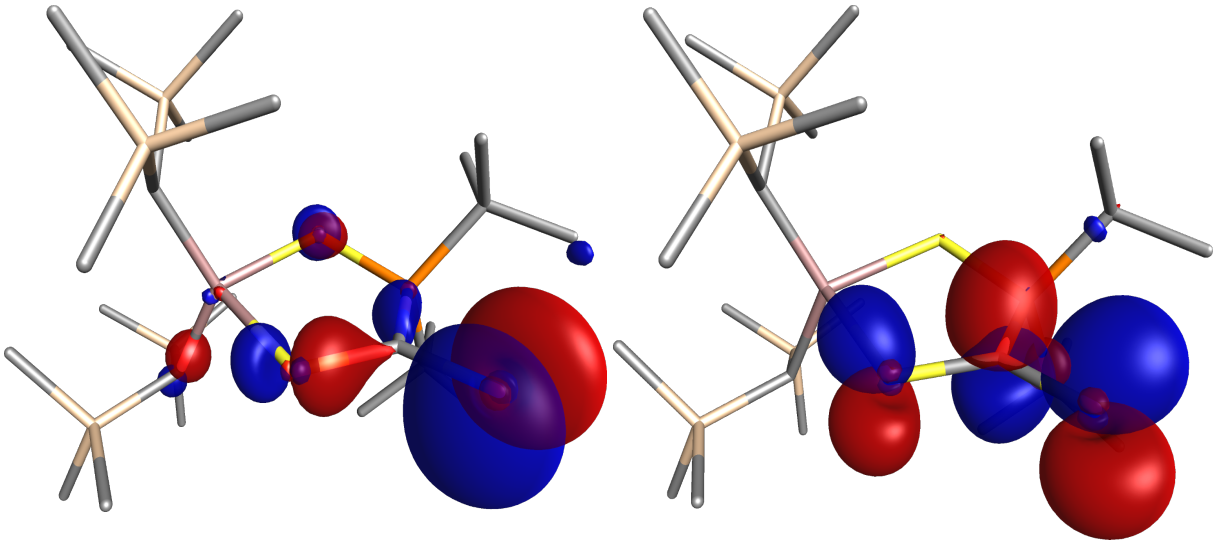

| HOMO (-6.4061) | LUMO (-2.5779) |
|---|---|

**Table S14**. Frontier molecular orbitals (isosurfaces 0.05 a.u.) and respective energies (eV) in PBE0-D3BJ/def2-TZVP calculation of **AlSP**·$CO_2$.

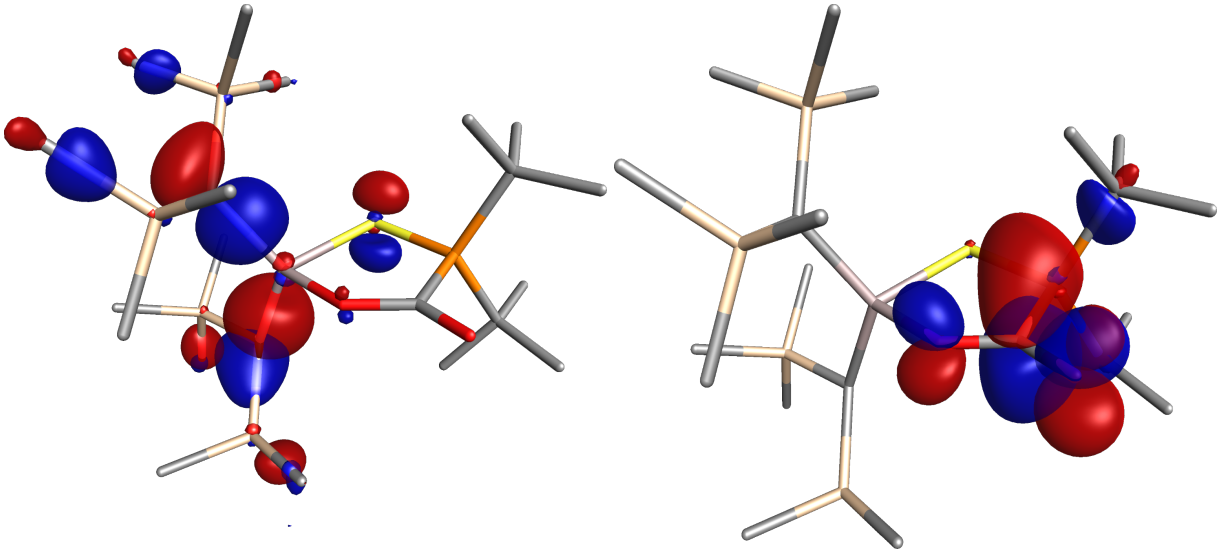

| HOMO (-6.6660) | LUMO (-0.8201) |
|---|---|

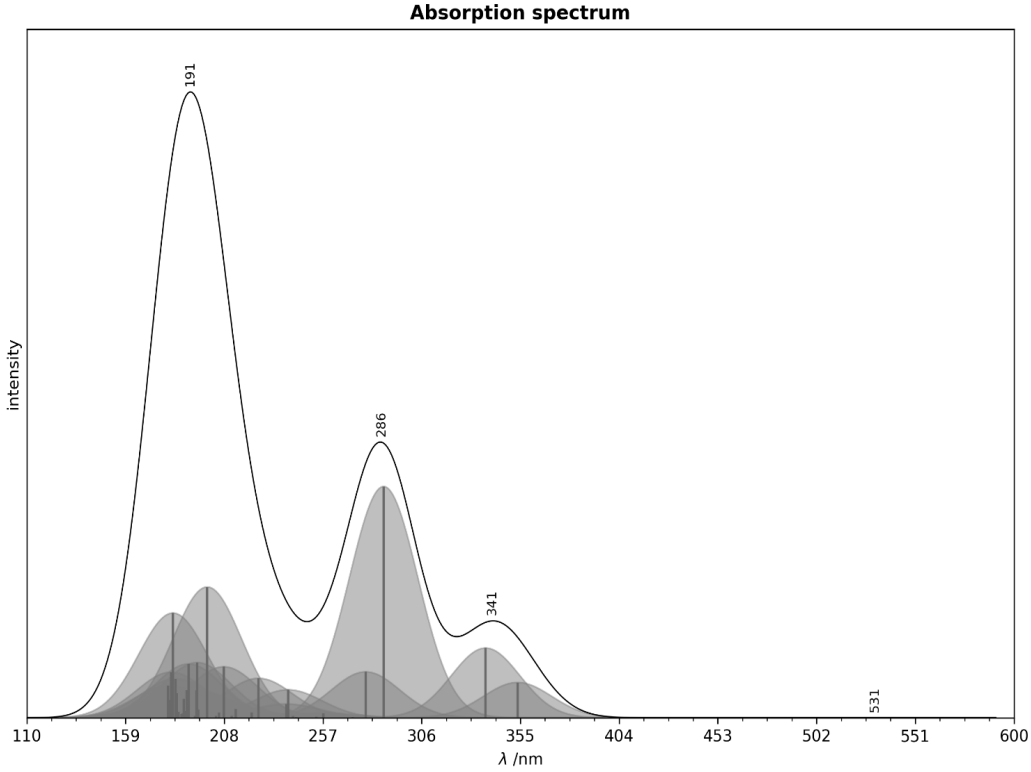


**Figure S103**. Simulated UV-Vis spectrum of **GaOP**·$CS_2$ based on TD-DFT calculation. Individual transitions are shown as vertical sticks and are approximated as Gaussian functions (grey areas with 20 nm FWHM). Full line is the sum of all Gaussians. No empirical shift has been applied to the transition energies.

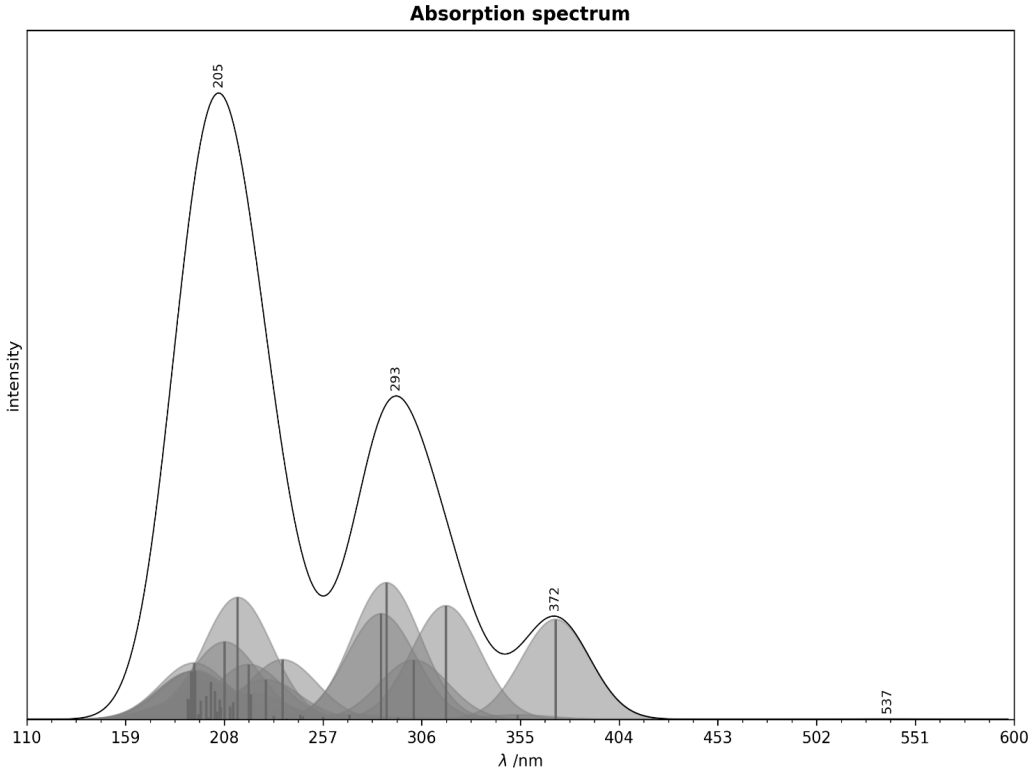


**Figure S104**. Simulated UV-Vis spectrum of **AlSP**·$CS_2$ based on TD-DFT calculation. Individual transitions are shown as vertical sticks and are approximated as Gaussian functions (grey areas with 20 nm FWHM). Full line is the sum of all Gaussians. No empirical shift has been applied to the transition energies.

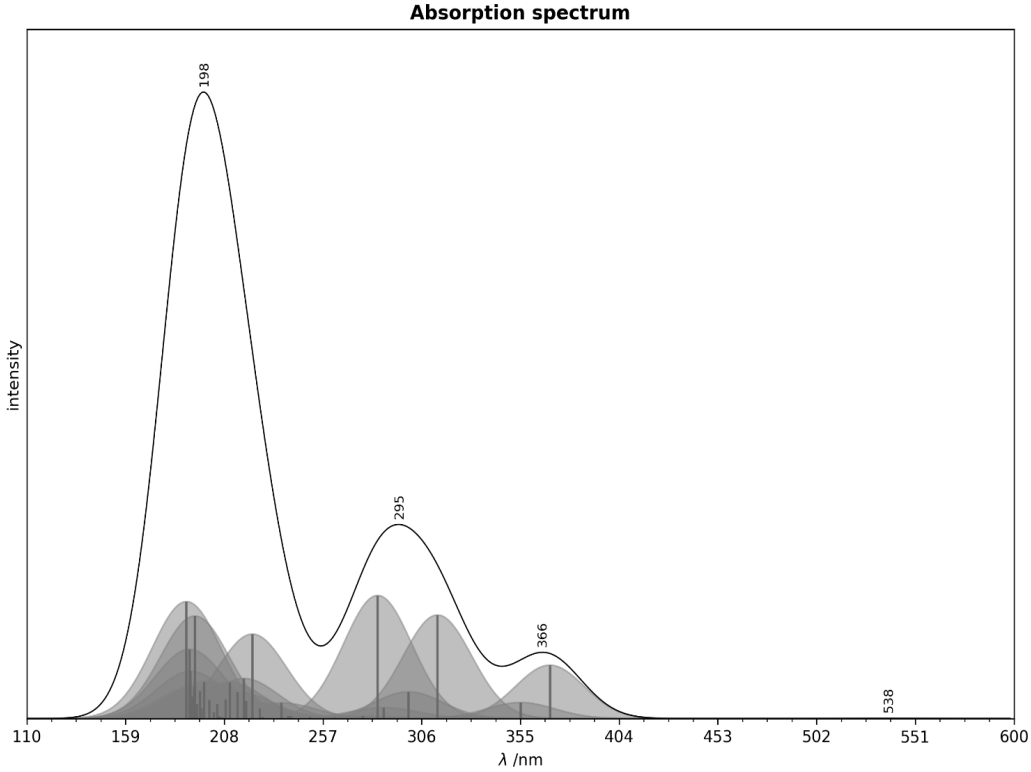


**Figure S105**. Simulated UV-Vis spectrum of **GaSP**·$CS_2$ based on TD-DFT calculation. Individual transitions are shown as vertical sticks and are approximated as Gaussian functions (grey areas with 20 nm FWHM). Full line is the sum of all Gaussians. No empirical shift has been applied to the transition energies.

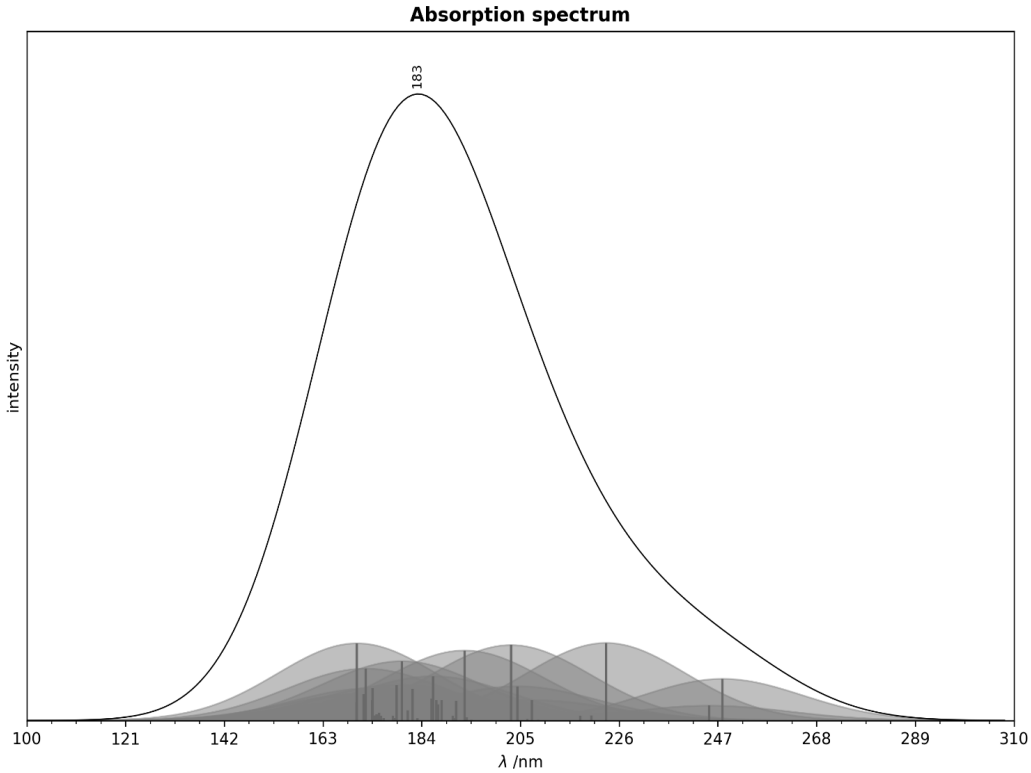


**Figure S106**. Simulated UV-Vis spectrum of **AlSP**·$CO_2$ based on TD-DFT calculation. Individual transitions are shown as vertical sticks and are approximated as Gaussian functions (grey areas with 20 nm FWHM). Full line is the sum of all Gaussians. No empirical shift has been applied to the transition energies.

## References


1 W. Uhl, L. Cuypers, R. Graupner, J. Molter, A. Vester and B. Neumüller, *Z. Anorg. Allg. Chem.*, 2001, **627**, 607–614.

2 J. Buth, M. J. Klingsiek, Y. V. Vishnevskiy, A. Mix, J.-H. Lamm, B. Neumann, H.-G. Stammler, N. W. Mitzel, *ChemistryEurope* **2025**, *0*, e20250030723.

3 J. Krieft, H. Koch, B. Neumann, H.-G. Stammler, J.-H. Lamm, A. Mix and N. W. Mitzel, *Dalton Trans.*, 2024, **53**, 16280–16286.

4 G. M. Sheldrick, *Acta Crystallogr., Sect. A:Found. Adv.*, 2015, **71**, 3–8.

5 O. V. Dolomanov, L. J. Bourhis, R. J. Gildea, J. A. K. Howard and H. Puschmann, *J. Appl. Crystallogr.*, 2009, **42**, 339–341.

6 G. M. Sheldrick, *Acta Crystallogr., Sect. C:Struct. Chem.*, 2015, **71**, 3–8.

7 L. J. Bourhis, O. V. Dolomanov, R. J. Gildea, J. A. K. Howard and H. Puschmann, *Acta Crystallogr., Sect. A:Found. Adv.*, 2015, **71**, 59–75.

8 F. Kleemiss, O. V. Dolomanov, M. Bodensteiner, N. Peyerimhoff, L. Midgley, L. J. Bourhis, A. Genoni, L. A. Malaspina, D. Jayatilaka, J. L. Spencer, F. White, B. Grundkötter-Stock, S. Steinhauer, D. Lentz, H. Puschmann and S. Grabowsky, *Chem. Sci.*, 2021, **12**, 1675–1692.

9 F. Neese, *WIREs Comput. Mol. Sci.*, 2022, **12**, e1606.

10 S. Grimme, J. G. Brandenburg, C. Bannwarth and A. Hansen, *J. Chem. Phys.*, 2015, **143**, 054107.

11 F. Neese, F. Wennmohs, A. Hansen and U. Becker, *Chem. Phys.*, 2009, **356**, 98–109.

12 C. Adamo and V. Barone, *J. Chem. Phys.*, 1999, **110**, 6158–6170.

13 S. Grimme, S. Ehrlich and L. Goerigk, *J. Comput. Chem.*, 2011, **32**, 1456–1465.

14 F. Weigend and R. Ahlrichs, *Phys. Chem. Chem. Phys.*, 2005, **7**, 3297.

15 S. Grimme, *Chem. –Eur. J.*, 2012, **18**, 9955–9964.